109

SATELLITE & MESOMETEOROLOGY RESEARCH PROJECT

Department of the Geophysical Sciences
The University of Chicago

A STUDY OF SATELLITE-OBSERVED CLOUD PATTERNS OF TROPICAL CYCLONES

by

Ekundayo E. Balogun

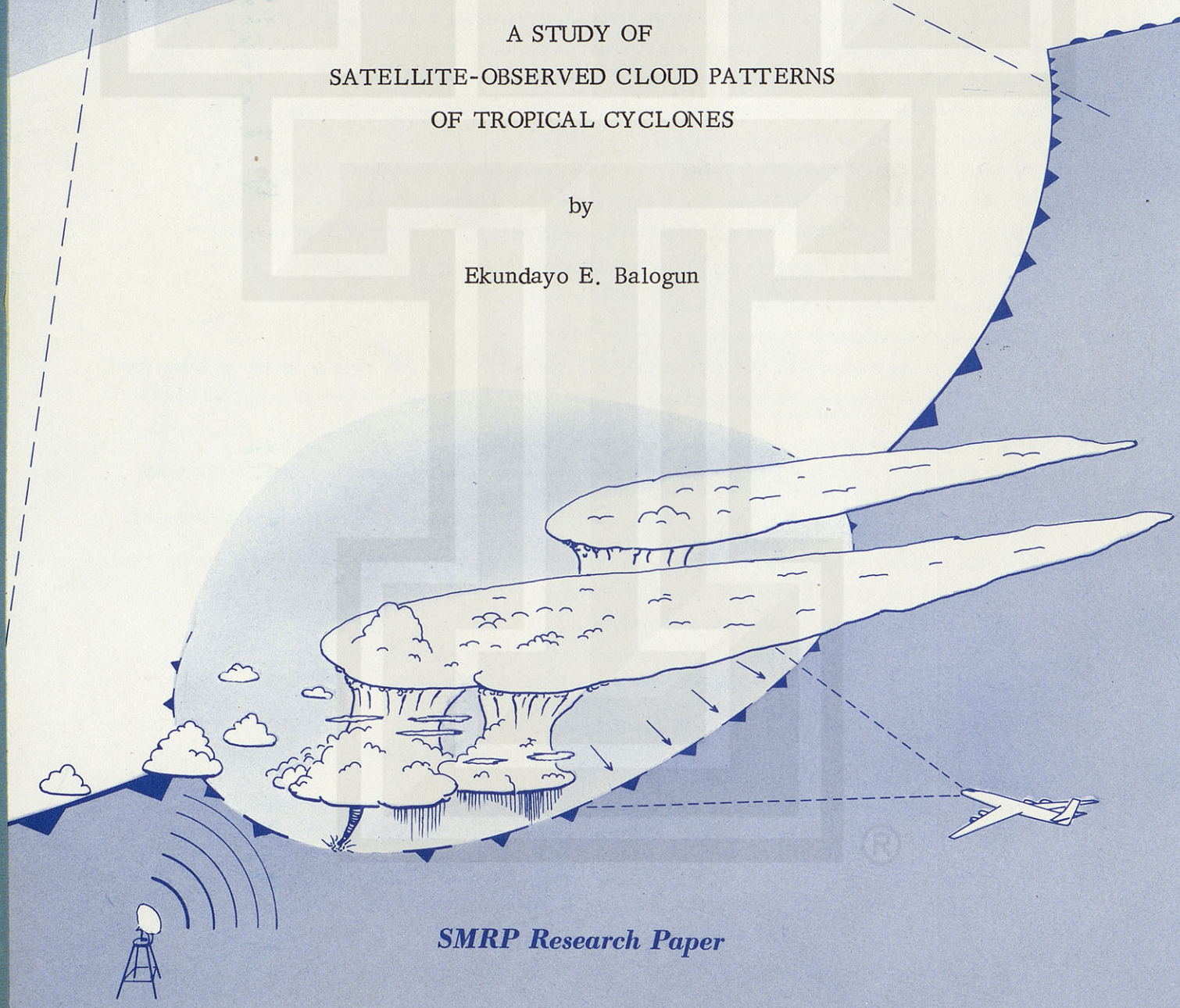

SMRP Research Paper

MESOMETEOROLOGY PROJECT --- RESEARCH PAPERS

1.* Report on the Chicago Tornado of March 4, 1961 - Rodger A. Brown and Tetsuya Fujita

2.* Index to the NSSP Surface Network - Tetsuya Fujita

3.* Outline of a Technique for Precise Rectif.cation of Satellite Cloud Photographs - Tetsuya Fujita

4.* Horizontal Structure of Mountain Winds - Henry A. Brown

5.* An Investigation of Developmental Processes of the Wake Depression Through Excess Pressure Analysis of Nocturnal Showers - Joseph L. Goldman

6.* Precipitation in the 1960 Flagstaff Mesometeorological Network - Kenneth A. Styber

7.** On a Method of Single- and Dual-Image Photogrammetry of Panoramic Aerial Photographs - Tetsuya Fujita

8. A Review of Researches on Analytical Mesometeorology - Tetsuya Fujita

9.* Meteorological Interpretations of Convective Nephsystems Appearing in TIROS Cloud Photographs - Tetsuya Fujita, Toshimitsu Ushijima, William A. Hass, and George T. Dellert, Jr.

10.* Study of the Development of Prefrontal Squall-Systems Using NSSP Network Data - Joseph L. Goldman

11. Analysis of Selected Aircraft Data from NSSP Operation, 1962 - Tetsuya Fujita

12. Study of a Long Condensation Trail Photographed by TIROS I - Toshimitsu Ushijima

13. A Technique for Precise Analysis of Satellite Data; Volume I - Photogrammetry (Published as MSL Report No. 14) - Tetsuya Fujita

14. Investigation of a Summer Jet Stream Using TIROS and Aerological Data - Kozo Ninomiya

15. Outline of a Theory and Examples for Precise Analysis of Satellite Radiation Data - Tetsuya Fujita

16. Preliminary Result of Analysis of the Cumulonimbus Cloud of April 21, 1961 - Tetsuya Fujita and James Arnold

17. A Technique for Precise Analysis of Satellite Photographs - Tetsuya Fujita

18.* Evaluation of Limb Darkening from TIROS III Radiation Data - S.H.H. Larsen, Tetsuya Fujita, and W.L. Fletcher

19. Synoptic Interpretation of TIROS III Measurements of Infrared Radiation - Finn Pedersen and Tetsuya Fujita

20.* TIROS III Measurements of Terrestrial Radiation and Reflected and Scattered Solar Radiation - S.H.H. Larsen, Tetsuya Fujita, and W.L. Fletcher

21. On the Low-level Structure of a Squall Line - Henry A. Brown

22.* Thunderstorms and the Low-level Jet - William D. Bonner

23.* The Mesoanalysis of an Organized Convective System - Henry A. Brown

24. Preliminary Radar and Photogrammetric Study of the Illinois Tornadoes of April 17 and 22, 1963 - Joseph L. Goldman and Tetsuya Fujita

25. Use of TIROS Pictures for Studies of the Internal Structure of Tropical Storms - Tetsuya Fujita with Rectified Pictures from TIROS I Orbit 125, R/O 128 - Toshimitsu Ushijima

26. An Experiment in the Determination of Geostrophic and Isallobaric Winds from NSSP Pressure Data - William Bonner

27. Proposed Mechanism of Hook Echo Formation - Tetsuya Fujita with a Preliminary Mesosynoptic Analysis of Tornado Cyclone Case of May 26, 1963 - Tetsuya Fujita and Robbi Stuhmer

28. The Decaying Stage of Hurricane Anna of July 1961 as Portrayed by TIROS Cloud Photographs and Infrared Radiation from the Top of the Storm - Tetsuya Fujita and James Arnold

29. A Technique for Precise Analysis of Satellite Data, Volume II - Radiation Analysis, Section 6. Fixed-Position Scanning - Tetsuya Fujita

30. Evaluation of Errors in the Graphical Rectification of Satellite Photographs - Tetsuya Fujita

31. Tables of Scan Nadir and Horizontal Angles - William D. Bonner

32. A Simplified Grid Technique for Determining Scan Lines Generated by the TIROS Scanning Radiometer - James E. Arnold

33. A Study of Cumulus Clouds over the Flagstaff Research Network with the Use of U-2 Photographs - Dorothy L. Bradbury and Tetsuya Fujita

34. The Scanning Printer and Its Application to Detailed Analysis of Satellite Radiation Data - Tetsuya Fujita

35. Synoptic Study of Cold Air Outbreak over the Mediterranean using Satellite Photographs and Radiation Data - Aasmund Rabbe and Tetsuya Fujita

36. Accurate Calibration of Doppler Winds for their use in the Computation of Mesoscale Wind Fields - Tetsuya Fujita

37. Proposed Operation of Intrumented Aircraft for Research on Moisture Fronts and Wake Depressions - Tetsuya Fujita and Dorothy L. Bradbury

38. Statistical and Kinematical Properties of the Low-level Jet Stream - William D. Bonner

39. The Illinois Tornadoes of 17 and 22 April 1963 - Joseph L. Goldman

40. Resolution of the Nimbus High Resolution Infrared Radiometer - Tetsuya Fujita and William R. Bandeen

41. On the Determination of the Exchange Coefficients in Convective Clouds - Rodger A. Brown

* Out of Print
** To be published

(Continued on back cover)

A STUDY OF

SATELLITE-OBSERVED CLOUD PATTERNS OF TROPICAL CYCLONES

Dissertation Submitted
by

Ekundayo E. Balogun
Department of the Geophysical Sciences
The University of Chicago
for the
Degree of Doctor of Philosophy

The research presented in this paper was sponsored by the National Oceanic and Atmospheric Administration, NHRL grant E-22-24-71 G and in part by MSL grant E-198-68 G.

TABLE OF CONTENTS

A Study of

Satellite-Observed Cloud Patterns of Tropical Cyclones

Ekundayo E. Balogun

Abstract

Quantitative estimates of the cloud cover of tropical cyclones as shown in satellite photographs are made using a photometric method. These estimates are then analyzed for series of photographs depicting the life history of three tropical cyclones as the cyclones develop from tropical disturbances to severe storms.

The photometric estimates of the cloud cover are made along nine concentric circles. The observed or reported center of the cyclones is used as the common center of the concentric circles, and the principle of harmonic analysis is applied to the cloud cover estimates along the circumference of the circles. The distribution of the cloud cover estimates N (measured in tenths), and the orientation of the cloud patterns are quantitatively described by parameters V_r, r_N, α_r and also by the phase angles of the harmonic components considered. These quantities have been computed as functions of radial distances and time. The distribution and changes in these quantities are interpreted in terms of the physical processes suspected to be going on in the tropical cyclone systems.

The changes in the mean value of cloud cover estimates N along each circle are found to be small and of the order of one- to two-tenths for cyclones developing in favorable environment. Cloud patterns of cyclones developing in unfavorable environments often show changes in the cloud cover estimates of about three-tenths or more. Such cyclones do not usually develop into full grown storms.

The quantity V_r is a normalized range of cloud cover estimates at various radial distances from the center of the cyclone system. It indicates the circumferential variation of cloud cover along each circle with time. Areas near the cyclone center are usually characterized by small values of V_r, V_r. The quantity increases outward from the center of the cyclone.

The parameter r_N is defined as the radial distance r from the center of the cyclone at which a value N of the estimated cloud cover is most frequent. As several patterns in a series are considered, the quantity r_N for a particular N changes. The quantity therefore provides an objective means of studying the changes in the areal extent of the cloud cover in tropical cyclones as the cyclones develop. It is found that the parameter changes in the same manner for the different cyclones studied but no unique value of r_N can be identified with a particular stage of the cyclone. This conclusion emphasizes the difficulty of determining the intensity of the tropical cyclone from the size of the cloud cover of the cyclones.

The quantity a_r is a measure of the asymmetric distribution (non-uniform circumferential distribution) of cloud cover estimates about the center of the cyclone. It is the normalized amplitude of the first harmonic component. This quantity, plotted as a function of radial distance for each cloud pattern, shows maximum values near the center of the cyclone at early stages of the cyclone. As the cyclone matures the position of the maximum value of the parameter is located farther away from the center of the cyclone.

It is also found that the first two harmonic components account for most of the variation of the cloud cover estimates along the circles. The first harmonic component is the more prominent. The curves joining the phase position along each of the nine circles for the first two components and for each pattern are identified as 'phase curves' and are used to study the changes in the orientation of the cloud patterns. These curves are identified with cloud bands and are found to oscillate about a particular direction at the early stages of the cyclones but rotate cyclonically near the center of the cyclone (within seven degrees) as the cyclone intensifies. At the outer regions the curves rotate anticyclonically. The rate of rotation is found to be much slower than the rate of rotation of air parcels. The modes and the origin of these motions of the phase curves are still not clear. The motions, however, reflect the displacements of some fields of convergence in the cyclone system.

From the study of various cloud patterns of tropical cyclones for the major tropical cyclone forming regions during the 1968-1970 seasons, model cloud patterns illustrating the evolution of tropical cyclone cloud patterns from the I. T. C. Z. cloud band are established and the analyses of the model cloud pattern are used as guides in the interpretation of the analysis of cloud patterns in actual cyclones.

CHAPTER I

INTRODUCTION

1.1 General Introduction

Tropical cyclones are either spawned by disturbances superimposed on the Intertropical Convergence Zone (ITCZ) or by disturbances in the trade wind belts. The former disturbances are results of the intensification of some members of the numerous wave trains which move from east to west along the ITCZ. The latter disturbances, usually indicated by the so-called cloud clusters, also develop from wave activities in the trade winds. After their formation near the equator (rarely within 5° latitude of the equator), the tropical cyclones generally move westward, intensify, recurve poleward around the subtropical high pressure cells and finally enter the circulation of the westerlies where they dissipate and degenerate into extratropical depressions. During their lifetime, they exhibit different cloud patterns.

The aim of this study is to analyze quantitatively the various cloud patterns associated with the different stages of the development of the cyclone system as shown from satellite photographs with a view to investigating the changes in the cloud patterns and the nature of the cloud distribution within those patterns as the cyclone system is transformed from a weak disturbance to a severe storm. Although it is overly optimistic to expect that the different mechanisms of the development of tropical cyclones can be completely understood by simply analyzing the cloud patterns of the cyclones, yet the quantitative analyses of the cloud patterns as carried out in this study promises a better insight into the collective effects of the different processes that produce and maintain the cyclone cloud patterns without going into the details of these processes. Moreover, in the data-sparse regions of the tropics, where the initial disturbances that give rise to the tropical cyclone form, the satellite data becomes a major source of information about these disturbances. Furthermore, the approach taken in this study may provide a means of assessing quantitatively, from satellite photographs, the results of the effect of large scale seeding of tropical cyclone cloud systems.

For this study, satellite photographs of tropical cyclones for the various cyclone-forming regions of the tropics, i.e., North Atlantic Ocean, East and West Pacific Ocean, Indian Ocean, Bay of Bengal, Arabian Sea, etc., for the tropical cyclone seasons of 1968, 1969 and 1970 were inspected and studied in some detail. Documenting every type of cloud organization which the cyclones were capable of assuming tended not only to be monotonous but also to be time- and effort-consuming. However, despite the variety of individual cyclone cloud pattern, there were some general features common to all cloud patterns during particular stages of development of the cyclones. Some of these general features are used in this study to characterize the different stages of the development of the cyclones. The results from the detailed quantitative analysis of three tropical cyclones are presented in this study.

1.2 The basic problems and the specific goals of this study

The problems connected with the use of satellite photographs for the cloud study of the atmospheric disturbances fall into two major parts. The first is the photogrammetric problem which involves both optical and geometric problems. The second, and the more challenging to a meteorologist, is the problem of determining the meteorological information that can be obtained from the photographs. The first problem is not of major concern in this work. It is sufficient to mention the nature of the problem. The optical problem varies with the kind of lens used with the cameras on the satellites. Wide-angle lenses are required when a large field of view is desired. However, the use of wide-angle lenses results in severe radial distortion and aberration in the final image obtained. The use of narrow angle lenses can prevent distortions, but the area that can be surveyed by the spacecraft cameras is thereby seriously limited. Electronic distortions are also introduced into the final photographs through the imperfections of the electronic equipment that receive and retransmit to earth visible radiation reflected from the earth surface. To control these problems, a detailed record of the optical and electronic distortions associated with each camera system is kept before the cameras are carried into space so that proper allowances for the distortions can be made when the pictures from the cameras are used. The principal geometric problem is that of rectifying the photographs obtained from satellites. This means that there must be adjustment of the photographs for the varying angles from which the cameras carried by the satellites viewed the earth. If a satellite directs its camera axis straight downward for every picture, most of the variations in the viewing angles can be removed. The photographs used in this study have been rectified.

To obtain any meteorological information from satellite photographs of the clouds associated with the atmospheric disturbances, the cloud features must be recognized and identified. There are many factors which make the problem of cloud feature recognition very formidable. An important factor is the resolution of the camera system of the satellites. The resolution, that is, the amount of detail that can be seen on the photographs, depends on the number and width of the raster lines of the satellite camera system. The camera system functions very much like the ordinary television cameras. The raster line limitations of the photographs (obtained from the Environmental Survey Satellites - ESSA and the Application Technological Satellites - ATS) used in this study prevent seeing cloud features smaller than two miles for pictures obtained by use of wide angle lenses and features smaller than 0.2 miles for pictures obtained from narrow angle lenses. Since the entire cloud system associated with the tropical cyclones have dimensions greater than the dimensions defined by the raster-line limitations, there is very little or no problem in recognizing tropical cyclones on the satellite photographs. The problem here is that cloud types cannot always be identified because individual cloud cells cannot be resolved by the satellite camera system. Since the aim of this study is not to study the individual cloud types but to study the entire cloud system, the problem mentioned here does not hinder this investigation. Moreover, the cloud types in a tropical cyclone are well known but the mechanisms responsible for the formation and the distribution of these cloud types, especially at the early stages of the tropical cyclone formation, are still the subject of active research.

Another factor that makes the recognition of cloud structures and patterns difficult in a satellite picture is that the reflected solar energy from the cloud areas is not directly proportional to the spatial density of cloud elements in the field of view of the satellite camera. The reflections from a cloud area are mainly due to the nature of the underlying surface and the thickness and shape of cloud tops. There is also a tendency for the clouds to be unduly bright when viewed with the satellite looking to the sunward side of the vertical and in, or near, the vertical plane that includes the sun and the satellite. The apparent brightness of the cloud photographs from satellite therefore varies not only with the type of cloud system viewed but also with other factors such as time of day, angle of view of the cloud and photographic processing.

Because of the problems stated above, care must be taken in interpreting cloud photograph solely on the basis of brightness. On the other hand, good brightness variation in a photograph can provide a good basis for the initial recognition of features in the satellite photographs. For example, oceans appear black, land areas, especially those with vegetation, appear dark grey, thin clouds or scattered small clouds appear light grey, clouds of average thickness appear white and very thick clouds are usually white.

The cloud image as seen in satellite photographs may be the final result of a series of degradations that the original image of cloud (as would have been seen from satellite height) has suffered. Some important features of the cloud may have been lost through degradation which usually takes place during the following processes:

a. when the cloud image goes through the sensors;

b. during the data selection, processing and storage in the satellite systems;

c. during transmission to earth station. Degradation at this point is mainly due to electromagnetic noise;

d. during ground processing in which some data may be deliberately or inadvertently discarded.

In addition to the problems raised above, it is necessary to note that malfunction of the satellite either as a result of faulty engineering design or as a result of inadequate orbital characteristics, can lead to poor data from satellite. Such data must be used, if at all, with reservations.

The difficulty of identifying the correct geographical location of the cloud elements can be minimized by the proper gridding of the photographs.

In spite of the foregoing, photographs from artificial satellites still provide the best information about atmospheric disturbances in data-sparse regions of the tropics. The problem of estimating cloud cover from photographs are discussed in subsequent chapters.

The specific goals of this study can be stated as follows:

(a) To estimate quantitatively the cloud cover in the patterns of clouds of tropical cyclones as observed from satellites and to use such information to study the characteristics of the patterns at the different stages of development of tropical cyclone.

(b) To apply the principle of harmonic analysis to the analysis of the cloud cover. The harmonic analysis will be performed on the estimated cloud cover along circles of varying radius from the reported or suspected center of the cyclones. An attempt will then be made to interpret the cloud cover distribution in terms of the amplitude and phase of the harmonic components obtained from the analysis of the cloud cover. Each stage of the cyclone is then identified according to the dominant harmonic components.

(c) To interpret physically the result of the harmonic analysis of the cloud cover of the tropical cyclone. An attempt will be made to explain some known and heretofore speculated characteristics of the tropical cyclones in the light of the cloud analysis carried out in this investigation.

(d) To explore the usefulness of the methods used in this investigation as diagnostic or prognostic tools in the study of tropical cyclones.

In support of the conclusions arrived at from the cloud analysis of the cyclones, information from the analysis of relevant surface and upper air synoptic charts will be used in this report.

Such charts, however, will not be included in this study partly because of high degree of uncertainty in the contour analysis of observations obtained from conventional sources (especially for observations obtained over the ocean areas) and partly because most of the charts contain very little or no information about the flow field in which the tropical cyclone pattern is imbedded.

1.3 Review of previous studies on tropical cyclone cloud structures

The use of artificial earth satellites as platforms for meteorological observation of the tropical cyclone is very recent. It is, therefore, necessary to mention, at the outset, some of the early research efforts of the tropical cyclones based on conventional observation because the interpretation of satellite photographs of these cyclones has been strongly influenced by these efforts. In later paragraphs, some of the published research work on the tropical cyclones based on satellite photographs will be discussed.

From the time of Ferrel (1911) to the early nineteen thirties, the convective nature of tropical cyclones has been recognized and very exhaustive, but mainly descriptive treatises on the birth and death of tropical cyclones have been written. A new approach to the study of tropical cyclones was initiated as a result of the pioneering investigations of Visher (1925), Regula (1936) and Dunn (1940) into the disturbances of the tropics. These investigations led to more research into the general condition under which tropical cyclones form and move. Palmen (1948), and Riehl (1948, 1954) made fundamental contributions to the understanding of the motion fields, thermodynamic

conditions, physical structure and the general functioning of the tropical cyclone. Great improvements have been made upon the works of Riehl and Palmen due to the development of aircraft reconnaissance techniques which provided means of obtaining meteorlogical data from all sectors and at various levels of the tropical cyclone. Data obtained from airborne observation platforms enable researchers to modify or extend their conclusions about the mechanism of tropical cyclones made only from the analysis of ground-based observation procedures. Information from such reconnaissance flights have resulted in research papers such as those of Riehl and Malkus (1961), Malius, et al. (1961) in which the role of the cloud systems, especially towering cumulonimbus clouds, in the functioning of the tropical storm was clearly described. Since then, other scientific papers combining ground based observations with airborne observations of tropical cyclones have been published. These papers discussed factors favoring or suppressing hurricanes and influencing their tracks. They have also provided observational bases for the development of theoretical investigations and theoretical models of the cyclone. The process of formation of tropical cyclones, however, has not been treated satisfactorily, either through analysis of observation data (Yanai, 1968, made a very commendable attempt) or from theoretical reasoning.

Very few of these papers have been devoted exclusively to the study of cloud structures of the tropical cyclone. Since clouds are the results of integrated motions in the atmosphere, it may be possible to explore the dynamical implications of the cloud patterns by studying the variations in the cloud distributions relative to the center of the tropical cyclones. One attempt at mapping the clouds in a tropical cyclone system was carried out by Malkus et al. in 1961. The cloud structure of Hurricane Daisy of 1958 was investigated by them. The salient points of the investigation were: First, the pattern of clouds associated with the hurricane was remarkably persistent over the duration of the study. The major cumulonimbus rows and cirrus shield were formed in nearly the same coordinates relative to the storm center. Secondly, the cloud patterns exhibited a slow and gradual evolution toward a symmetrical distribution about the center; an evidence of the maturing of the storm. The symmetrization was achieved by gradual extension of cumuli rows and cirrus shield into the forward quadrants with small changes elsewhere. Thirdly, penetrative convection was extremely restrictive in area and occurred only in the major lines of cumulonimbi. Fourthly, over the duration of the investigation of the storm, the S. E. quadrant of the storm contained twice as many cumulonimbi as did the remaining quadrants. The concentration of cumulonimbi was found to be reflected in the temperature field. Such asymmetry in convective activity may be of importance in hurricane dynamics. Fifthly, the study raised the possibility of 'finger printing' the tropical cyclones by cloud patterns.

Before artificial earth satellites became a reality, Wexler (1954) had speculated on what to expect from a photograph of the earth taken from a distance of 4,000 miles out of space. Even though he underestimated the scales of the cloud patterns of some atmospheric disturbances, most of his speculations have been vindicated by subsequent research with actual satellite photographs of these disturbances from outer space.

The earlier studies of tropical cyclones using satellite photographs as a basic research tool dealt essentially with qualitative pattern recognition of the different stages of tropical cyclones. From these studies, however, some useful knowledge about the

cyclone development and growth were obtained. For example, Fritz (1962) described the cloud features associated with the early development stage of tropical cyclone and suggested that it developed from an easterly wave which travelled from the coast of West Africa into the West Atlantic. Similar studies were carried out by Frank (1963) and Erickson (1963, 1967). Sadler (1964) studied the tropical cyclones of the eastern north Pacific Ocean utilizing TIROS satellite observations. His conclusion was that hurricanes of the Eastern Pacific form from pre-existing weak vortices in the zone between the N. E. trades and the westerly branch of the turned S. E. trades north of the equator. By studying satellite photographs, Fett (1964) arrived at a model of tropical cyclone development deduced from associated cloud patterns. He found that the development of cloud pattern associated with the developing cyclone system could be subdivided into four stages ranging from elongated cloud mass along the wave axis to that of a well developed cirrus shield over the mature hurricane. Other models showing the sequence of development of the tropical cyclone have been presented by Merrit (1964), Fritz et al. (1966) and Oliver (1968). In all the literature cited above, cyclones were characterized mainly in terms of the areal coverage, the position of the major cloud over cast in relation to the entire tropical cyclone, the degree of circularity of the spiral bands and whether the center of the spiral band structure was located inside the major cloud mass of the cyclone.

Other use of cloud photographs in the study of cyclones includes the estimation of the motion field in the tropical cyclone and its environment by computing the motion of small cloud elements. The motion field obtained is then used for kinematic analysis of the storm. Although much useful information about tropical cyclones and tropical disturbances has been obtained by that method (Fujita 1968), the procedure is still at an experimental stage.

The present investigation attempts to quantify the information obtained from satellite photographs of tropical cyclones by describing the behavior of the cloud patterns of these cyclones by the numerical parameters obtained from the analysis of the satellite observed cloud cover of the cyclones.

CHAPTER II

QUANTITATIVE ESTIMATION OF CLOUD COVER FROM SATELLITE PHOTOGRAPHS

2.1 The problem of quantitative estimation of cloud cover from satellite photographs

Although the recognition of cloud features from satellite photographs and the gridding of the photographs can prevent enormous problems, the problem of quantitatively determining the cloud cover from the photographs is of a high order of magnitude. Two major problems arise when visual estimation of clouds is made in a designated area (for example 1° x 1° latitude-longitude area) on a satellite photograph. First, it is not always possible to distinguish between a high cloud and a low cloud within the area. Secondly, it is usually difficult to assign a single cloud estimate to a designated area if the area is covered by clouds of varying degree of brightness. One must distinguish the case in which the area is totally covered by a thick convective cloud from that in which the area is totally covered by a thin cirrus cloud. The situation is further complicated if the area is partly covered by one type of cloud and partly covered by another type. As noted earlier, the variations in the reflection of solar energy from any cloud area are due to many causes and very bright areas may not necessarily indicate an area of thick and well developed clouds.

In this investigation, the first problem was solved by avoiding it. There was no distinction made between high clouds and low clouds. It was assumed that all the cloud elements that made up the tropical cyclone cloud pattern result from integrated motions in the system. The study of the entire pattern, without making any distinction between high and low clouds was, therefore, still capable of revealing some characteristics of the tropical cyclone system. Errors in the determination of the cloud cover due to the second problem was reduced by careful treatment of the photographic data, and by using an objective method which takes into account the spatial variation and the intensity of brightness of an area in the estimation of the cloud cover over the area. Because of the investigator's familiarity with the cloud structures of tropical cyclones, any unusual features in the photographic products used were easily recognized and corrections were made for them. Where corrections of deficiencies could not be carried out, the photographs were not used.

The problem of estimating the total cloud cover over an area had been discussed by a few researchers. Young (1967) reported an experiment in which ten qualified weather observers, experienced but uninitiated in the use of satellite photographs were asked to estimate visually the amount of cloud cover in designated areas of some satellite photographs. The result of the study could be summarized as follows: First, the study showed that there was human variability and errors in making visual estimates of the amount of cloud from satellite photographs. Secondly, it showed that the subjective methods of cloud cover estimation led to greater errors when the total cloud cover in an area ranged between 40% and 60%. The study further indicated that human estimation errors could influence the results of meteorological analysis when subjectively determined cloud cover was used in such an analysis.

Earlier in this study, a test analysis was made of tropical cyclone cloud patterns from cloud amounts determined visually from satellite photographs. Although repeated tests showed that the results of the analysis were fairly consistent, it was concluded that appreciable subjectivity was still involved in the method of visual estimation of cloud amount. The method was abandoned in favor of a more objective one. The objective method is described in the next section.

2.2. Quantitative estimation of satellite observed cloud cover by photometric method

The measuring device used to estimate the cloud cover of tropical cyclones from satellite photographs consisted essentially of a light meter, a 45° prism, a 100-watt light bulb and a variable auto-transformer. These components were assembled as shown schematically in Figure 1.

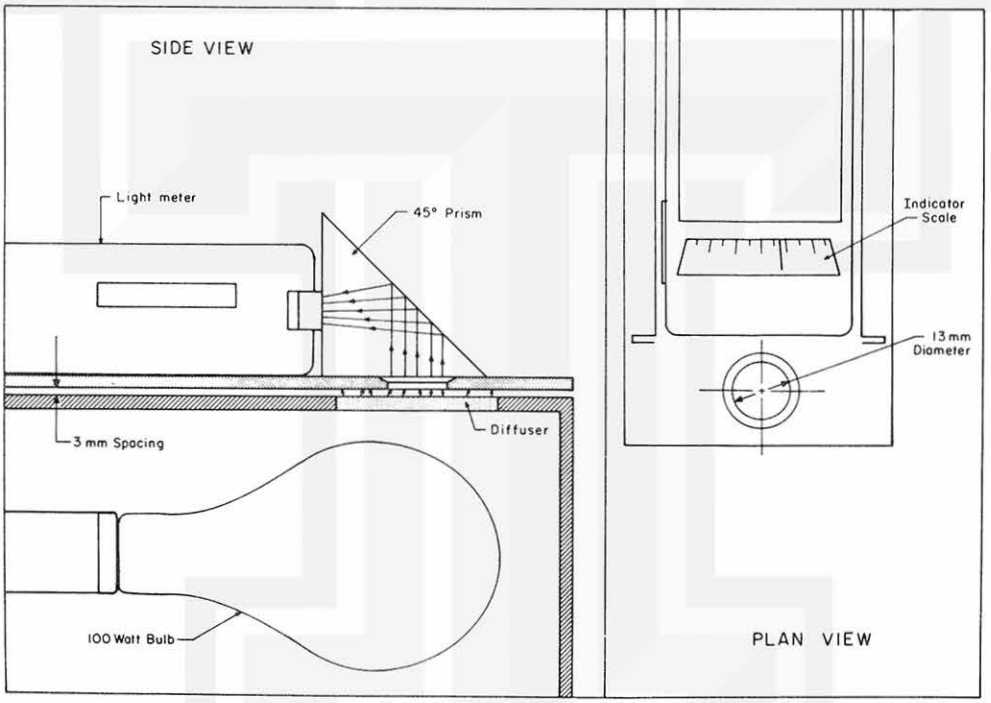

Fig. 1. Photometer arrangement.

The 100-watt bulb was enclosed in a wooden box which has a hole, covered by ground glass to act as a diffuser, at its upper part to allow a beam of light to pass through to the outside. A sheet of plexiglass was placed on the top of the box in such a way as to allow a satellite photograph to slide freely between the top of the box and the glass sheet. The light meter and the 45° prism were arranged on the glass sheet so that diffused light from the hole could be totally internally reflected and be recorded by the light meter. The light meter was secured on its sides, except on the side that contained its window, to prevent its movement during cloud cover estimation. The

45° prism was held down by black adhesive tape so that each of its perpendicular sides face very closely the window of the light meter and the hole on top of the box. The black adhesive tape also served the purpose of preventing light rays from the surrounding area from influencing the reading of the light meter. The 100-watt bulb was connected to an auto-transformer so that the intensity of light from the bulb could be varied as desired.

To make cloud cover estimates over a desired area of a satellite photograph, the photograph was moved in the space between the top of the box and the plexiglass so that the area was brought over the hole on the top of the box. The area was then illuminated by diffused light from the ground glass. The light transmitted by the area of the photograph underwent a total internal reflection in the prism and was recorded by the light meter. The light meter recorded the resultant of the transmitted light from the different parts of the illuminated area of the photograph. The recorded light depended not only on the degree of the whitness of the area but also on the percentage of the area covered with clouds. This was an advantage over the visually determined cloud cover. The reading on the light meter was converted into percentage cloud cover by a procedure to be explained later in this section. The cloud cover estimates over the area by the present procedure therefore reflected both the intensity and the spatial distribution of the cloud over the area.

The light meter used had a photoconductive cell which changed its conductivity in the presence of light. The indicator needle which showed those changes was deflected by a system of small mechanical levers and gears powered by tiny mercury batteries. The data provided by the manufacturers of the light meter indicated that the amount of light recorded in foot lamberts by the light meter was related to the indicator scale by the exponential relation $L = k\,2^{s}$ where

L = the amount of light recorded by the light meter in foot lambert;

s = indicator scale reading; and

k = constant with value 0.00105 .

The curve $L = k2^{s}$ was plotted on a linear scale and used as the calibration curve for the determination of cloud cover. See Figure 2.

The following steps were followed in the estimation and the analysis of the cloud cover for each tropical cyclone.

Step one. A set of (at least) five photographs showing the cloud patterns of a tropical cyclone at various stages of development was made on special non-stretching photographic paper. Care was taken to ensure that all the photographs in the set were of the same exposure.

Step two. One degree by one degree grids (made up of longitude and latitude lines) were imposed on the photographs to be analyzed. The grids were slightly adjusted so that the observed or estimated center of the cyclone was at a grid point. Each photograph in the set was inspected for the darkest areas -- usually cloudless

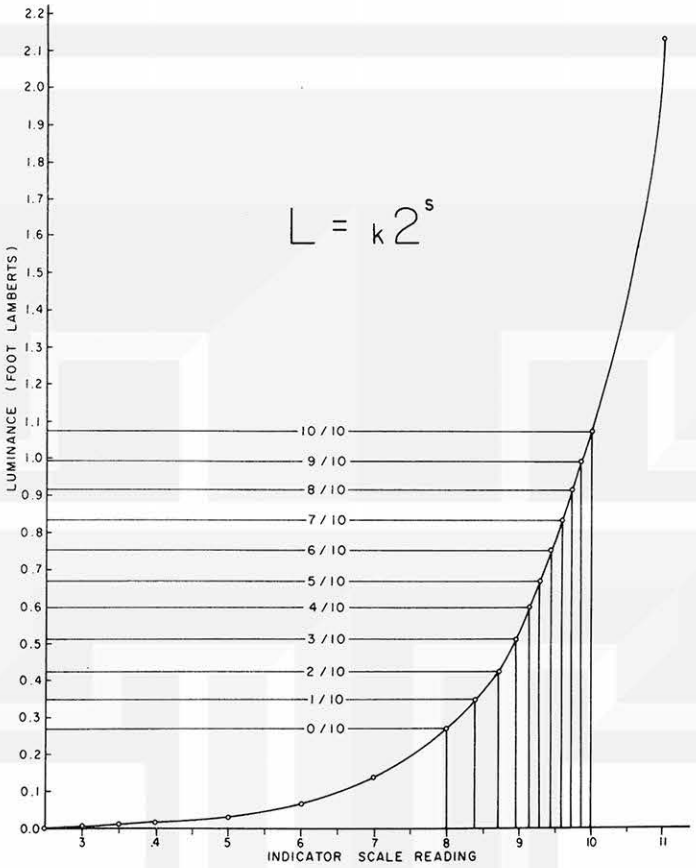

Fig. 2. Calibration curve for the determination of satellite observed cloud cover.

ocean areas — and for the brightest areas — areas with well developed cumulonimbus clouds with glaciated tops. Each photograph was illuminated in the device described earlier. For each photograph an indicator reading s_1 for the darkest area and s_2 for the brightest area were recorded. For properly processed set of photographs of a tropical cyclone, the variations in the s_2 readings and the variations in the s_1 readings did not exceed one-tenth. It was possible then to use a single calibration curve for that set of photographs. The light from the 100-watt bulb was kept constant during the two readings. The transmitted light by the photograph in each case is related to the corresponding amount of light L_1 and L_2 given in foot lamberts by the expressions:

$$L_1 = k 2^{s_1}$$

$$L_2 = k 2^{s_2}$$

The difference in transmitted light from these two areas is therefore

$$L_1 - L_2 = k(2^{S_1} - 2^{S_2})$$

Any dark area with a reading corresponding to L_1 was assigned zero-tenths cloud cover and any bright area with reading L_2 was assigned ten-tenths cloud cover.

Caution was taken in assigning values to the areas where light meter reading fell between the two extremes. The following points were put into consideration when values were being assigned to such areas. First, the density of the photographic paper prints, that is, the amount of chemicals deposited by the exposure of the paper, varied from one area of the paper to the other. The relationship between the density of the paper and the relative brightness of areas on the paper often follows the general pattern of the curve shown in Figure 3. From the graph it is observed that initially the density

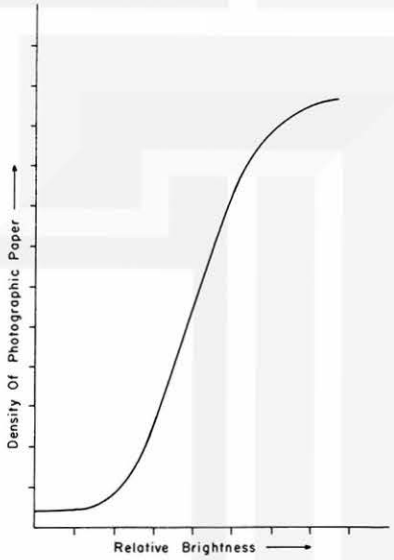

3. Curve illustrating the relationship between relative brightness and density of photographic paper.

does not increase directly as very dark areas become progressively brighter. Then the density increases directly as the areas of the photograph become brighter and continues to be so until a saturation point is reached. At that point, the density no longer increases as areas on the photograph become excessively bright. A linear relationship therefore exists between the density and the brightness on the straight line portion of the graph. It is assumed that most of the measurements made lie on the straight line portion of the curve. The assumption is made in the light of the fact that in the photographs used in this investigation, the extreme cases of zero-tenths cloud cover and ten-tenths cloud cover are much fewer than the cases in which the amount of cloud cover recorded lie between the extreme values. The second point to be emphasized is that a controllable source of light was used to illuminate the photographs. It was possible to adjust the source of light until a steady reading was obtained for the

dark areas After proper adjustment, the amount of light recorded on the light meter increased almost directly as the cloud amount increased. The third point was that the assumption of a linear relationship between the density of the paper and the brightness of the cloud features facilitated the estimation of the cloud cover.

To determine the amount of satellite observed cloud cover in areas where the amount of light transmitted by the photograph fell between L_1 and L_2 the following procedure was followed:

a. The quantity $L_2 - L_1$ in foot-lamberts was divided into ten parts of identical fraction illumination, that is $\frac{L_2 - L_1}{10} = \Delta L$. In a specific case s_1, the indicator scale reading and the corresponding measurement of light transmitted, L_1 were found to be 8.0 and 0.2688 foot-lamberts, respectively. For the same case, s_2 and L_2 were found to be 10.0 and 1.0748 foot lamberts, respectively. ΔL was calculated to be 0.0806 foot-lamberts. The cloud cover for any area on the photograph was then determined by measuring the light transmitted by the area and then converting the reading on the indicator scale to the appropriate cloud cover by using the calibration curve $L = k 2^s$. For example, the light transmitted by an area in a picture gave an indicator reading of 9.2. The amount of light transmitted was estimated to be .5912. Since the light transmitted was $L_1 + L \Delta L$ foot-lamberts, the cloud cover was estimated as four-tenths. A similar procedure was employed in estimating the cloud cover on all the photographs used in this investigation.

b. With the observed or estimated center of the storm as center, concentric circles of radii 1°, 2°, ... 9° latitude were drawn on the photograph for which cloud cover has been determined. From the same center, radial lines were drawn at an azimuthal interval of 10° so that the radial lines intersect each circle at 36 equally spaced points. See Figure 4. All azimuthal distances were measured from the north.

c. A weighted estimate of the satellite-observed cloud cover (to eliminate errors that may arise in using point values and to smooth the data) was then determined at each of the thirty-six points along each circle by the following procedure. Each of the thirty-six points was made the center of a square with length of each side equal to six grid lengths. The cloud cover at the point in question was then determined by considering the contribution to the cloud cover of points within the square. The contribution from each grid point was weighted by a factor $e^{-\sigma y_i}$ where y_i, the distance of a grid point from the point where the cloud cover estimate was being determined, was less than or equal to two grid lengths, and σ was a factor determined by assuming that $e^{-\sigma y_i}$ had a value 0.1 at $y = 2°$. From that assumption, the value of σ was found to be 1.15. The specification of a six grid length square was for computational convenience.

The cloud cover estimate N at each of the thirty-six points on each of the circles was then computed from the expression:

$$N = \frac{\Sigma N_i e^{-\sigma y_i}}{\Sigma e^{-\sigma y_i}}$$

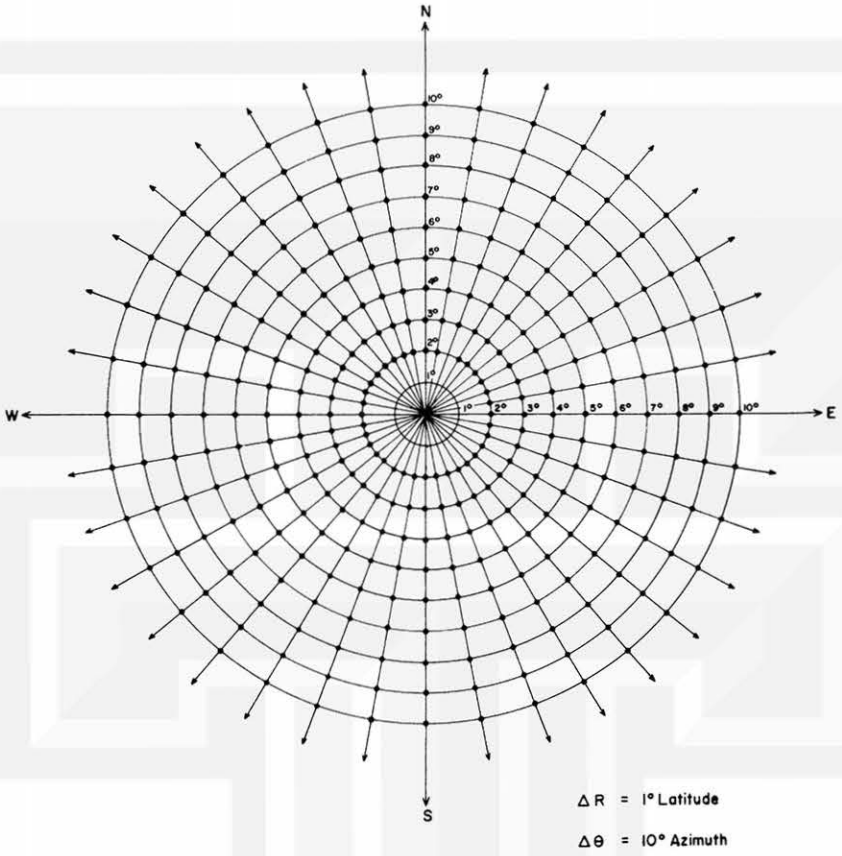

Fig. 4. Polar grid for the determination of satellite-observed cloud cover.

where Ni was the satellite-observed cloud cover estimate at distance yi within the square box. The cloud cover was thus determined for all the thirty-six points on each circle. The computation involved in this procedure was enormous, but it was accomplished by use of IBM 360 computer system at the University of Chicago Computation Center. The choice of 0.1 for $e^{-\sigma y_i}$ at $y_i = 2$ grid lengths was based on the assumption that a grid point value at that distance from the center of the square should not contribute more than one-tenth of its value to the cloud cover value at the center of the square. N is henceforth referred to as satellite-observed cloud cover or simply, cloud cover.

Figures 5 and 6 show the results of the estimates from one satellite photograph.

The definition of satellite observed cloud cover as given in the last paragraph necessitates the discussion of some methods employed in the estimation of cloud cover from satellite photographs vis-a-vis the estimation of cloud cover by a ground based observer. To an observer on the ground, the cloud cover is simply the proportion

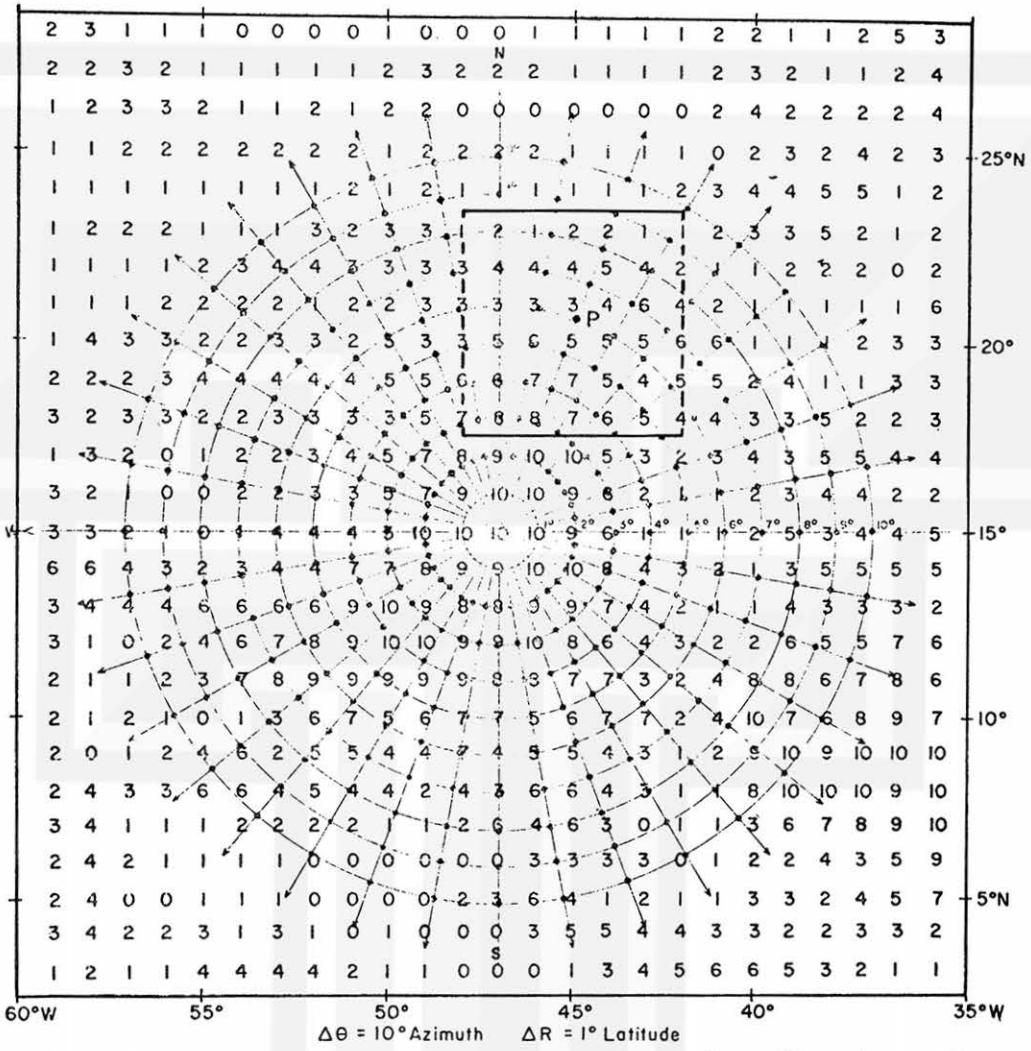

Fig. 5. An example of photometric computation of satellite-observed cloud cover. Hurricane Debbie, August 16, 1969 (1232Z).

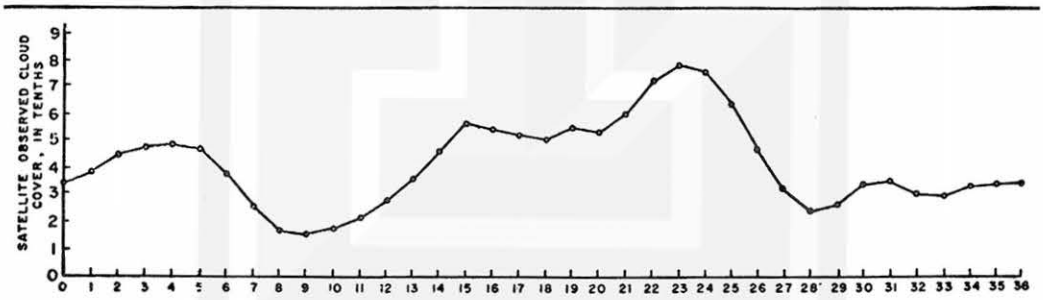

Fig. 6. Weighted cloud cover estimated at thirty-six data points along the circle R = 6° latitude in Fig. 5.

of the sky covered by clouds as seen from his location. This proportion is usually expressed either in eighths or in tenths. The observed sky in this case is limited by the horizon. The meteorological satellite on the other hand gives information which includes detailed cloud patterns associated with many different types of weather conditions and systems over a much wider area. The dimensions of the area covered simultaneously vary from a few thousand kilometers to an entire hemisphere. The use of satellite photographs in the study of cloud patterns therefore demands the establishment of a new system of defining the amount of clouds over an area of the earth surface as seen from satellites. There is at present no standard way of doing this. Average cloud amount in terms of the fraction of the sky covered with clouds has been obtained by some researchers from nephanalysis derived from cloud pictures. This procedure requires manual (or visual) interpretation of satellite cloud pictures to produce a nephanalysis and then interpreting the nephanalysis to estimate cloud amount over the area of interest. This procedure is very subjective. In spite of its deficiencies, Clapp (1964, 1968) has made estimates of Northern Hemisphere cloud cover from nephanalysis from TIROS (Television and Infra-Red Observation Satellites) photographs for selected seasons. Sadler (1968) has used variations of satellite derived total cloud amount in specified latitude-longitude squares as indicators of processes in the large scale general circulation over ocean areas. The nephanalysis procedure of estimating cloud amount from satellite photographs has some merits when cloud estimates thus obtained are used for climatological purposes as in the above cited literature but the procedure is not adequate for the present research.

Rather than estimating satellite cloud cover in terms of the proportion of a specified area covered by clouds, some researchers have averaged and composited digital representation of brightness of clouds (reflected visible radiation from cloud tops) obtained from satellites for specified areas for long periods of time to delineate consistently cloudy parts of the area from consistently cloud free parts of such areas. In this regard, Kornfield (1967), Booth and Taylor (1969), Hubert (1969) and others have made contributions. Hubert et al. 1969 have used these data to delineate the seasonal mean locations of the intertropical convergence zone. This procedure has yielded useful results in determining cloud and no-cloud areas for climatological purposes. It is not, however, adequate for the present research.

It is clear from the above discussion that there are several methods by which the cloud cover shown in satellite photographs can be estimated and that each method depends on the kind of information desired from the satellite photographs. In this study a photometric method has been used to estimate the cloud cover over tropical cyclones as shown in the photographs. The values obtained were further subjected to a weighting process before they were finally used in computation. The weighted values have been called satellite-observed cloud cover and denoted by N for the purpose of this investigation. No relationship has been established between N and the cloud cover as observed from the ground. The quantity N is simply a quantitative estimate of the cloud cover of tropical cyclone system as shown in satellite photograph.

The merit of the photometric method of estimating cloud cover is that it is objective. The quantity N is assumed to be capable of showing the variation in the cloud cover of tropical cyclones as shown in satellite photographs as the cyclones develop.

CHAPTER III

COMPUTATIONS INVOLVED IN THE HARMONIC ANALYSIS OF ESTIMATED CLOUD COVER

The principle of harmonic analysis has been applied in various ways to the study of many geophysical problems. Some of the previous applications of harmonic analysis similar to the way the concept is applied in this study are those reported by Barret (1961) and Piexoto, et al. (1964). Barret applied the principle to the study of some characteristics of the zonal components of the wind circulation around the globe. Piexoto, et al. studied the global distribution of the topography of the earth surface using the harmonic analysis as the tool of analysis. The present study is an attempt to apply the same principle to the study of cloud patterns in a tropical cyclone system.

3.1 Mathematical expressions for the harmonic analysis of estimated cloud cover

Any function estimated at equal intervals around each circle on the analyzed photographs involves a total change of azimuth angle of 360. The physical interpretation of such a function can be studied by the representation of the function as a fourier series.

In general, if a function $f(t)$ of a variable is periodic with the period T ie $f(t+T) = f(t)$ and exists in a region $-x \leq t \leq x$ and also satisfies the following two conditions, viz:

(a) In any period, $f(t)$ has only a finite number of jump discontinuities within the region.

(b) In any period, $f(t)$ has only a finite number of maxima and minima, then the function may be represented by the infinite fourier series,

$$f_{n(t)} = \overline{f_{n(t)}} + \sum_{n=1}^{\infty} \left(An \sin \frac{2\pi nt}{T} + Bn \cos \frac{2\pi nt}{T} \right) \qquad 3.1\,(i)$$

where the coefficients An , Bn are defined respectively as

$$An = \frac{2}{X} \int_0^X f(t) \sin \frac{2\pi nt}{T}\, dt \qquad 3.1\,(ii)$$

$$Bn = \frac{2}{X} \int_0^X f(t) \cos \frac{2\pi nt}{T}\, dt \qquad 3.1\,(iii)$$

$$f(t) = \frac{1}{2X} \int_0^{2X} ft\, dt \qquad 3.1\,(iv)$$

and $$T = 2X \qquad 3.1\,(v)$$

$f_{n(t)}$ is called the n^{th} fourier component of the function $f(t)$.

In this study, estimate of cloud amount at thirty-six equally spaced points along a circle is approximated by a function $N(\theta t)$. It is assumed that $N(\theta t)$ is a

well-behaved function (satisfies the above conditions) of the azimuthal distances and can be represented in terms of azimuthal mean plus a fourier series of sinusoidal components:

$$N(\theta_t) = \overline{N(\theta_t)} + \sum_{n=1}^{\infty} A_n \sin K_n \theta_t + B_n \cos K_n \theta_t \qquad 3.1\ (vi)$$

where $N(\theta_t)$ = function expressing distribution of estimated cloud cover along a circle.

$K_n = \frac{2\pi n}{l}$ is the azimuthal wave number.

l = the distance around a circle.

n = is the number indicating the number of 'waves' around a circle. It identifies the harmonic of $N(\theta_t)$.

θ_t = azimuthal distance from the north.

The coefficients A_n and B_n are calculated by multiplying both sides of 3.1 (vs) by $\frac{\sin 2\pi m\theta_t}{l_t}$ and integrating along a circle. From orthogonality relationships,

$$\int_0^{l_t} \sin\frac{2\pi n\theta_t}{l_t} \quad \sin\frac{2\pi m\theta_t}{l_t} = \begin{cases} 0 & n \neq m \\ l_t/2 & n = m \end{cases} \qquad 3.1\ (vii)$$

we obtain, using summation notation since discrete values are considered,

$$A = \frac{2}{l} \sum_{n=1}^{\frac{l_t}{2}-1} N(\theta_t) \sin\left(\frac{360}{l} n\theta_t\right) \qquad 3.1\ (viii)$$

and

$$B = \frac{2}{l} \sum_{n=1}^{\frac{l_t}{2}-1} N(\theta_t) \cos\left(\frac{360}{l} n\theta_t\right) \qquad 3.1\ (ix)$$

The expression in 3.1 (vi) can be rewritten in the form,

$$N(\theta_t) = \overline{N(\theta_t)} + \sum_{n=}^{\infty} H \cos\frac{360}{l_t} n(\theta_t - \epsilon_n) \qquad 3.1\ (x)$$

where $H_n = (A_n^2 + B_n^2)^{1/2}$ and represents the amplitude of the harmonic component.

l_t = 36 and represents the number of data points along the circle.

t = identifies points on the circles.

ϵ_n = phase of the harmonic component given by

$$\epsilon_n = \frac{l_t}{360} \text{ arc } \tan \frac{A_n}{B_n}$$

The first harmonic has a period l_t equal to 36, the number of data points along a circle. The second harmonic has a period l_t equal to 18 and the n^{th} harmonic correspondingly as a period of $\frac{360}{n}$. The mean and the eighteen possible harmonics in this analysis should describe the cloud cover estimates along a given circle completely. It is, however, not necessary to compute all the eighteen harmonics. The variation of cloud cover along each circle can be described adequately by the first few harmonics. In this investigation, therefore, computations are made for the first four harmonics. The number of harmonics computed is thought to be within the limits of usefulness of the concept of harmonic analysis for this purpose. If many harmonics are required to account for the cloud cover variation, then it will be concluded that the cloud cover function is not sinusoidal. The harmonic analysis can still provide a mathematical representation of the function, nonetheless. For clarity the subscripts for $N(\theta_t)$ and $\overline{N(\theta_t)}$ are dropped in the subsequent discussions.

3.2 Cloud cover parameters obtained from harmonic analysis

The mean of the cloud cover along a circle, $\overline{N}$, the amplitude H_n , and the phase angle ϵ_n corresponding to the harmonic component n were the basic parameters used in the description of the cloud patterns.

For each photograph showing a cloud pattern of a tropical cyclone under study, these parameters, or other parameters derived from them, were computed as a function of the radial distance from the center of the cyclone. Similar graphs were prepared for a set of photographs showing the cloud pattern at different stages of development of the tropical cyclone.

(a) The mean of the cloud cover estimates

The mean of the satellite observed cloud cover estimates is the zeroth harmonic. The changes in the graphs of $\overline{N}$ from one picture to another were indicative of the redistribution, development and dissipation of clouds as the cloud patterns changed from one stage of development to another.

(b) The amplitude (H_n) of the cloud cover estimates

In the harmonic analysis, the amplitudes (or half ranges) show the maximum excursion of cloud cover values from the mean value. The significance of the amplitudes of a particular harmonic component is usually dependent on the magnitude of the mean value. To eliminate the influence of the mean cloud cover from the amplitudes, the amplitudes are expressed as percentages of the appropriate mean cloud cover. For example, for a circle with radius (r) where the mean cloud is $\overline{N}$,

the quantity $\hat{H}_n$ is computed, and $\hat{H}_n = \frac{H_n}{N} \times 100$ is identified as relative amplitude of the component along circle r .

Where there is a non-zero cloud cover N, at only one of the thirty-six data points along the circle, the mean cloud cover along the circle is defined as usual as $\frac{N}{36}$. In that case, the amplitude value for all components will be $\frac{2N}{36}$, and $\hat{H}_n$ will be 200%. The situation mentioned here arises where there are highly localized cloud concentrations at certain radial distances from the center of the cyclone. Along any circle where there is uniform, almost uniform cloud cover, or complete absence of cloud cover, the amplitudes are expected to be zero or very small.

In the discussion of harmonic analysis of certain oscillations it is customary to regard the square of the amplitude H_n as a measure of power or energy associated with the oscillations. This is true in the harmonic analysis of mechanical or electrical oscillations. In the present application of the harmonic analysis principle such an interpretation of H_n^2 cannot be made. However, the computation of H_n^2 is still of value in this study as will be shown in the following paragraphs.

One of the objectives in this study is to be able to characterize each cloud pattern by a particular harmonic component. It was necessary therefore to identify the predominating harmonic components with which the analyzed cloud pattern can be characterized. The fraction of the total variance of the cloud cover along each circle (with radius r) accounted for by a single harmonic component (n) is given by the quantity $H_n^2/2$. In the case of the last harmonic which is not computed here the quantity was H_n^2 . The total variance of the cloud cover along a circle is given by S^2 where ,

$$S^2 = \frac{(N - \bar{N})^2}{t_t} \qquad 3.1\,(xi)$$

The quantity $1/2\,\frac{H_n^2}{S^2} \times 100$, here represented by η_r , is then the percentage of the total variance of the cloud cover along the circle r accounted for by the harmonic component n . For each cloud pattern, η_r is computed as a function of the radial distance and the wave numbers.

For a particular circle of radius r , $\hat{\eta}_r$, represents a cumulative value of η for each of the four harmonic components considered, so that for the circle r ,

$$\hat{\eta}_r = \sum_{n=1}^{4} \eta_r \qquad 3.1\,(xii)$$

(c) The relative standard deviation ($\hat{S}$)

This parameter is computed by expressing the square root of the variance S^2 as a percentage of the mean. That is

$$\hat{S} = \frac{S}{N} \times 100. \qquad 3.1\,(xiii)$$

(d) The phase angle ϵ .

For each circle, the phase angle ϵ_n indicates the azimuth distance from the North where the first maximum of N corresponding to the component n is

located. Additional maxima are located at $(+\frac{2\pi\alpha}{n})$ for each integral value of α up to n-1. For each cloud pattern studied, a polar diagram showing the pattern of the distribution of phase angles, is drawn for at least the first and second harmonic components.

The quantity ϵ_n is usually determined from the expression

$$\epsilon_n = \frac{L_t}{360_n} \text{ arc tan } \frac{A_n}{B_n} \qquad 3.1\,(\text{xiv})$$

ϵ_n is capable of having two values by the equation 3.1 (xiv), the correct value of ϵ_n is determined by the condition that

$$\epsilon_n = \frac{L_t}{360_n} \text{ arc sin } \frac{A_n}{B_n} \qquad 3.1\,(\text{xv})$$

Other parameters derived in the course of this study to clarify the results are discussed in subsequent chapters.

CHAPTER IV

HARMONIC ANALYSIS OF MODEL CLOUD PATTERNS OF TROPICAL CYCLONES

4.1 Sequence of model cloud patterns in the evolution of tropical cyclones

From the general appearance of the tropical cyclone in satellite photographs for the various cyclone forming regions during 1968-1970 season, schematic representations of clouds during the stages of development of the cyclones were established. To have a feel for the nature of results to be expected from the harmonic analysis of the cloud pattern in actual cyclones, the principle of harmonic analysis was first applied to the model patterns. Figure 7a represents the earliest indication of the formation of a tropical cyclone on the Intertropical Convergence Zone (I. T. C. Z.). This stage is identified as Stage One.

In reality, the I. T. C. Z. marks the boundary between the N. E. trades and the low level cross equatorial flow. It is a narrow band about 2° -3° latitude wide extending east and west and comprising lines of active meso-scale cumulus convection. The I. T. C. Z. is usually most prominently defined, and persistent in the ocean areas. It is most sharply defined in the North Atlantic, Eastern and Central North Pacific between

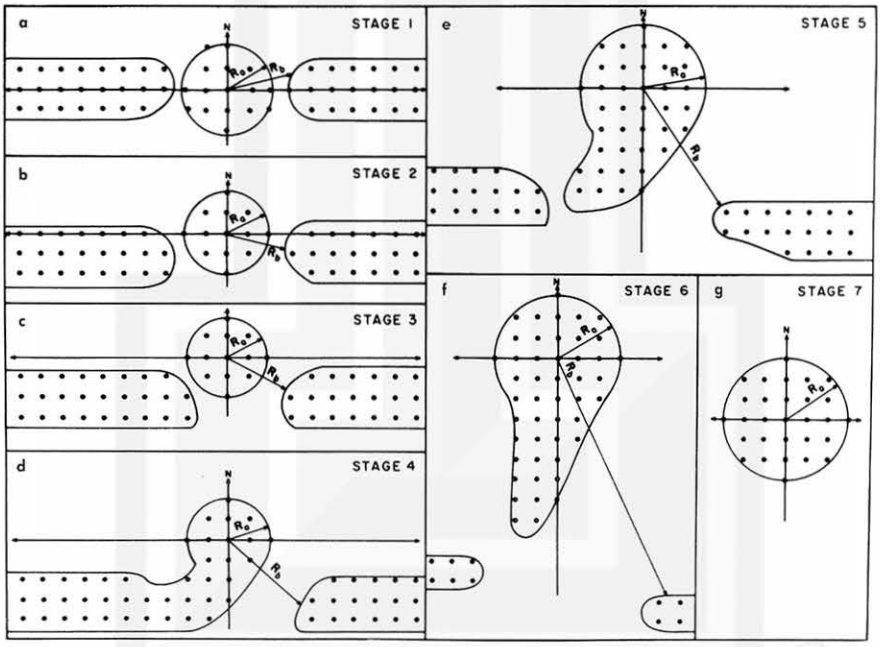

Fig. 7. Sequence of model cloud patterns in the evolution of tropical cyclones.

Lat. 5°N and 10°N and sometimes noticeable between Lat. 5°S and 10°S in the Eastern Pacific Oceans. In other ocean areas and over the land masses (except over West Africa), the I. T. C. Z. is not well defined. The intensity of convection along the I. T. C. Z. undergoes both daily, seasonal and other aperiodic variations. It also undergoes various distortions due to the passage of wave disturbances. Sometimes, the I. T. C. Z. exhibits a double cloud band structure in the East Central Pacific with the Equator lying in the cloud-free areas in between the cloud bands. Increased convective activity along the I. T. C. Z. often manifests itself in the form of an amorphous cloud mass composed mainly of cumuliform clouds. Such activity may indicate the presence of the developing tropical cyclone within the I. T. C. Z. cloudiness.

The subsequent stages in the evolution of the tropical cyclone were represented in Figures 7b and 7c. The figures illustrated the gradual northward protrusion from the I. T. C. Z. of the clouds associated with the disturbances. At such stages, the reflection of the disturbances in the surface isobars are usually not very noticeable. But they are very evident in the mid-tropospheric wind field, especially at the 700 mb level. The tropical cyclones at these stages are called tropical disturbances. Figure 7D was a model of the tropical cyclone in the tropical depression stage. It was identified as stage four in this study. At that stage, closed isobars may or may not be evident on surface maps. In the schematic representation, as in actual case, the cloud patterns assume a N-SSW orientation with the SSW portion still attached to one arm of the I. T. C. Z. Figure 7e illustrated the Tropical Storm stage. At this stage, closed isobars are usually observed on surface maps with the cyclone developing winds up to 45 knots. Noticeable at this stage, as indicated in the model pattern and in many cyclones, is the development of a trailing convective cloudiness. This characteristic of the developing tropical cyclone was also observed by Fett (1964). Figure 7f represents the Hurricane stage At that stage, the tropical cyclone has developed winds up to at least 65 knots. The trailing convective cloudiness has become pronounced and in actual cyclone situations, characterized by cirrus outflow. This stage illustrates the characteristic comma shape generally associated with the northward moving tropical cyclone system. The trailing convective system and the cirrus streamers from it generally appear directed toward the equator.

Model cloud patterns have not been made for cyclones originating from wave disturbances within the trade wind circulation, because the cloud sequence in such cyclones is very similar to that explained above, especially after the initial stage of development. Tropical cyclones forming within the trade wind circulation often first appear as the so-called 'cloud clusters'. A cloud cluster appears in satellite photographs as almost circular solid white mass about 3°-6° degrees in diameter. The appearance of the clusters is due to the large cirrus canopies typically associated with them. A harmonic analysis of a cluster should show that the mean cloud cover describes the pattern adequately especially within 2°-3° degrees from the geometric center of the cluster. A cloud cluster that may eventually develop into a tropical cyclone generally becomes elongated in the North-South direction with a circulation center developing to its west. This stage is therefore similar to stage four of the sequence described earlier except that there is no I. T. C. Z. cloudiness in its vicinity. Further development from that stage on follows the same patterns as suggested earlier.

In all the stages illustrated in the model, areas are either assigned ten-tenths cloud cover, or no cloud cover at all. A square grid with grid-lengths of one unit is imposed on the cloud pattern so that the geometric center of the schematic cloud pattern coincided with a grid point. One unit length represents one degree. With the assumed center of the pattern as a center, twelve concentric circles, instead of nine for better coverage of the schematic patterns, are drawn on the patterns. The estimation of cloud cover (in this case, cloud cover of model patterns) at the thirty-six points on each circle is accomplished by the procedure explained earlier. Along the circles close to the center, the quantity, $R\Delta\theta_t$, the distance between the data points is small and most of the thirty-six data points lie in cloud areas. Along the outer circles, however, the distance between data points becomes large and very few of the thirty-six points actually lie in the cloud areas. However, because of the procedure adopted in assigning values to the data points, some points immediately outside the cloud areas still have some cloud cover assigned to them and, therefore, there is a gradual change in the cloud cover amount as one proceeded along one of these outer circles from cloud areas to areas with no clouds. The thirty-six data points on each circle are used in the harmonic analysis.

4.2 Presentation of results of the analysis of the model cloud pattern

From the analysis of the schematic models, it is possible to study the relative importance and the contribution of each harmonic component to the appearance of the model cloud patterns. The results obtained are useful as guides for the proper interpretation of the analysis of the cloud patterns of real tropical cyclones. The parameters discussed in Section 3.2 are used to describe the features of each cloud pattern.

(a) Cloud patterns of stages one, two, and three

The mean cloud cover $\overline{N}$ or the zeroth harmonic is plotted as a function of the radial distance from the center of the model cloud patterns as shown in Figures 8a-c. The curves for these three stages are very similar as the mean cloud cover at all the radial distances for the stages is almost the same. On the same graphs, the curves of the appropriate relative standard deviation $\hat{S}$ (standard deviation expressed as a percentage of the mean) are also plotted. At outer radii there are large deviations from the mean. That reflected the fact that at those outer radii, the cloud cover becomes highly localized along the circles and the mean values along each circle are very small.

For stage one, the most prominent harmonic component is the second harmonic component as shown in Figure 9a. The component accounts for the largest part of the total variance of the cloud cover along each circle as shown in the table for $\hat{H}_n$ and $\hat{\eta}_r$ in Appendix I. As the cloud pattern of the tropical cyclone moves out of the general I. T. C. Z. cloudiness, as depicted in stages two, three and four, this component becomes less prominent. Figure 10 shows the gradual development in amplitude of the first harmonic component as the second harmonic component diminishes in importance from stage one to stage three. Figure 11 shows the mean cloud cover estimate for stages one to three. The first harmonic component gradually becomes very important as more clouds are left to the south during the northward movement of the cyclone-associated cloud cover, while the mean cloud cover at each radial distance remains virtually the same.

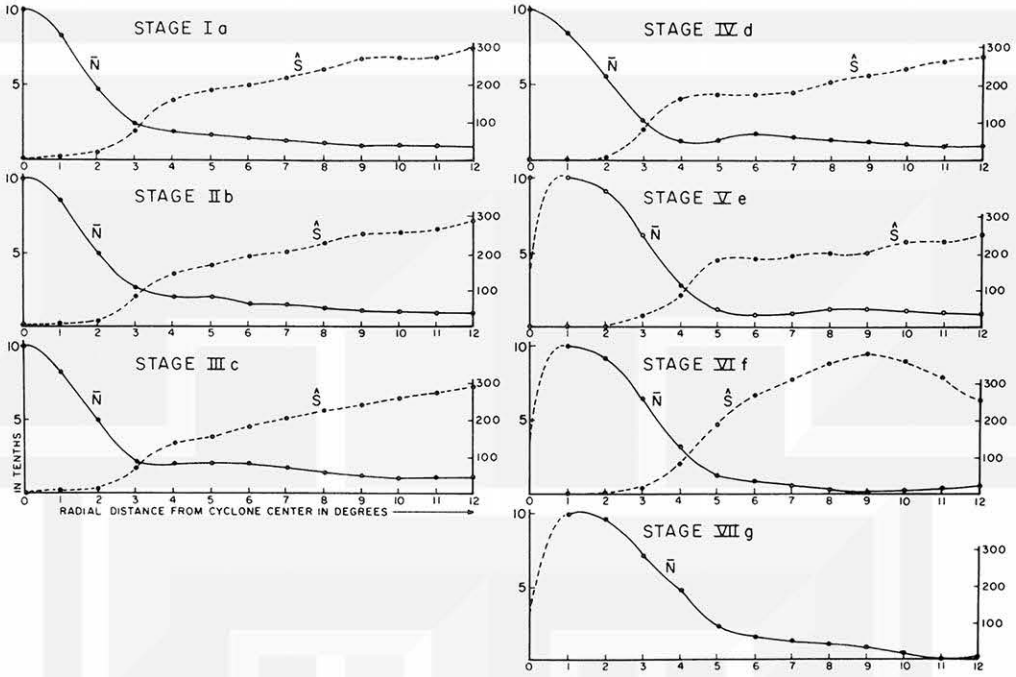

Fig. 8. Mean cloud cover N and relative standard deviation S for model cloud patterns.

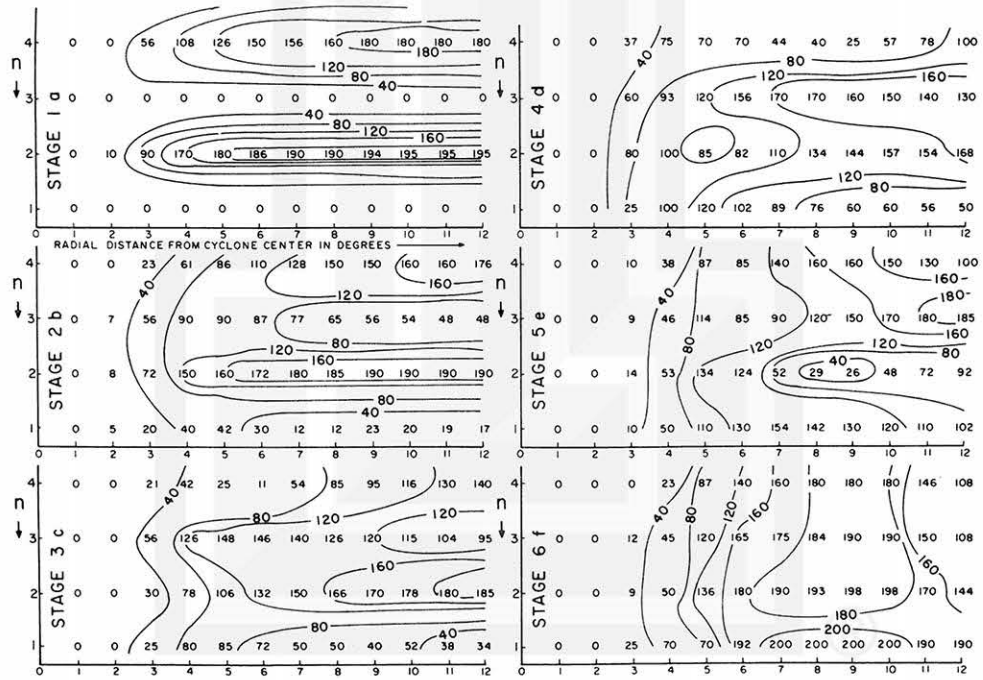

Fig. 9. Distribution of relative amplitudes in model cloud patterns.

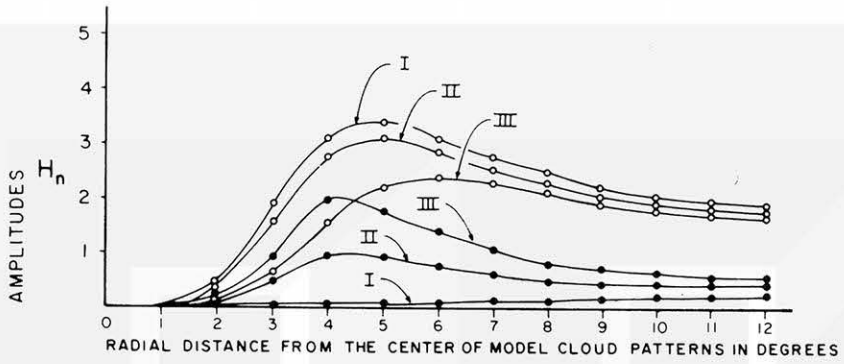

Fig. 10. A comparison of the amplitudes of the first and the second harmonic for stages one to three of model cloud patterns.

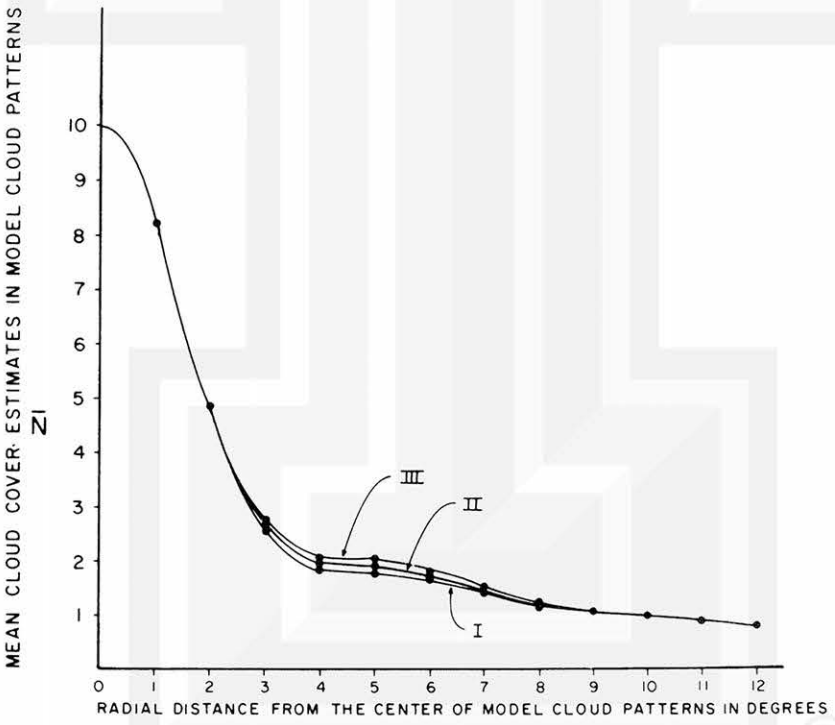

Fig. 11. Mean cloud cover estimates for stages one to three.

During stage one, there are no contributions to the cloud pattern by the odd harmonics, and the contribution by the even harmonics is largely from the second harmonic. For stages two and three the contribution from the odd harmonics, especially the first and third harmonics, increased. The polar diagrams composed from amplitudes and phase angles for the second and fourth harmonic component for stage one are shown in Figure 12. The polar diagram for the second harmonic component shows positive contours in the E-W direction and negative contours in the N-S direction. The positive contours reflect the E-W orientation of the model cloud pattern for that stage. The negative contours, however, have no physical meaning as negative cloud cover cannot be defined. Since the negative contours appear in the no-cloud areas, positive contours should appear in those areas when polar diagrams for other harmonics are drawn for the model cloud pattern of the same stage, to neutralize the negative contours. The polar diagram for the fourth harmonic, for stage one, for example, shows positive contours in the North, East, South and West directions. There are, therefore, a succession of negative and positive contours in no-cloud areas as other harmonics are considered. The polar representation of amplitudes and phase for the first and second harmonic for stage six of the cloud patterns is shown in Figure 13.

(b) Cloud patterns of stage four, five, six and seven

In discussing these stages, each harmonic component will be considered separately.

(i) The mean cloud cover. -- As in the first three stages, all the curves for these stages indicate large values of mean cloud cover near the center of the model cloud patterns as expected. The mean cloud cover decreases outwards as in the other stages. For stage seven, the mean cloud cover reduces almost to zero at outer radii. The graphs of S also showed very large deviation from the mean (Fig. 8), at the outer radii.

(ii) The first harmonic component. -- Figure 9d and Figures 9e and f indicate the importance of the component for these stages especially near the cyclone center. The phase angles of the component indicated that there was more cloud to the south of the cyclone center than to the north. As the cloud pattern moved further north from the I. T. C. Z. cloudiness the amplitudes of the component decreased but are still relatively large in comparison with the amplitudes of the other components.

(iii) The second harmonic component. -- The directions of the vectors indicate the azimuth distances from the north where the amplitude of the cloud cover for the second harmonic component is a maximum. Similar vectors are drawn for the first harmonic component, Figure 14. After an initial increase, the amplitudes of the component increased gradually from stage four to stage six, and the distribution of phase angles shows a gradual change in orientation of the polar diagram pattern of this component from the general E-W orientation of the earlier stages through a NE-SW orientation to a North-South orientation. This change in orientation is emphasized in Figure 15. Figure 15 shows the amplitudes represented in form of vectors.

(iv) The third harmonic component. -- The amplitudes of this component are only pronounced at outer radii at all stages. This reflects the fact that the 'arms' of the I. T. C. Z. cloudiness has been kept in model cloud patterns. This component increased in importance during stages one to five, especially at outer radii. For stage seven the amplitudes of this component and for other components reduce to zero.

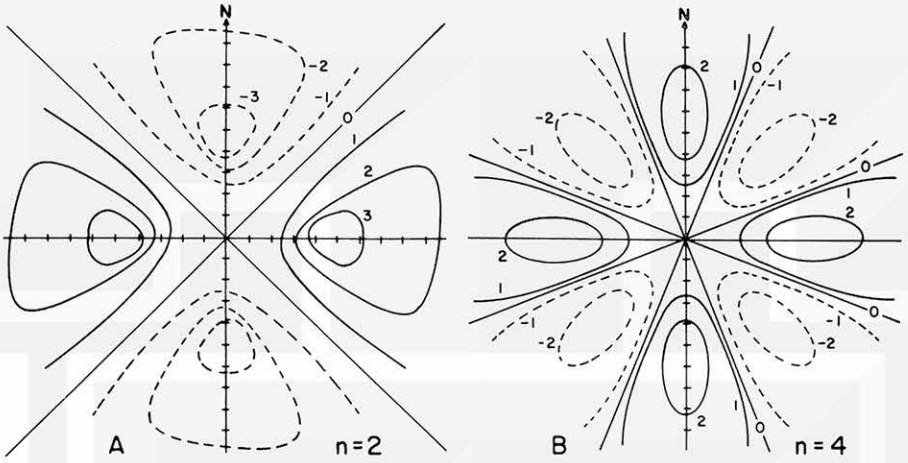

Fig. 12. Polar representation of amplitude and phase for the second and the fourth harmonic for stage one of model cloud patterns.

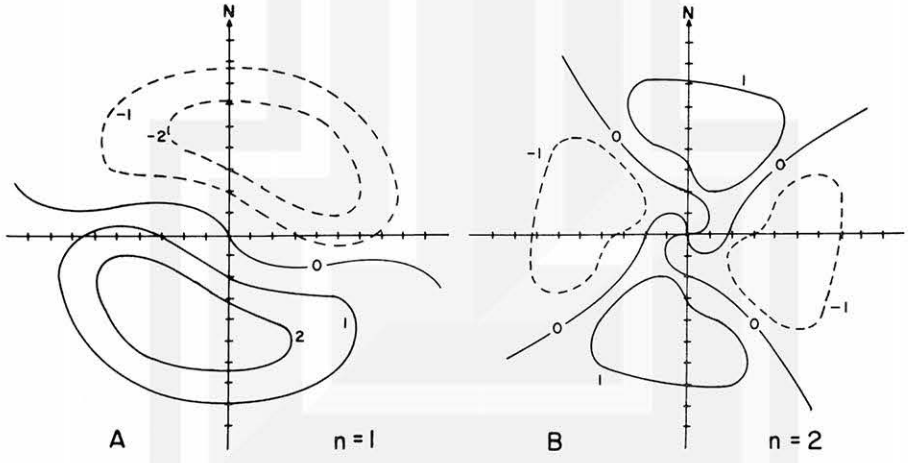

Fig. 13. Polar representation of amplitude and phase for the first and the second harmonic for stage six of the model cloud patterns.

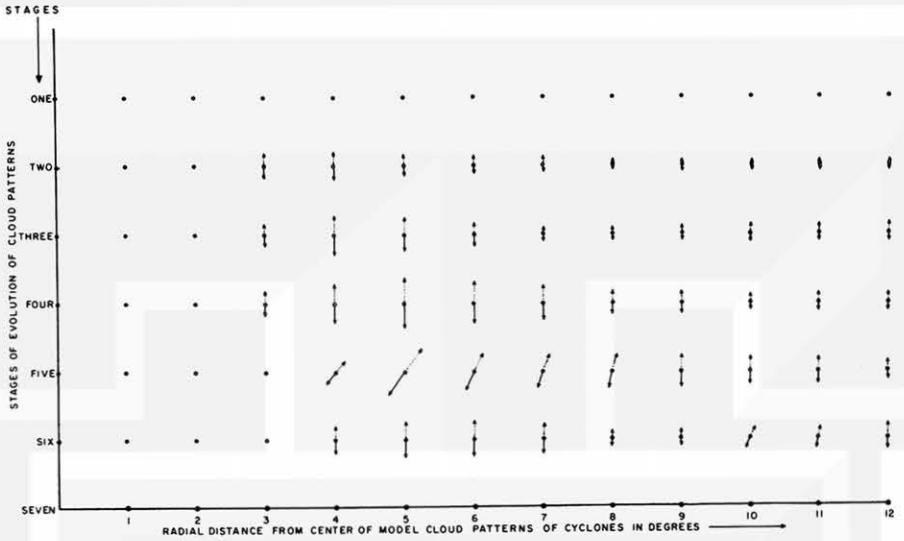

Fig. 14. Vector representation of amplitude and phase for the first harmonic drawn for the different model cloud patterns as function of radial distances.

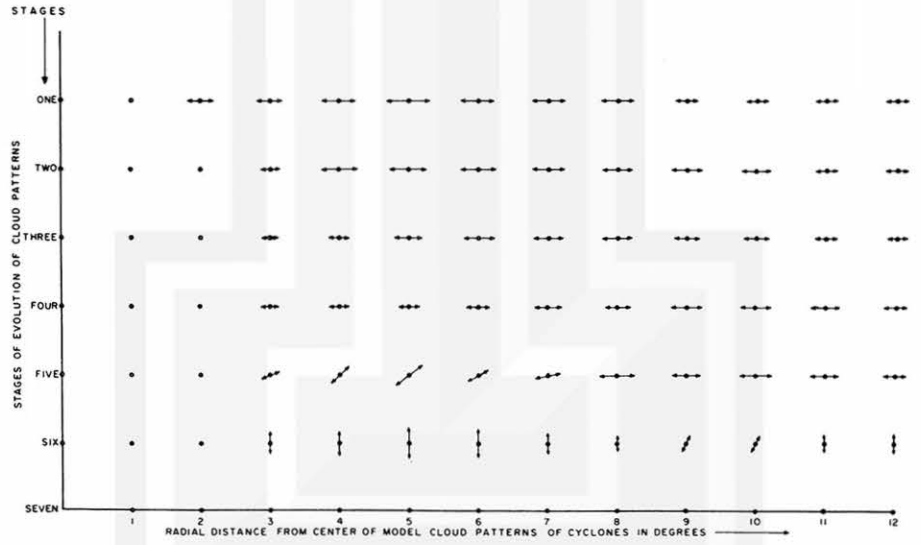

Fig. 15. Vector representation of amplitudes and phase for the second harmonic for the different model cloud patterns as function of radial distances.

(v) The fourth harmonic component. -- For the patterns illustrating the third and fourth stages, there is a marked reduction in relative amplitude of the component. Figure 9 shows that this component is most prominent on the outer circles for the three stages.

(c) Comments on the analysis of the model cloud patterns

(i) The model cloud patterns do not make any distinction between the types or heights of cloud cover. Such distinction is not necessary for the kind of information desired from the harmonic analysis of the cloud patterns. Table 1 shown in the Appendix, shows that four harmonics will account for about 90% of the variance of the original cloud distribution along most of the circles, especially along those circles near the center of the cyclone cloud pattern. It can be concluded that the mean cloud cover and the four harmonic components convey the same information about the patterns as the thirty-six cloud cover amounts on each of the circles drawn on the patterns. The fourth harmonic, the highest computed, has a wave length of 90° azimuth. Considering only four components, therefore, amounts to investigating the concentration of clouds in four quadrants of the model patterns.

(ii) Harmonic analysis is carried out in this study with the circumference of the circle as fundamental wave length. Considering all the concentric circles it must be noted that the wave lengths of any particular component increases with distance from the center of the cyclone. The wave length of any component along the circle of radius 8° is four times larger than the wave lengths of components along the circle of radius two degrees.

(iii) In relation to the various model patterns considered, it is necessary to define the following terms: Axis-symmetry and asymmetry.

In mathematics an axis of symmetry is defined as a line drawn within a body or a set of points in such a location and direction that a rotation of the body or the set of points through an angle $\frac{2\pi}{p}$ radians about the line as an axis, p being an integer greater than unity, results in a configuration indistinguishable from the original configuration. A body or a set of points having such an axis is said to have a p-fold symmetry, and the line is said to be a p-fold axis. As p approaches infinity, the body or the set of points becomes circular symmetric and there are very little circumferential variations in the body or in the distribution of the set of points.

The polar representations of amplitudes and phase for the second harmonic or wave number n = 2 in Figure 12a has,by the above definition, a two-fold symmetry with respect to an axis through the center of the model cloud pattern. If the pattern is rotated through 180 degrees, it will remain unchanged. Similarly, the polar diagram of the fourth harmonic,Figure 12b,shows a four-fold symmetry pattern. The polar diagram for the first harmonic, as exemplified in Figure 13a, has to be rotated through 360 degrees about an axis through the assumed center of the model cloud pattern before the original pattern can be obtained. By the above definition, the axis of rotation cannot be regarded as an axis of symmetry. The model cloud pattern of clouds in which the first harmonic is most prominent is therefore referred to as an asymmetric cloud pattern. Those patterns in which the clouds are circular are referred to as

circular or axially symmetric cloud patterns. The cloud patterns in which the second harmonic is most prominent are identified as two-fold symmetry cloud patterns.

In actual cyclones, the deviations from circular symmetry of the cloud patterns are of interest. Quantitative estimates of such deviations, referred to in this study as non-axis-symmetry or asymmetry, are estimated for actual cyclones and are discussed in Chapter Seven.

CHAPTER V

APPLICATION OF HARMONIC ANALYSIS TO ATS III PICTURES OF TROPICAL CYCLONES

The Applications Technological Satellites were spacecrafts designed to conduct research in synchronous earth orbit at 22,500 miles above the Equator. Since the orbital period of the ATS was equal to the sidereal rotation of the earth, the satellite remained fixed to the sub-satellite point of the earth. The satellite could thus provide a continuous meteorological observation of the earth below it.

The photographs used for parts of this investigation were from the ATS III satellite. The ATS III was located above the equator south of the United States. The cameras on the ATS had a resolution of about 2.5 miles at the sub point. The ATS was capable of sending photographs to earth every ten to thirty minutes.

5.1 Analysis of ATS photographs of tropical cyclones at one hour intervals

Since photographs from low-orbit satellites, for example ESSA satellites, is available only once every day, it is not possible to study short time changes in the cloud structure of tropical cyclones from them. For this part of the study, several (ATS) photographs of Hurricane Debbie of 1969, are analyzed at intervals of approximately one hour on the 16th August, 1969. The history of that tropical cyclone and the analysis of the daily photographs of the cyclone are given in Chapter VI.

The ATS photographs used are shown in Figure 16. The photographs were gridded and the cloud cover amount estimated at the grid points are transferred to a mercator map. A polar diagram (as in Figure 4) is super-imposed on the cloud estimates and the cloud cover values are determined at thirty-six points along each circle, according to the procedure given in Chapter II. Figure 5 shows the cloud cover estimations at 1232 Z . Similar estimations are made for the other photographs.

(a) The distribution of satellite observed cloud cover estimate

To have a proper understanding of the cloud patterns in a tropical cyclone as observed from the ATS photographs, it is useful to study the distribution of the cloud cover estimates N at the various radial distances from the center of the cyclone. For that purpose, frequency intervals of cloud cover is established and the number of cloud cover amount falling in the interval is counted and recorded. The procedure is carried out for nine concentric circles on each tropical cyclone cloud pattern studied. The intervals are: 0 - 0.45; 0.5 - 1.45; 1.5 - 2.45; 2.5 - 3.45; 3.5 - 4.45; 4.5 - 5.45; 5.5 - 6.45; 6.5 - 7.45; 7.5 - 8.45; 8.5 - 9.45; 9.5 - 10.00. The central values of each interval is correspondingly 0, 1, 2, 3, 4, ..., 10. Zero and ten are respectively chosen as the central value for the first and last intervals as it is neither possible to have cloud cover values less than zero nor possible to have values greater than 10. The frequency of cloud cover estimates for each interval is identified with the central value of the interval. For example, if for a particular circle, the number of cloud cover estimates between 4.50 and 5.45 is twenty, then there are twenty points (out of the possible 36) with five-tenths cloud cover. Twenty, therefore, represents the

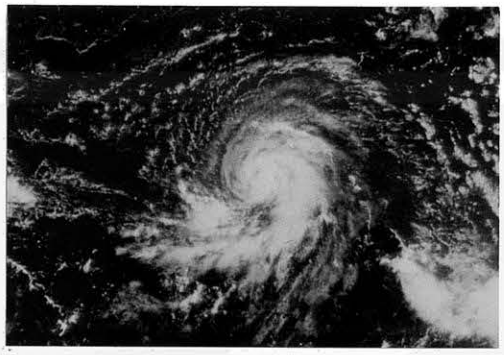

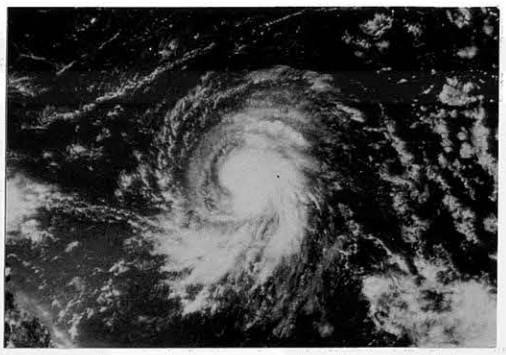

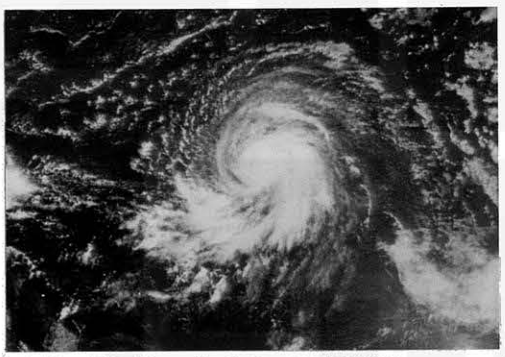

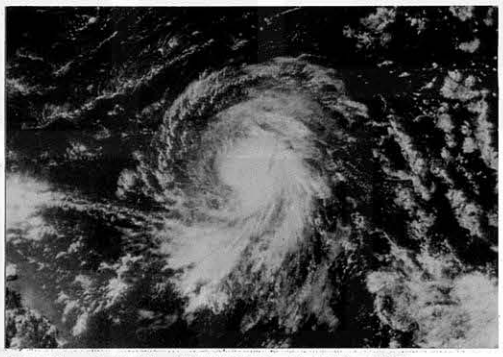

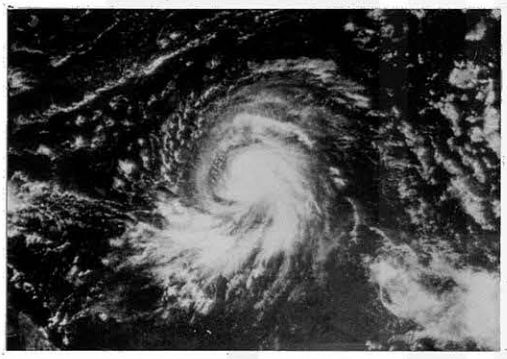

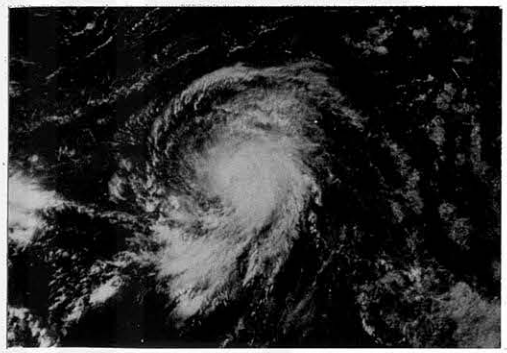

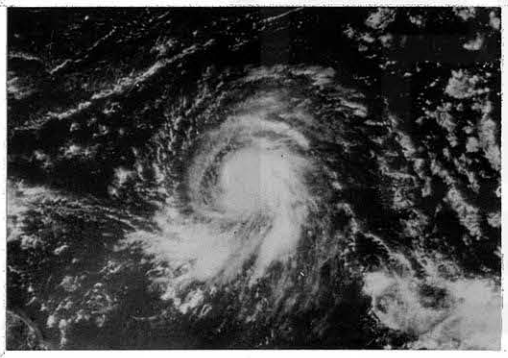

Fig. 16. Sequence of photographs for hurricane Debbie, August 16, 1969. From 1233 Z to 1930 Z.

absolute frequency of cloud cover for the interval 4.50 - 5.45. The use of absolute frequency is preferred to the use of relative frequency or cumulative frequency because it affords an easier method of assessing the increase or decrease of clouds at a particular radial distance from the center of the cyclone as the cyclone developed.

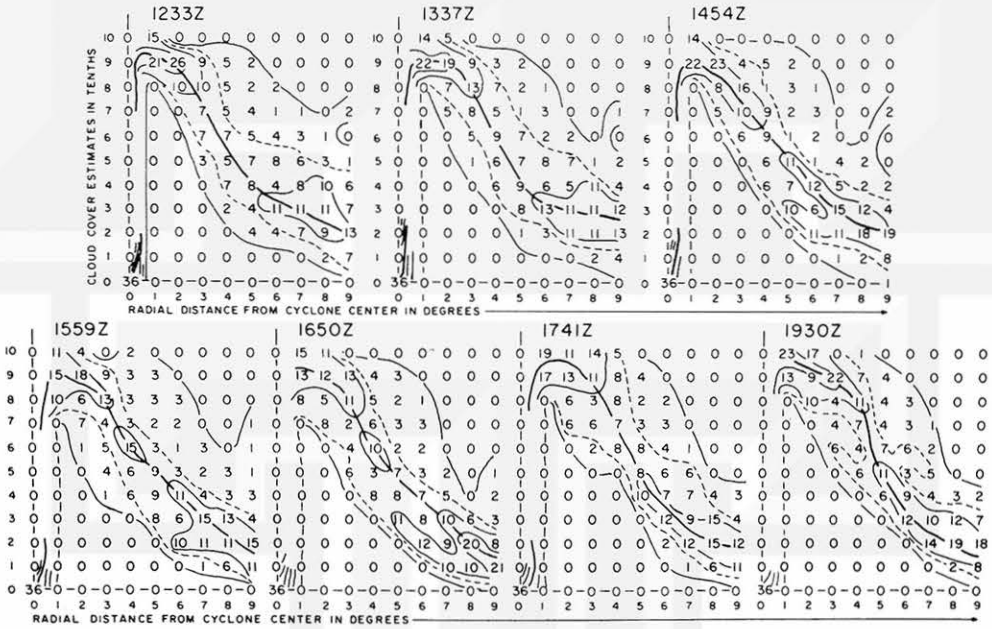

Fig. 17. Frequency distribution of cloud in hurricane Debbie on Aug. 16, 1969 from ATS III photographs.

Figure 17 shows the distribution of cloud cover as function of radial distance from the cyclone center for each of the seven photographs analyzed. One general feature of the frequency distribution requires special mention. Namely, by drawing isolines of frequency on the frequency distribution, at intervals of 10 (the isolines for frequency of 5 were indicated by broken lines), an axis of maximum frequency of cloud cover could always be defined. The axis could be continuous or broken. The entire axis or parts thereof could shift in response to the redistribution of cloud cover. From these diagrams it was possible to define a parameter r_N as the radius of maximum frequency of a particular cloud cover estimate N. For example, the radius of maximum frequency of five-tenths cloud cover estimate at 1233 was 4.5. Figure 18 shows the changes of r_N with time, for r_N equal to three-, five-, and eight-tenths. The implications of the changes in r_N values as the tropical cyclone developed will be discussed in later chapters.

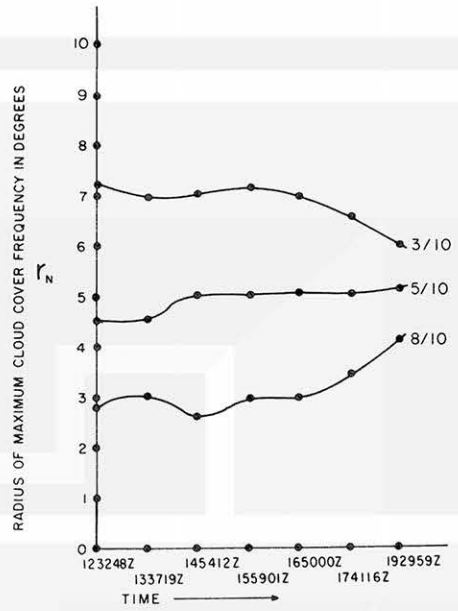

Fig. 18. Graphs of three-tenths, five-tenths and eight-tenths cloud cover as function of radial distances and time computed from Fig. 17.

(b) The harmonic analysis of cloud cover

Harmonic analysis was carried out for cloud cover values obtained from each photograph in Figure 16. The results of the analysis were summarized in the form of polar diagrams shown in Figure 19. On those diagrams, the amplitudes Hn have been written at the appropriate radial distances on the curves joining the points indicating the phase angles along each circle for the harmonic components considered. The diagrams show the distribution of actual amplitude and phase for the first and second harmonic.

5.2 Presentation of the results of analysis

The ATS photographs analyzed are those taken during the gradual development of Hurricane Debbie from the stage of a tropical storm to that of a full grown cyclone, with hurricane force winds.

Figure 20 shows the curves for the mean satellite observed cloud cover and those for relative standard deviation S as functions of radial distance. At the inner radial distances 0° - 3° the values of the relative standard deviations are small. The values increase outwards and, at distances greater than 7°, the standard deviations are greater than the mean.

By estimating the changes in the mean values of the cloud cover at particular radial distances from the center of the cyclone, the diagram shown in Figure 21 was prepared.

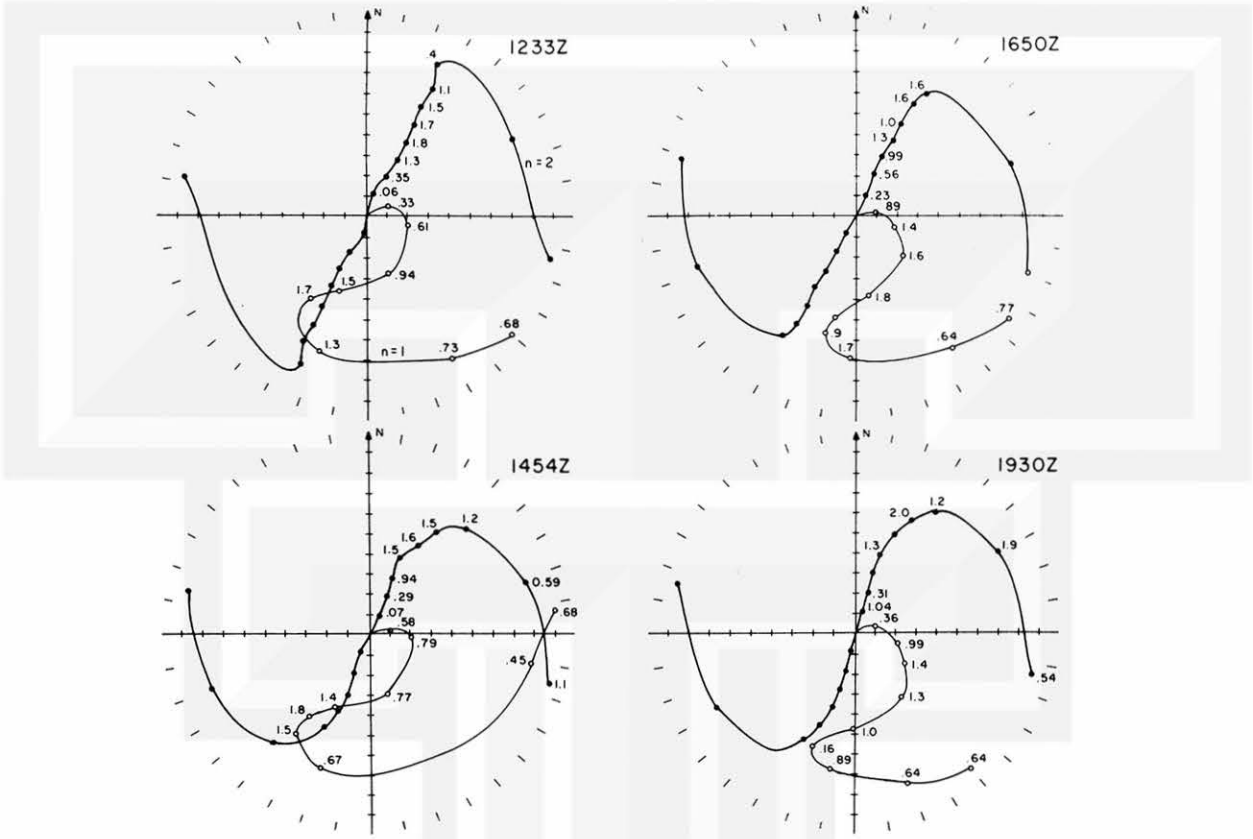

Fig. 19. Polar diagram showing phase curves obtained from the harmonic analysis of some of the photographs in Fig. 16.

Figure 21 shows that very little or no changes occur in the cloud cover estimates during the entire seven hour period. From reports, the tropical cyclone developed hurricane force winds at 1800 on August 16, 1969. This is reflected in the increase of about one-tenth between 1700 and 1800. What is noteworthy in the figure is that the increase is more noticeable at the outer radial distances (outside 3° radius), that is along the spiral bands, during that period. The only substantial decreases noted are at the outermost parts of the storm.

The polar diagrams in Figure 19 show that there are very little but noticeable changes in the phase angles as the different cloud patterns are considered. Thus, the general pattern of the cyclone remained virtually the same over a period of seven hours. This confirms the observation of Malkus et al. (1961) that the cloud development in a tropical cyclone tended to take place at approximately the same position relative to the center of the cyclones, and because of the orientation of the curves shown in Fig. 19 a conclusion can be drawn that the preferred direction of production of clouds is along

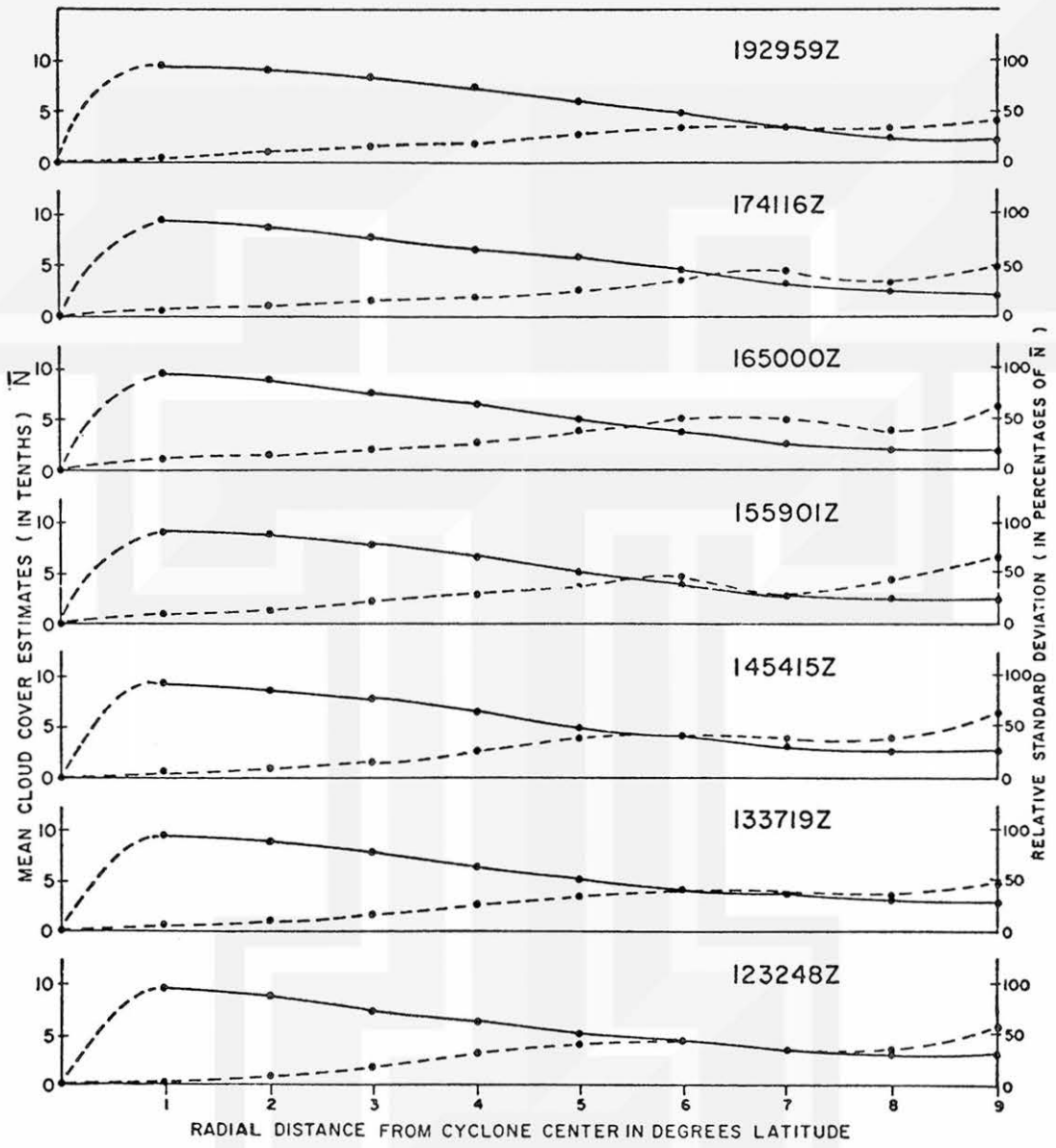

Fig. 20. Cloud cover estimates N and relative standard deviation S for hurricane Debbie, August 16, 1969 as a function of radial distances and time.

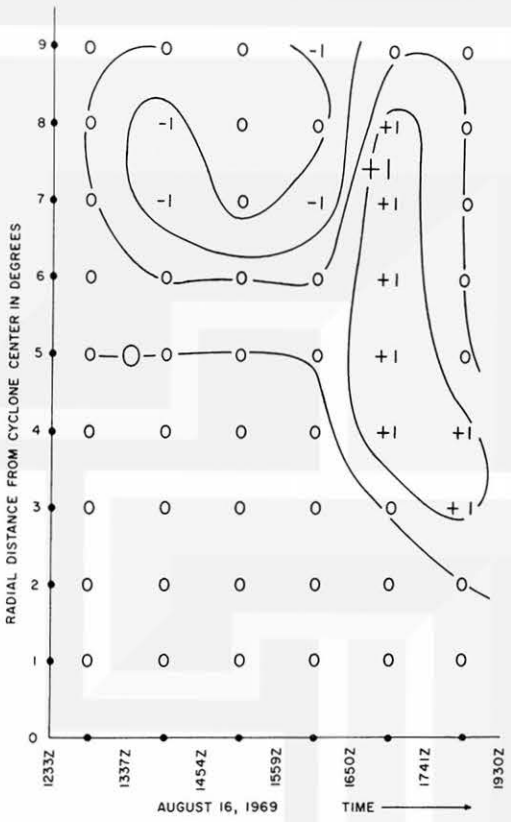

Fig. 21. Hourly changes in cloud cover estimates at various radial distances and time for hurricane Debbie on August 16, 1969.

an axis extending NE - SW at that particular stage of development of the cyclone. An examination of the phase angles, however, shows that there are measurable and organized changes in the phase angles for both the first and the second harmonic components during the seven-hour period. The implications and the significance of this observation are further discussed in Chapter Seven. In the next chapter, the results of the analysis of the daily changes in the cloud patterns of Hurricane Debbie and two other cyclones are discussed.

CHAPTER VI

APPLICATION OF HARMONIC ANALYSIS TO ESSA PHOTOGRAPHS OF TROPICAL CYCLONES

6.1 Analysis of daily ESSA photographs of tropical cyclones

The ESSA satellites were launched into a near polar sun synchronous orbit -- an orbit such that the orbital plane rotated about the earth at exactly the same rate as the earth orbits the sun. The orbits of the satellites were at altitudes of about 1400 - 1500 km. Those orbital characteristics assured that the satellites would cross the Equator at the same local sun time every day and also that all parts of the earth (except those in polar night) could be photographed once every twenty-four hours.

Photographs from ESSA 3 and ESSA 5 in the ESSA series of satellites are used in this study. The photographic products used are in the form of composite rectified mosaic on Mercator projection from several passes of the satellites. The products were available once a day. Because the satellites crossed the equator at the same local sun time every day and because the cyclones were slow moving (5-15 knots), the time interval between one analyzed photograph and the other was approximately twenty-four hours.

From the photographic products, an area approximately 30 latitude by 30 longitude containing a tropical cyclone cloud pattern is enlarged to fit a mercator projection map of known scale. The tropical cyclone cyclone cloud pattern is positioned as much as possible at the center of the map. Sometimes it is necessary to join two frames of original photographic product to achieve a good coverage of the cloud pattern under study. On occasions, grids on the original products are in error of about 1/4 - 1/2 of a degree. Such errors are corrected by reference to the original single frame pictures from which the mosaics are made. Transparent mercator grids with longitude and latitude lines drawn at intervals of one degree are imposed on the photographs such that the eye of the cyclone is at a grid point. In cases where an eye is not visible, the grids are adjusted so that the estimated or reported center of the cyclone coincides with a grid point.

In carrying out computations on the mercator maps, the grids made up of longitude and latitude lines are used essentially as square grids with equal distances between the grid points. As the distances between any two parallels of latitude increase at higher latitudes, the mercator grids could hardly be regarded as square grids. The greatest virtue of the mercator map, however, is that it has some advantageous properties near the equator. Within reasonable limits, the map is conformal and isometric for areas in low latitudes. The area of a unit square of the projection at Lat. 30 is only 15 percent larger than the area of a unit square on the equator. For a small square close to the equator, the differential stretching of the north-south side is hardly noticeable.

The centers of the cyclones studied were situated well south of latitude thirty; therefore, the magnitude of the errors that could be introduced into the computations were not large enough to affect the results of the investigation.

6.2 Histories of three hurricanes analyzed from ESSA photographs

The day to day variations in cloud patterns of three tropical cyclones were studied from television pictures sent to earth from ESSA satellites. In this section, a brief history of the cyclones -- as given in U. S. Weather Bureau reports -- is provided as a background to the photographic analysis.

(a) Hurricane Debbie (August 13-25, 1969)

Debbie was a North Atlantic tropical cyclone; a map showing its path is shown in Figure 22. Debbie was identified as a tropical disturbance on August 13th and as a tropical storm at 1200 Z on the 15th. The storm intensified slowly as she moved NNW and became a hurricane at about 1800 Z on the 16th. She then moved NW while increasing her speed to about 90 kts. She was at her peak strength on the 20th with a central pressure of 950 mbs. Her winds dropped below hurricane force late on the 24th and by the 25th, the cyclone, then with a central pressure of 988 mbs, was identified as an extra-tropical cyclone.

In this study, the daily cloud patterns of the cyclone were studied from August 13 to August 19th (Fig. 23). The period thus covered the formative and development stages of the cyclone.

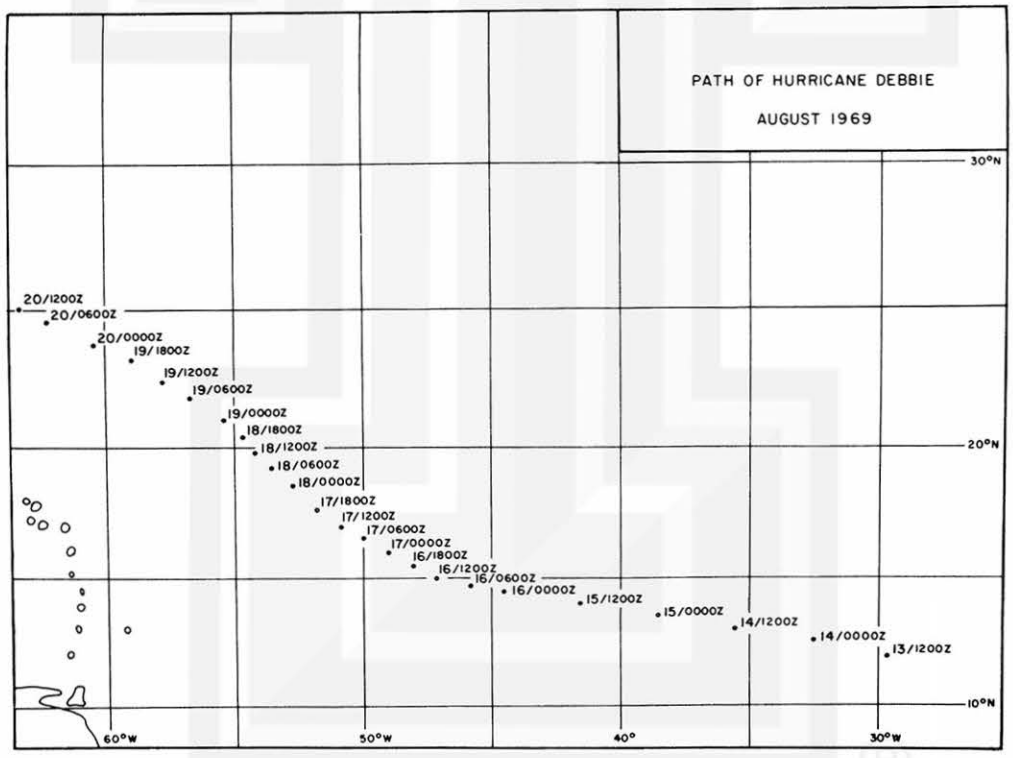

Fig. 22. Path of hurricane Debbie, August 13-19, 1969.

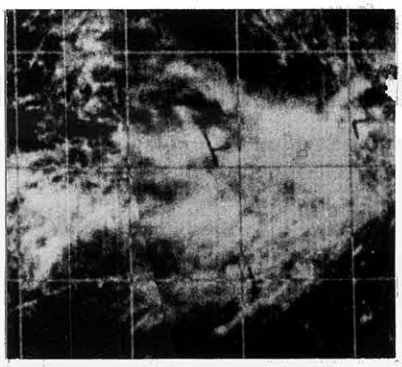

13 AUG 69

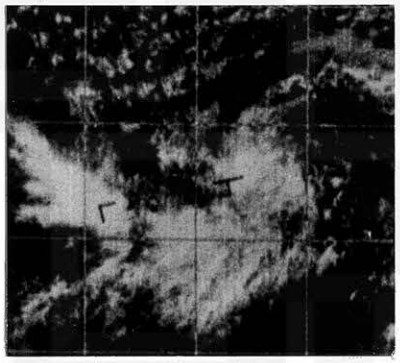

14 AUG 69

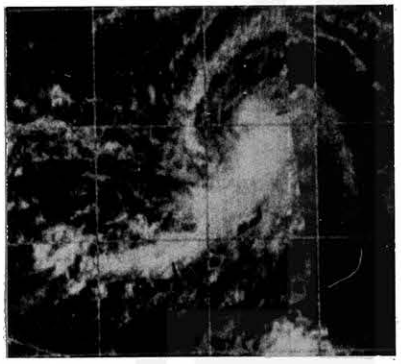

15 AUG 69

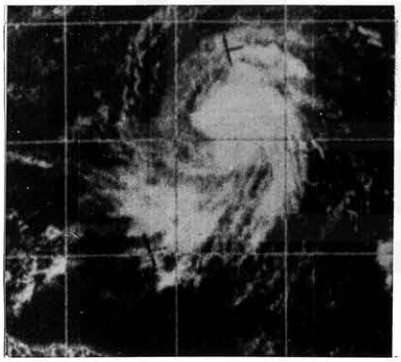

16 AUG 69

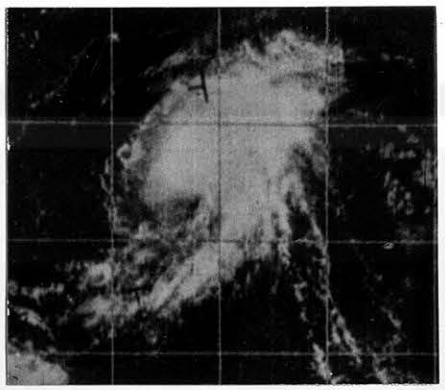

17 AUG 69

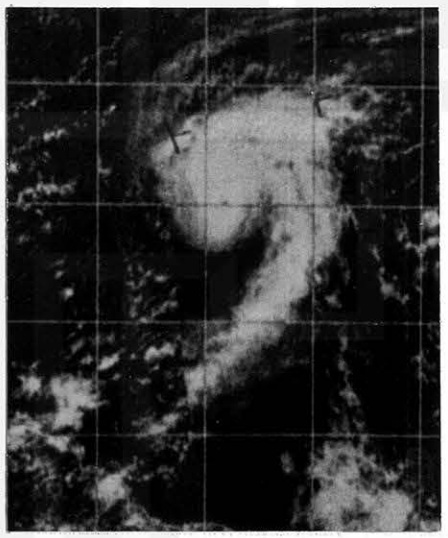

18 AUG 69

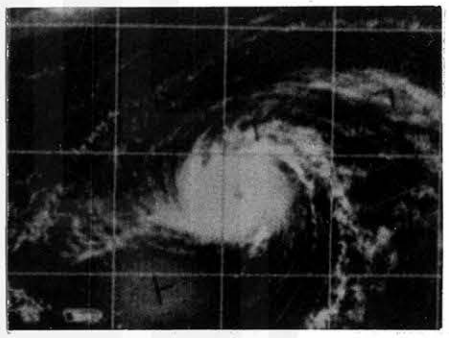

19 AUG 69

Fig. 23. Sequence of photographs showing the various cloud patterns in the evolution of hurricane Debbie between August 13 to August 19, 1969.

(b) Hurricane Holly (September 13-21, 1969)

The path followed by the cyclone is shown in Fig. 24, and the sequence of photographs showing the cloud patterns of the cyclone is shown in Fig. 25. The cyclone was an example of a North Atlantic Tropical Cyclone whose growth was stunted by an unfavorable tropical environment. She was identified as a tropitcal depression about 1200 Z on September 14th and as a tropical storm with top winds of about 40 kts by 2200 Z on the 14th. About 1600 Z on the 15th, she became a hurricane and attained her lowest pressure (992 mbs) and her highest winds (65 kts) shortly afterwards. She then moved in a WNW track and by late on the 17th, she had degenerated into a tropical storm again, with a maximum wind of 45 knots. She degenerated all the way down to an easterly wave by the 21st of September.

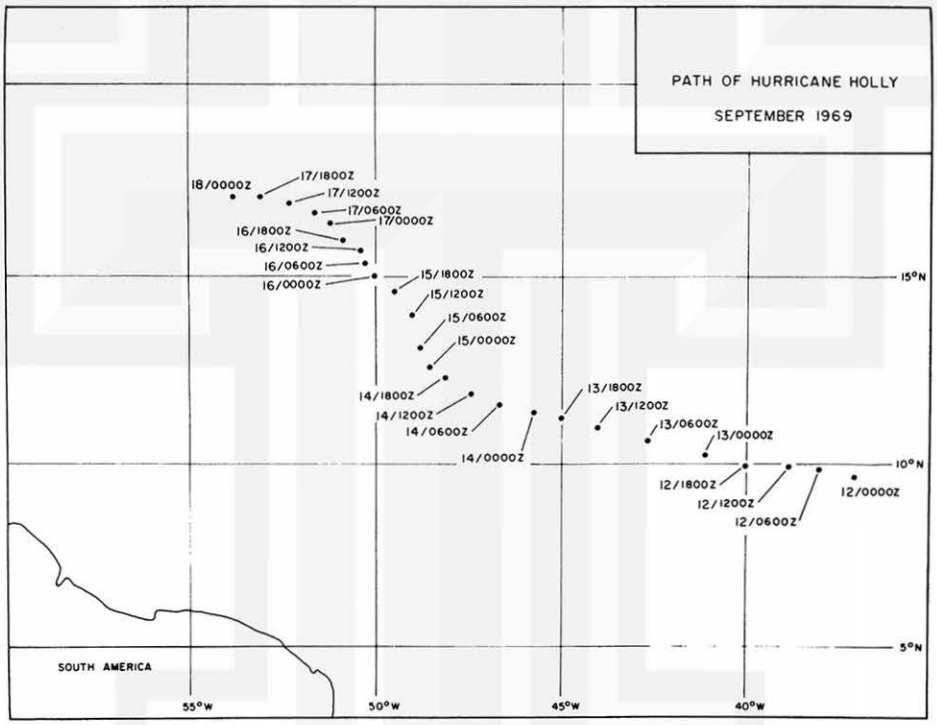

Fig. 24. Path of hurricane Holly, September, 1969.

(c) Typhoon Cora (August 14-23, 1969)

Cora was a tropical cyclone of the Western Pacific Ocean. She was identified first as a tropical depression early on the 14th of August and in less than twenty-four hours became a tropical storm with winds of about 45 knots. She became a typhoon later on the 17th of August and attained her peak wind of 85 kts with the lowest observed pressure of 948 mbs on the 19th of August. The path of the typhoon is shown in Figure 26 and the photographs of the typhoon are shown in Figure 27.

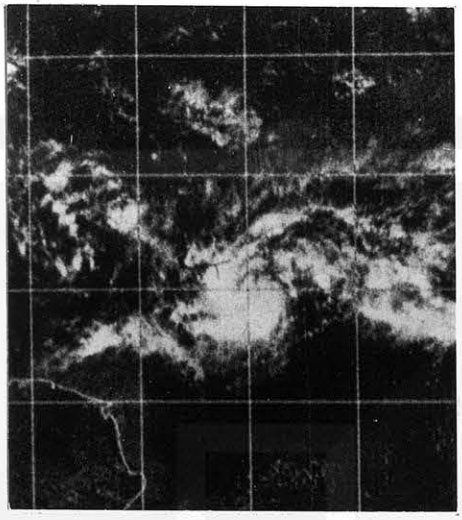

13 SEPT 69

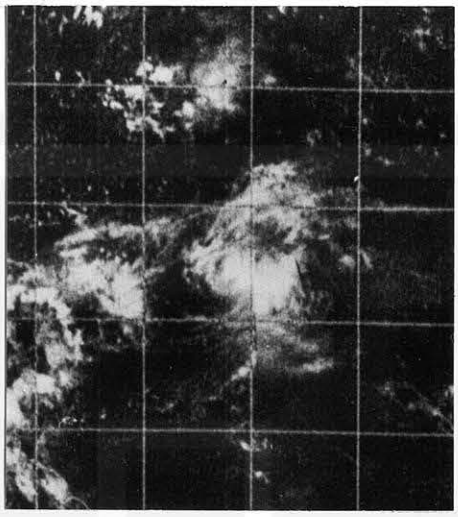

16 SEPT 69

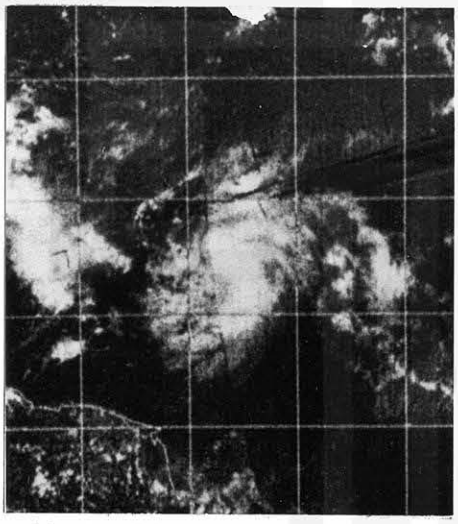

14 SEPT 69

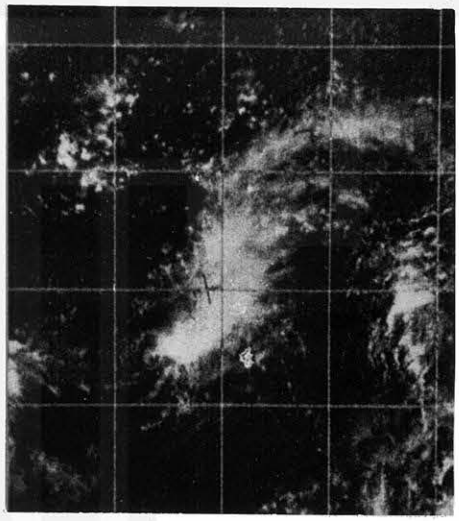

17 SEPT 69

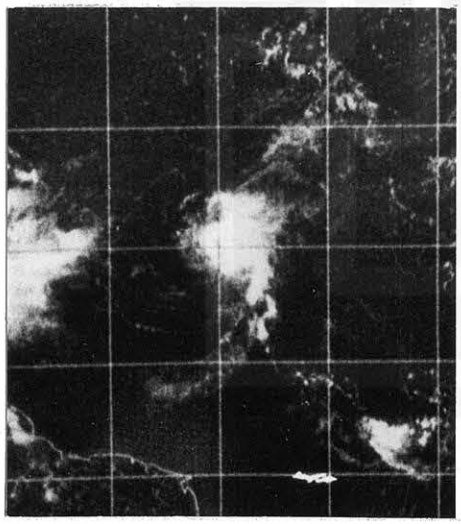

15 SEPT 69

Fig. 25. Sequence of photographs showing the various cloud patterns in the evolution of hurricane Holly between September 13 and September 17, 1969.

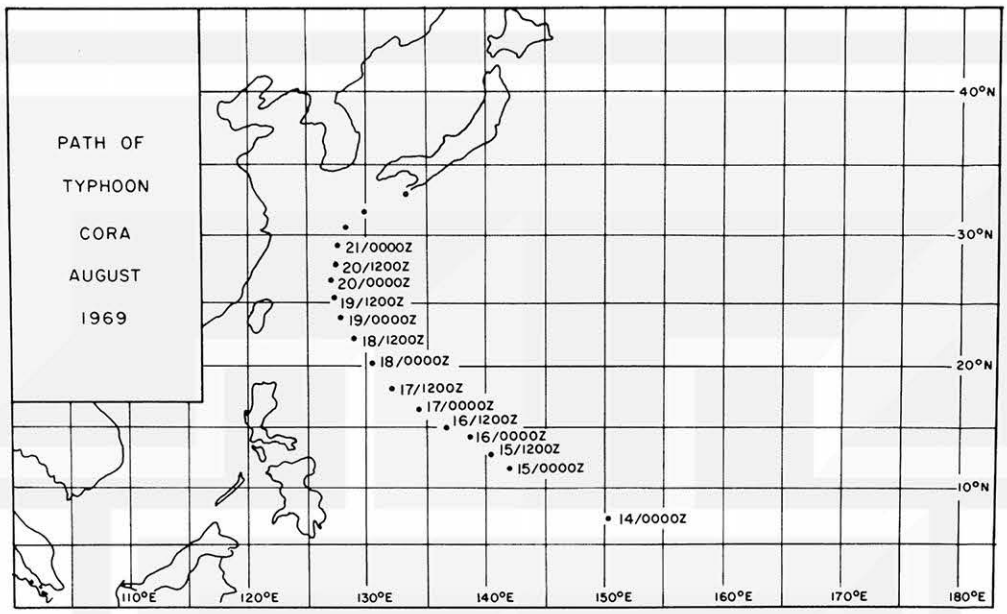

Fig. 26. Path of typhoon Cora, August, 1969.

As in all the other cases, only the cloud patterns at the formative and development stages were analyzed.

6.3. Harmonic analysis of cloud patterns and discussion of results

The cloud pattern analysis of the three tropical cyclones are discussed in the following sections by considering each of them in turn.

(a) Hurricane Debbie

The sequence of photographs studied was shown in Figure 23. From the sequence, photographs A, B, D, and G, could be identified as good examples of stages 3, 4, 5, and 7 of the model patterns discussed earlier.

(i) The distribution of cloud cover. -- Figure 28 shows the frequency distribution of the quantitative estimates of the cloud cover for each of the photographs shown in Figure 23. Axis of maximum cloud cover frequency are common features of all the cloud cover distribution. For photograph A, the frequency distribution shows a broken axis. This is characteristic of the distribution of clouds of tropical disturbances near the I. T. C. Z. in all cases studied. Figure 29 shows the variation of r_N with time. A general feature of that graph is that the radii of maximum cloud cover frequency decreased for all values of N considered during the tropical disturbance and tropical depression stages of the cyclone. The r_N increased as the tropical cyclone attained the tropical storm stage and decreased as the cyclone became a full grown hurricane. These curves are discussed in Chapter Seven.

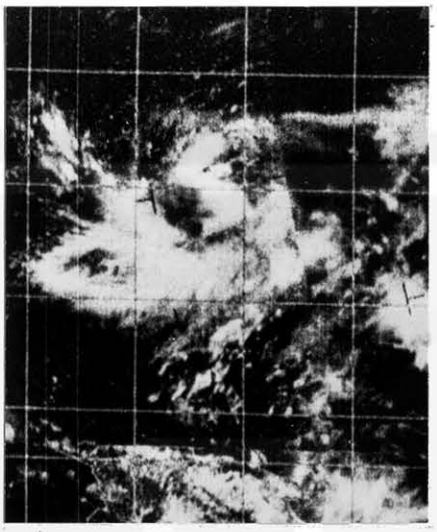

13 AUG 69

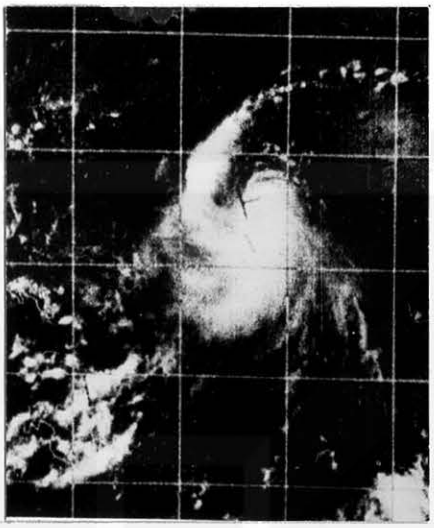

16 AUG 69

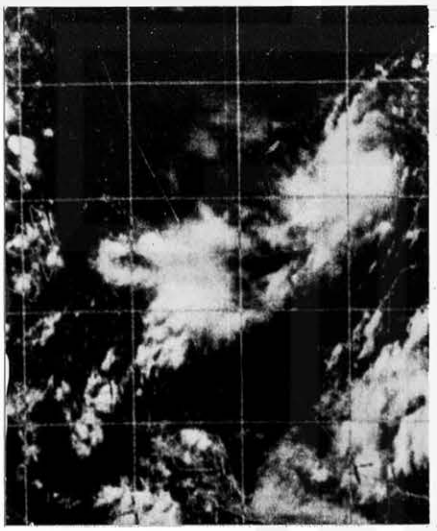

14 AUG 69

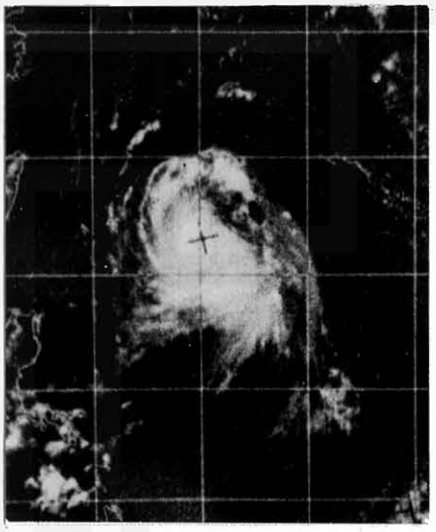

17 AUG 69

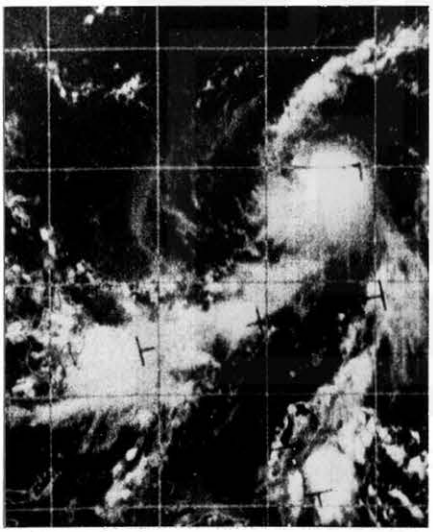

15 AUG 69

Fig. 27. Sequence of photographs showing the various cloud patterns in the evolution of typhoon Cora, August 13 to August 17, 1969.

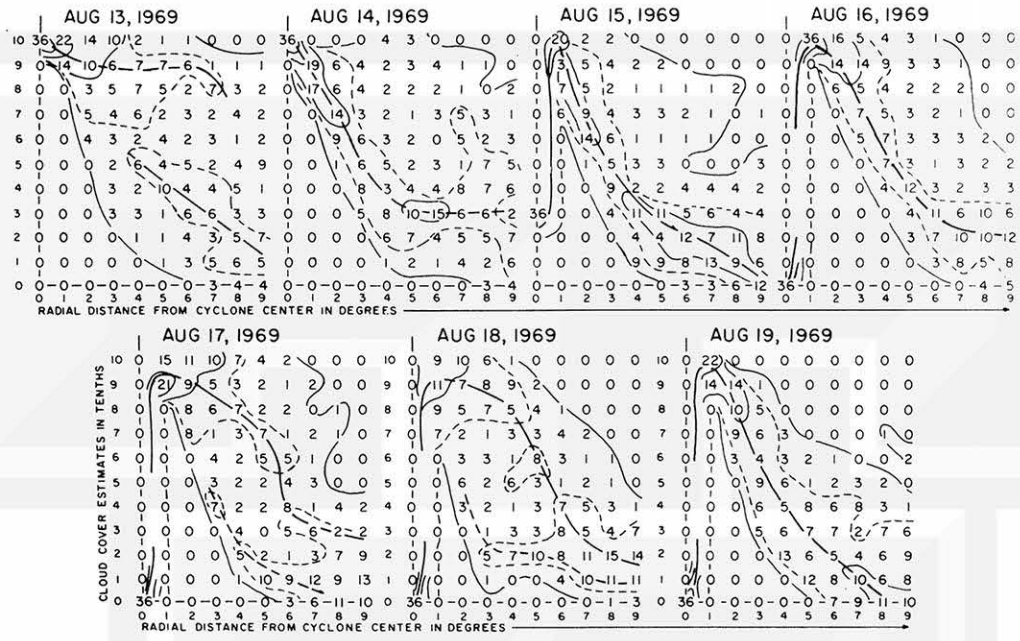

Fig. 28. Frequency distribution of cloud cover estimates in hurricane Debbie, August, 1969.

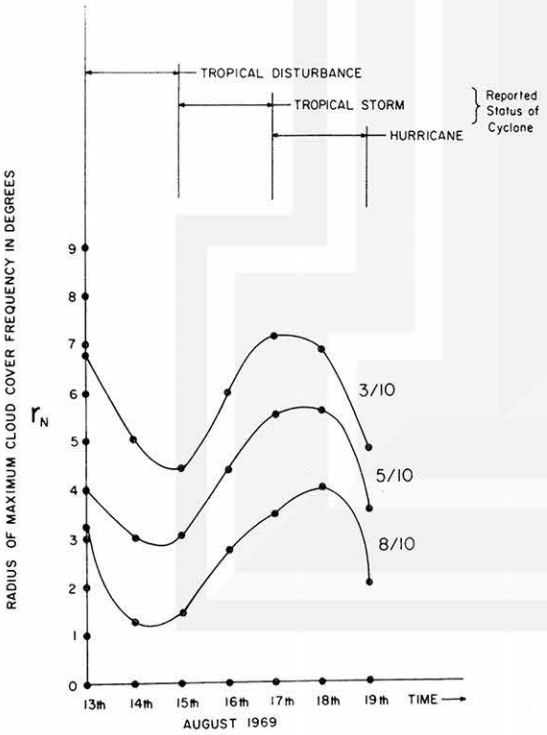

Fig. 29. Graphs showing variation of r_N with time for N equal to three-, five-, and eight-tenths for Debbie, August, 1969.

(ii) Harmonic analysis of the quantitative estimates of the cloud cover. --

Table 2 in Appendix I emphasizes the importance of the first harmonic component in all the stages of development of Hurricane Debbie. In photograph A, the reported center of the developing tropical cyclone is near the northern boundary of the I. T. C. Z. cloudiness. Hence, at radial distances close to the center, the first harmonic component is most predominant. At the outer radial distances, however, the second harmonic is the most predominant, reflecting the association of the disturbance with the I. T. C. Z. cloudiness. The stage depicted in photograph A, approximates that indicated in stage three of the model cloud pattern discussed earlier. In that model, as in the stage shown in photograph A, the concentration of the I. T. C. Z. cloudiness immediately to the south of the center is responsible for the predominance of the first harmonic component at radial distances close to the center. The stage of development of Debbie shown in photograph F, is a very good example of stage 6 of the model cloud patterns discussed in Chapter Four, while photograph G approximates the seventh stage.

Table 3 in Appendix I shows that the variance of cloud cover along the circles drawn on the cloud patterns is accounted for essentially by the first and second harmonic component. Figure 30 shows daily changes in the satellite observed cloud cover of hurricane Debbie.

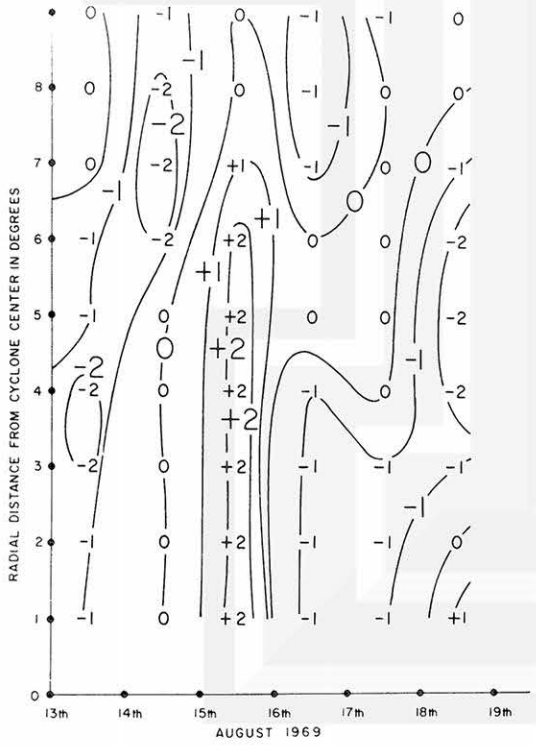

Fig. 30. Daily changes in cloud cover estimates at various radial distances for hurricane Debbie, August, 1969.

The curves on the polar diagram showing the phases for the first and second harmonic (Fig. 31) reflected different patterns assumed by Debbie during its evolution. The curves for the first harmonic indicated the general direction of cloud development. Because of the predominance of that component, it can be inferred from the polar diagram that the preferred direction of major cloud concentration and development is the SW-SE direction (especially near the center) during the early stages. As the cyclone matured, the direction of major cloud development shifts N-NE. The inspection of the sequence of curves for the first harmonic in the polar diagram indicated a cyclonic rotation of the portion of the curves near the center of the cyclone, while the portion of the curves further away from the center tended to recede in general.

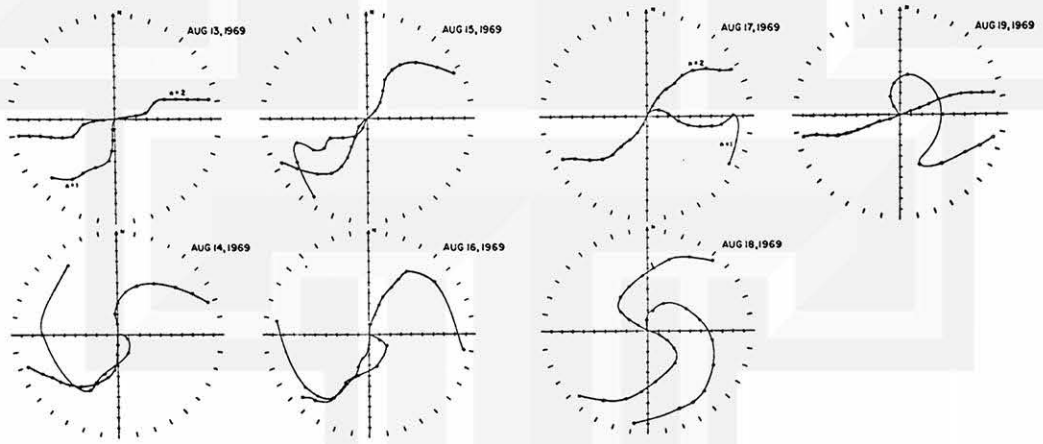

Fig. 31. Polar diagram showing phase curves obtained from the harmonic analysis of satellite-observed cloud cover of hurricane Debbie, August, 1969.

The same observation is noted for the curves for the second harmonic. One important feature of the curves for the second harmonic is that they closely indicate the general orientation of the cloud patterns at all stages more closely than those of the first harmonic.

(b) Hurricane Holly

(i) Distribution of cloud cover. -- The sequence of cloud patterns analyzed were shown in Figure 25. Figure 32 shows the mean cloud cover and the relative standard deviation as functions of distances from the center of Hurricane Holly. The graphs, especially those for the 15th and 17th of September, show that the major cloud cover at outer radii were very localized. Spasmodic development of clouds during the life-time of the cyclone reflected the unfavorable environment in which it developed. This behavior is depicted in Figure 33. The photograph of the cyclone for the 17th of September shows that the cloud cover has dissipated appreciably by that time.

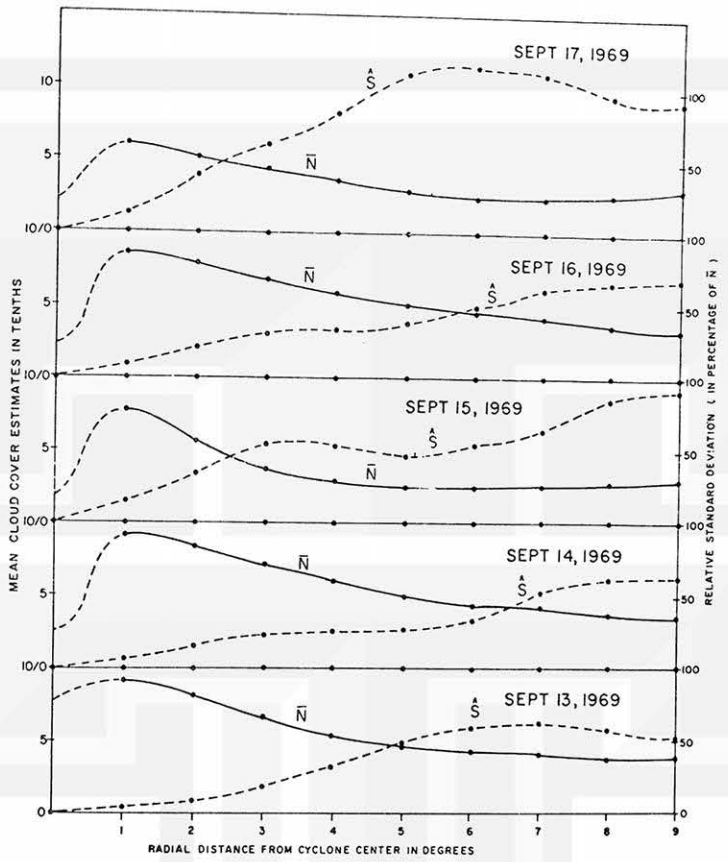

Fig. 32. Mean cloud cover estimate N and relative standard deviation in Hurricane Holly, September, 1969, as function of radial distances and time.

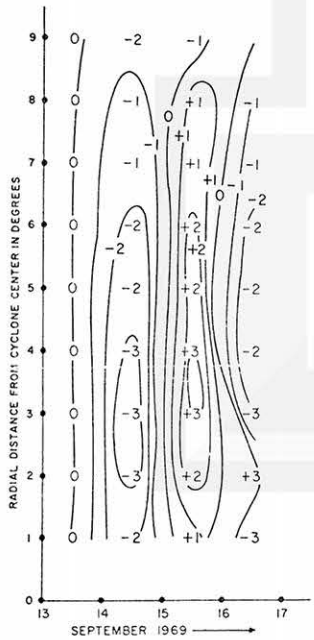

Fig. 33. Daily changes in cloud cover estimates at various radial distances and time for Hurricane Holly, September, 1969.

The distribution of the frequency of the cloud cover amounts follow the same general pattern as for Hurricane Debbie. Figure 34 shows the variations of r_N values, as the cyclone develops. The curves follow the general pattern as those for Hurricane Debbie. The distribution of $\hat{H}$ and $\hat{\eta}_r$ as functions of harmonic component and radial distances is shown in Tables 2 and 3, Appendix I.

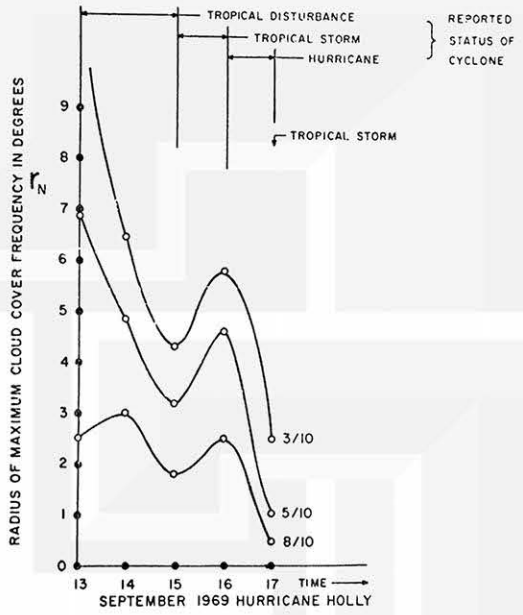

Fig. 34. Graphs showing variation of r_N with time for N equal to three-, five-, and eight-tenths for Hurricane Holly, September, 1969.

(ii) Harmonic analysis of cloud cover. -- As in the case of Hurricane Debbie, the first and the second harmonic are the most predominant for most of the cloud patterns. with the third harmonic showing some prominence at radial distances further away from the center of the cyclone, especially on the 15th and 17th of September. The relative importance of $\hat{H}$ and $\hat{\eta}_r$ for Hurricane Holly is shown in Tables 4 and 5 in Appendix I.

The polar diagrams showing the amplitude and phase for Hurricane Holly are shown in Figure 35, for the different cloud patterns. The same general comments apply for these curves as for Hurricane Debbie.

(c) Typhoon Cora (August 1969)

For comparison with the hurricanes of the Atlantic, the cloud pattern of some typhoons during the typhoon season of 1968-1970 were analyzed. The results for one of those typhoons are presented in Figures 36-39. In comparing these figures with those obtained for the Atlantic hurricanes, many common features of the cloud patterns were noted. The similarities in the patterns of clouds in tropical cyclones and the implications of the results obtained in the analysis of the three tropical cyclones are discussed in Chapter Seven.

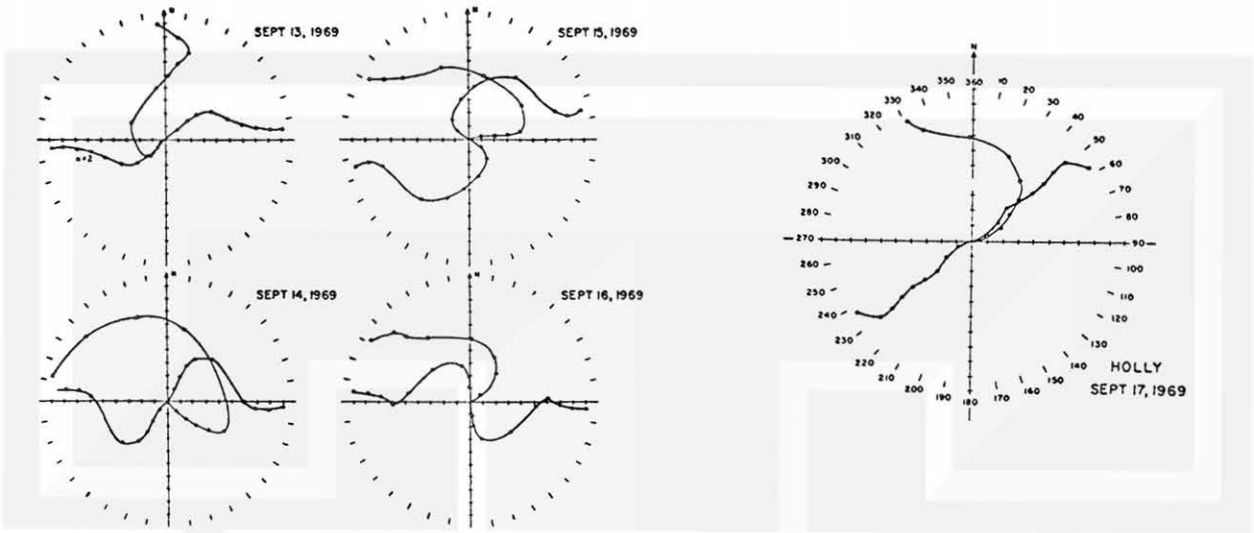

Fig. 35. Polar diagram showing phase curves obtained from the harmonic analysis of satellite-observed cloud cover estimates for Hurricane Holly, September, 1969.

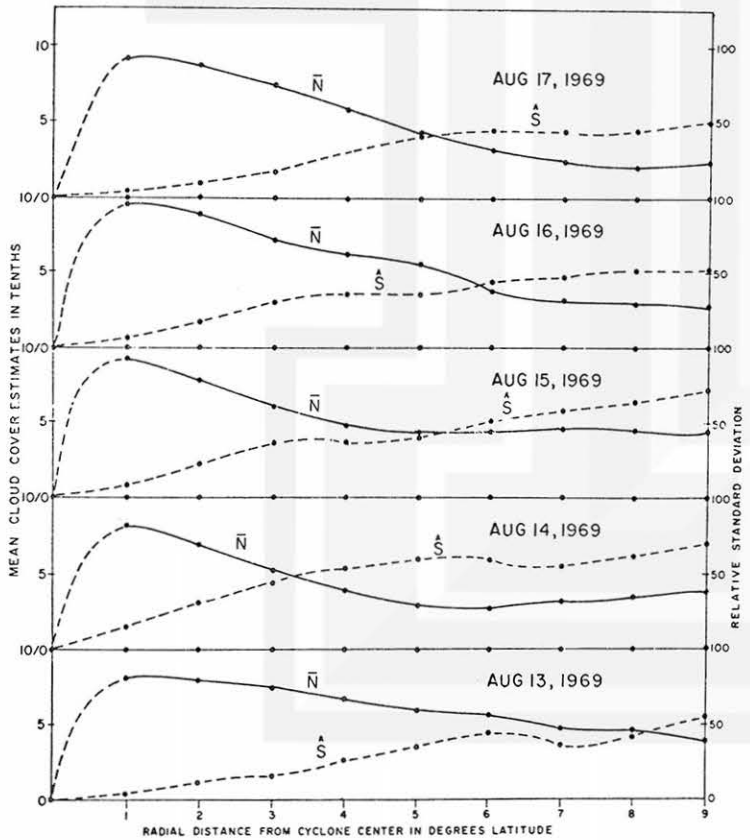

Fig. 36. Mean cloud cover estimate and relative standard deviation s in typhoon Cora, August, 1969 as function of radial distances.

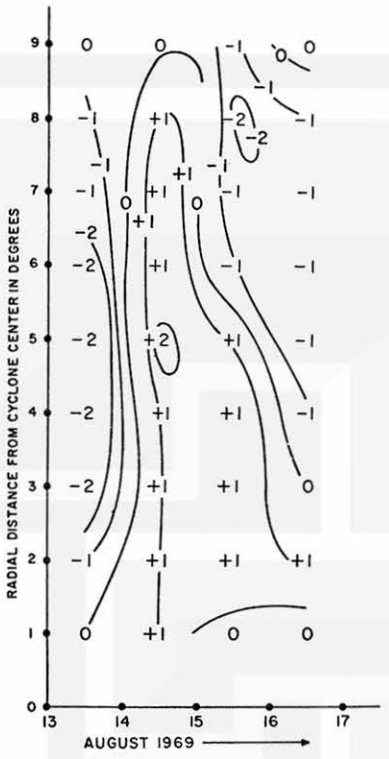

Fig. 37. Daily changes in cloud cover estimates at various radial distances for typhoon Cora, August, 1969.

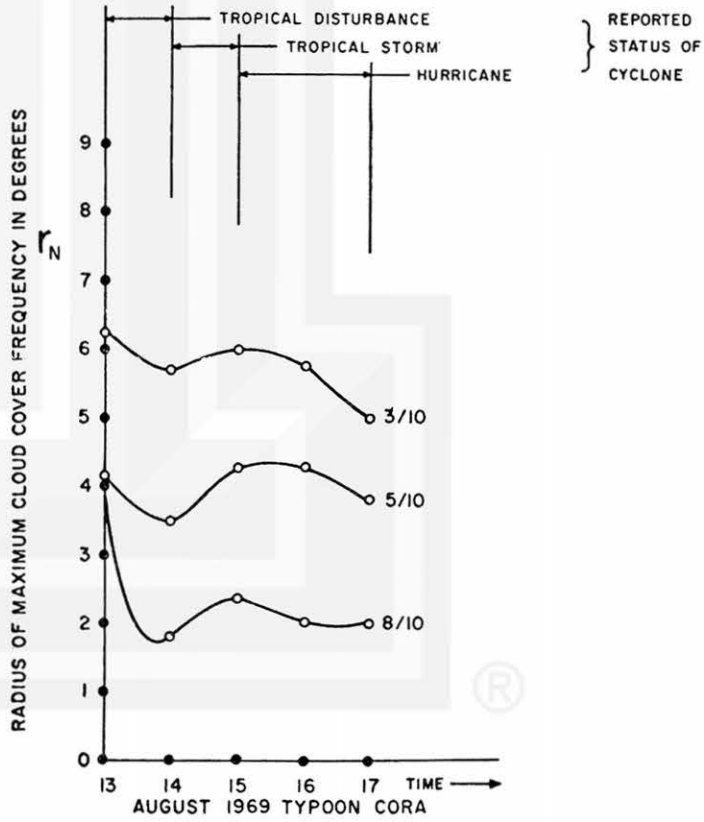

Fig. 38. Graphs showing variation of r_N with time for N equal to three-, five-, eight-tenths for typhoon Cora, August, 1969.

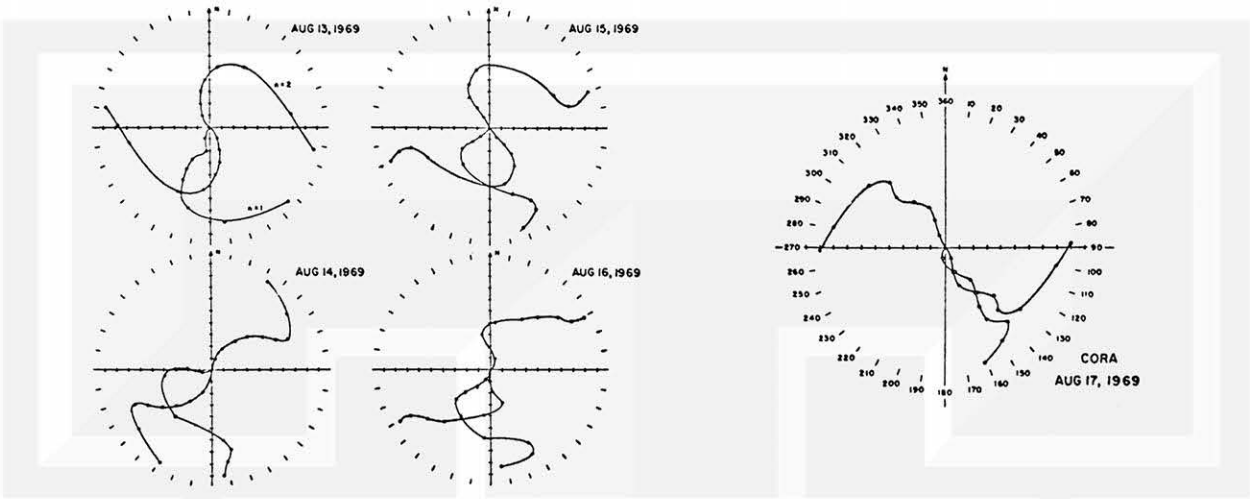

Fig. 39. Polar diagram showing phase curves obtained from harmonic analysis of satellite-observed cloud cover estimates for typhoon Cora, August, 1969.

(d) Further comments on the harmonic analysis of the satellite-observed cloud cover of tropical cyclones

(i) Origin of data points along concentric circles. -- In the harmonic analysis of the thirty-six equally spaced points on every circle drawn on each photograph, the azimuth distances have been measured from the true north and the point on each circle in the direction of the true north has been chosen as the origin of the thirty-six points. The direction of the true north has been chosen as the reference direction instead of the direction of motion of the cyclone for the following reasons:

The origin of the data points is immaterial as far as the amplitudes of the harmonic components are concerned. Regardless of the position along a particular circle chosen as the origin of the data points, the amplitudes of the data points still come out the same for that circle. Choosing a consistent direction, however, facilitates computation and avoids the necessity of changing the origin of the data points along the circles each time the cyclone changes its direction of motion. Secondly, since the information about the direction of motion of the cyclone is usually given in general terms (e. g. NW or NNW), except when the cyclone is investigated by a research aircraft, such information may be in error up to 20° azimuth. Errors in the direction of motion may, therefore, make the comparison of computed phase angles from one photograph to the other very difficult. The adoption of the true north as a reference direction makes the comparison of the phase angles easier. It may, however, make it impossible to isolate the changes in the phase angles due to the changes in the direction of motion of the cyclone from changes in the phase angles due to the rotation of the entire cloud pattern. This investigation has proceeded on the assumption that the

rotation of cloud patterns is independent of the direction of motion of the cyclone system. The definite shift in the phase angles for the analysis of the cloud patterns of hurricane Debbie on the 16th of August 1969 when the direction of motion of the cyclone was fairly constant supports this assumption.

(ii) Errors in the location of the origin of the polar diagrams drawn on the cloud patterns. -- The origin of the polar diagrams imposed on the cloud patterns of the tropical cyclones has been located at the reported (given by the U. S. Weather Bureau) center of the circulation accompanying the cyclone cloud pattern or at the eye of the cyclone when this is visible from the photographs. The center of the cyclone is determined from various sources, (e. g., aircraft reconnaissance reports, ship reports, from computation of the flow field accompanying the cyclones etc.) and it is assumed to be correct to within half a degree. There is no doubt that large errors in the location of the origin for the harmonic analysis computations will lead to errors in the amplitudes of the components. A nearly circular cloud pattern of a tropical cyclone in which the center of the cloud system has been correctly placed should be described only by the zeroth harmonic component. A small error in the location of the origin for such a case will show amplitudes for the first component especially at some distances away from such an origin. Quantitative estimates of such errors have not been carried out in this investigation mainly because considerable efforts have been made to place the origin correctly in each cloud pattern of tropical cyclones investigated. Errors that may arise from incorrect location of the origin are therefore considered small.

CHAPTER VII

PHYSICAL INTERPRETATION OF RESULTS

Because of the various shortcomings discussed earlier in the use of satellite photographs as basic tools in meteorological research, considerable caution must be exercised in making conclusions about the characteristics of the tropical cyclones from the satellite observed cloud patterns. Conclusions are only stretched to the extent that makes the present approach to the study of satellite observed cloud patterns of tropical cyclones useful.

In the following sections, some information about tropical cyclones provided by satellite photographs which are not obvious by mere observation of the photographs but which facilitate the understanding of some characteristics of tropical cyclones are discussed.

7.1 The distribution of the quantitative estimates of the satellite-observed cloud cover

The daily or hourly gain or loss in cloud cover estimates at various radial distances rarely exceeds three-tenths (Figs. 30, 33, 37). In fact, the extreme case of three-tenths change in cloud cover estimates are observed in tropical cyclones with rather precarious development as exemplified by the change in cloud cover estimates with time for Hurricane Holly, September 1969. The tropical cyclone had barely reached hurricane strength when she degenerated into a tropical depression. The pattern of changes in cloud cover estimates for Holly should be compared with those of Debbie and Cora (Fig. 30 and Fig. 37). In the case of the latter cyclones, less fluctuations are observed in the changes of the satellite-observed cloud cover. During the period of rapid growth -- August 16th and 17th for Debbie and August 14th and 15th for Cora -- an increase of one to two-tenths in the cloud cover estimates are shown for both cyclones. A general statement that can be made from the observation of the daily and hourly changes in the mean cloud cover estimates is that, although cloud production takes place continuously, during the life cycle of a cyclone, clouds grow and dissipate within the cyclone system at such rates that make the net changes in the cloud cover estimates small and gradual. Sudden and explosive development of tropical cyclone cloud cover was not observed during the course of this investigation. Very pronounced decrease or increase in the cloud cover estimates of a tropical cyclone can be attributed to the influence of other atmospheric systems (mostly of extra-tropical origin) on the tropical cyclone system.

Negative changes in the cloud cover estimates often take place at the outermost regions of the cyclones, especially during mature stages. This is indicative of the subsidence which is assumed to be taking place in those regions during those stages.

(a) The variation of cloud cover estimates about the center of the cyclone

The spread of the frequency distribution of cloud estimates values in Figures 17 and 28 clearly shows that (less markedly at radial 1° - 3° from the cyclone center) the cloud amount was not uniformly distributed azimuthally at all radial distances from

the center of the cyclone. This fact is obvious in certain cases from viewing actual photographs. However, a quantitative estimate of the variation of the distribution of the satellite observed cloud cover is made in this study by computing a parameter defined as follows

$$V_r = \frac{N_{max} - N_{min}}{\overline{N}}$$

where

V_r = the parameter measuring the variation of the satellite observed cloud cover at radial distances r from the cyclone center

N_{max} = the maximum cloud cover estimates at radius r from the cyclone center

N_{min} = the minimum cloud cover estimates at radius r from the cyclone center

$\overline{N}$ = the mean cloud cover estimates at radius r from the cyclone center

Figure 40 shows the distribution of V_r as functions of radial distances and time for the three tropical cyclones discussed. From these figures, the azimuthal distribution of the cloud cover estimates appears more uniform at distances close to the center of the cyclone than at outer distances.

While the variation parameter as computed indicates the non-axis symmetric character of the distribution of cloud estimates, a quantitative measurement of the non-axis symmetric character of the satellite observed cyclone cloud cover is better obtained in terms of the first harmonic component. The amplitudes of this fundamental component indicate the azimuthally varying nature of distribution of cloud in the cyclone cloud pattern. Moreover, the first harmonic component accounts for a large amount of the variance of clouds along most of the concentric circles drawn around the cyclone center. The graphical addition of the amplitudes of this component to the mean cloud amount at each radial distance from the cyclone center also yields a cloud field which approximates the original cloud field as shown by figures in Appendix II.

A quantitative measure of the non-axis symmetry of the cloud distribution is therefore given by a parameter, a_r, defined as the ratio of the amplitude of the first harmonic component to the mean cloud amount at a radial distance, r, from the center of the cyclone. The character of the curves of a_r (Figures 41-43) drawn as a function of radial distance from the cyclone center, changes with the stage of development of the cyclone. The quantity a_r has a maximum close to the center of the cyclone at the initial stages of the cyclone, but the location of this cyclone moves outward as the distribution of the cloud becomes more symmetric with respect to the center of the cyclone. This indicates that at early stages of tropical cyclones more cloud and hence more vigorous vertical motion is located in a particular azimuthal direction but then spreads completely around the center of the cyclone as the cyclone develops. The mechanism of the redistribution of vertical motion is not very clear.

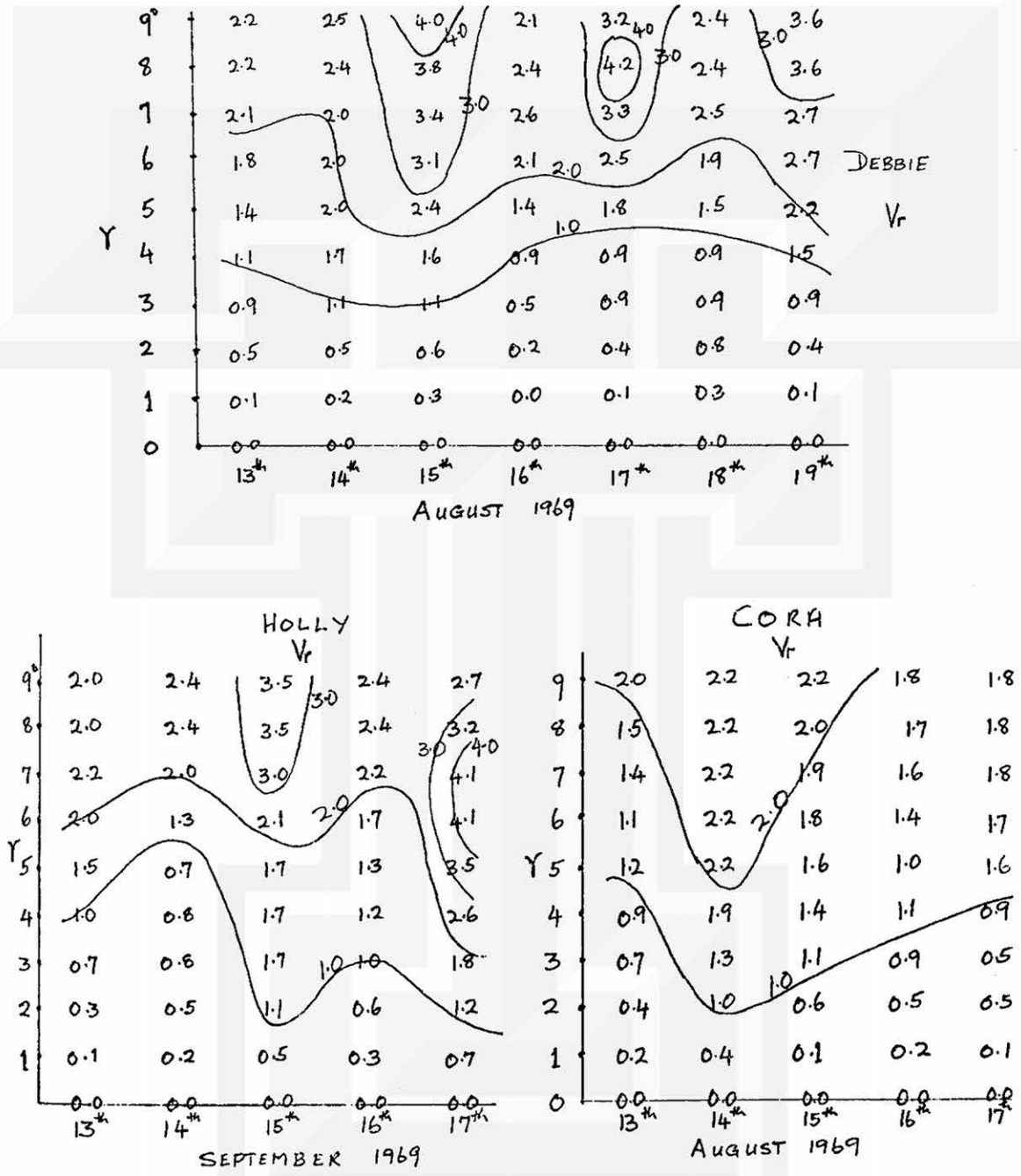

Fig. 40. The variation of parameter V_r of cloud cover estimates for the three cyclones as function of radial distance and time.

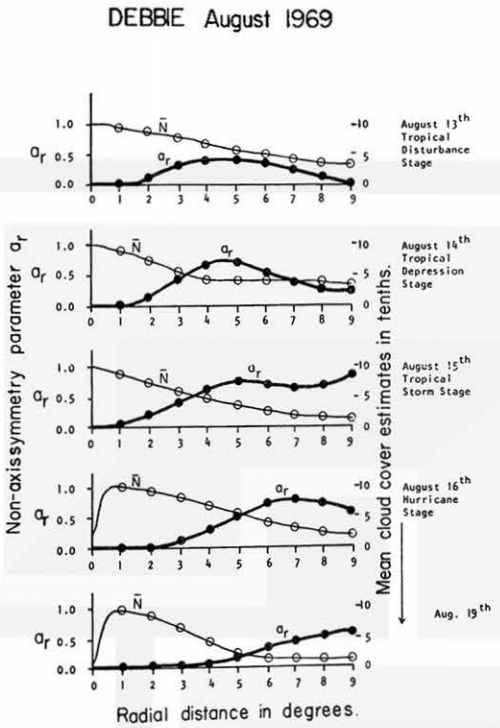

Fig. 41. Asymmetry parameter a_r as function of radius and time for hurricane Debbie, August, 1969.

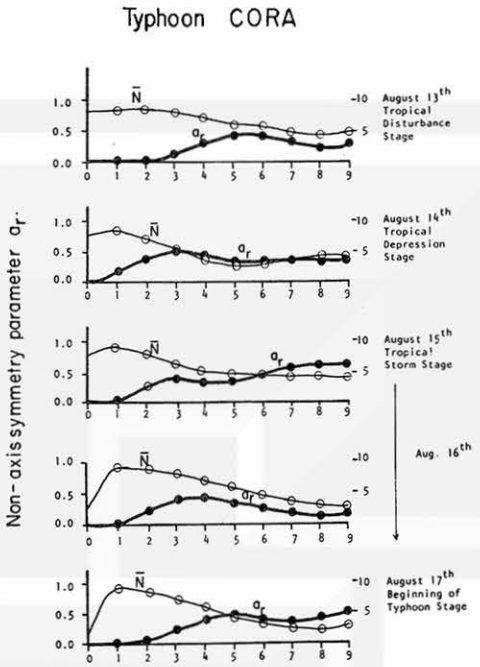

Fig. 42. Asymmetry parameter a_r as function of radius and time for typhoon Cora, August, 1969.

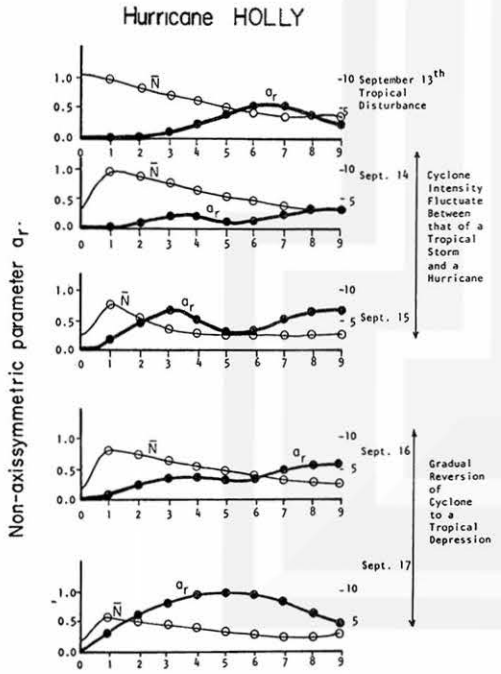

Fig. 43. Asymmetry parameter a_r as function of radius and time for hurricane Holly, September, 1969.

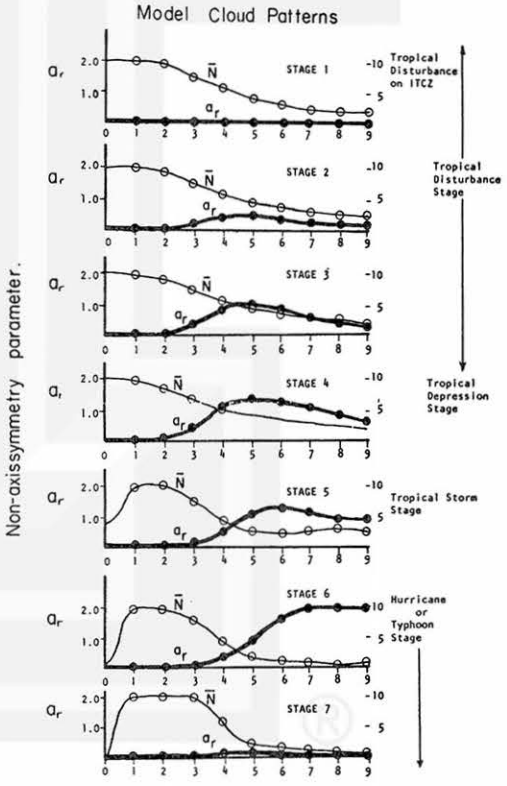

Fig. 44. Asymmetry parameter a_r as function of radius and stage of development for model cloud patterns.

(b) The relationship between the mean of cloud estimate and the most frequent cloud estimate

If, at any particular radial distance from the center of the cyclone, the distribution of the cloud estimates is normal, then the mean cloud estimate at that distance should be the most probable value of the cloud estimate. The most probable values of cloud estimates at each radial distance lie along the axis of maximum frequency of cloud estimates (Figures 17 and 28). Rather than comparing the mean cloud estimate with the most probable cloud estimate at every radial distance, comparison is made between the radius $r_{\bar{N}}$, the radial distance at which a specified mean cloud cover estimate (determined from graphs showing variation of $\bar{N}$ with radius) obtains in a particular cyclone pattern, with r_N , the radius of maximum frequency of cloud cover estimates corresponding to the specified mean cloud cover estimate $\bar{N}$. Such comparison is shown in Figure 45. The tables in the figure indicate that there are differences

DEBBIE
AUG. 16th 1969
1233Z - 1930Z

N	TIME	1233Z	1337Z	1454Z	1559Z	1650Z	1741Z	1930Z
8/10	$r_{\bar{N}}$	2.5	2.8	2.5	3.0	2.5	3.0	3.5
	r_N	3.0	3.0	2.5	3.0	3.0	3.5	4.0
5/10	$r_{\bar{N}}$	5.0	5.0	5.0	5.0	5.0	5.5	6.0
	r_N	4.5	4.5	5.0	5.0	4.7	5.0	5.0
3/10	$r_{\bar{N}}$	7.5	7.5	7.0	7.0	6.8	7.5	7.5
	r_N	7.0	7.0	7.0	7.0	7.0	6.5	6.0

DEBBIE
AUG. 13th - AUG 19th
1969

N	TIME	13th	14th	15th	16th	17th	18th	19th
8/10	$r_{\bar{N}}$	2.3	1.2	1.0	3.2	2.5	1.8	2.0
	r_N	7.0	1.2	1.5	3.0	3.5	2.0	2.0
5/10	$r_{\bar{N}}$	6.0	3.5	3.8	5.8	5.0	5.0	3.3
	r_N	4.0	3.0	3.0	5.5	5.8	5.5	3.5
3/10	$r_{\bar{N}}$	9.0	9.0	5.5	7.5	6.8	7.0	4.5
	r_N	6.5	5.0	4.0	6.0	7.0	7.0	4.8

HOLLY
SEPT. 13th - SEPT. 17th
1969

N	TIME	13th	14th	15th	16th	17th
8/10	$r_{\bar{N}}$	2.0	2.3	1.0	2.0	<1.0
	r_N	2.5	2.5	1.5	2.2	<1.0
5/10	$r_{\bar{N}}$	4.5	2.5	1.6	2.2	<1.0
	r_N	7.0	5.0	2.2	5.0	2.0
3/10	$r_{\bar{N}}$	>9.0	>9.0	4.0	9.0	4.7
	r_N	>9.0	6.5	4.2	6.0	2.5

CORA
AUGUST 13th - AUG. 17th
1969

N	TIME	13th	14th	15th	16th	17th
8/10	$r_{\bar{N}}$	2.5	1.3	1.7	2.7	2.7
	r_N	1.5	1.9	2.5	2.0	2.0
5/10	$r_{\bar{N}}$	7.0	3.5	3.7	5.5	4.5
	r_N	4.3	3.5	4.3	4.3	4.0
3/10	$r_{\bar{N}}$	>9.0	5.0	9.0	7.0	6.5
	r_N	6.0	5.7	6.0	5.5	5.0

Fig. 45. Comparison of r_N radius of maximum frequency of estimated cloud cover N and the radius $r_{\bar{N}}$ at which a mean cloud cover estimate of value $\bar{N}$ equal to N exists.

in many corresponding values of $r_{\bar{N}}$ and r_N for the specified values of N. There is, however, good agreement in many cases. Possible explanations of the disparity or similarity in the values of $r_{\bar{N}}$ and r_N are as follows: Since the cloud producing processes in a tropical cyclone are not usually independent of each other, one must not expect agreement between $r_{\bar{N}}$ and the corresponding r_N for the same value of satellite observed cloud cover, N. In cases where there are appreciable differences, it can be assumed that the azimuthal distribution of clouds are not normal. It is observed that when the cyclone is in a temporary or permanent steady state, for example during August 18th and 19th for Hurricane Debbie, there is good agreement between $r_{\bar{N}}$ and r_N. Sometimes compensatory interdependence exists between the factors responsible for the production and dissipation of clouds so that on the average, positive and negative factors cancel. In such cases, a specified mean cloud cover estimate N is therefore the most probable cloud cover estimate $r_{\bar{N}}$, and the corresponding r_N coincide. The azimuthal distribution of cloud estimate is therefore near normal in such situations.

(c) The relationship between satellite observed cloud cover of tropical cyclones and the intensity of the cyclone

In the atmosphere, the presence of large scale vertical motion is indicated by clouds. The relationship between ascending motion in tropical cyclones and the cloud cover of the cyclones is therefore more direct than the relationship between the cyclone intensity (determined by the strength of the tangential winds) and the cloud cover. Recent theoretical investigations into the relationship between the tropical cyclone and the cloud cover were based on computing the vertical and radial motions for a cyclone from specified tangential wind distributions using the equations of motion, and then correlating the computed motions with the cloud cover. Such theoretical investigations have shown qualitatively that strong tangential winds could be associated with strong and extensive upward motion, but the theoretical models are so far not realistic enough to quantify the relationship between upward motion in tropical cyclones and the cloud cover.

In this study, changes in the intensity and areal coverage of satellite observed cloud cover over a tropical cyclone are related to its reported stage of development as given by the U.S. Weather Bureau. A helpful parameter used in doing this is r_N, defined as before as the radial distance from the cyclone center where a specified satellite observed cloud cover estimate N (in tenths) is most frequent. Three concentric circles along which the most frequent cloud cover estimates are chosen are respectively, eight-tenths, five-tenths, and three-tenths. The radii of the three circles are then identified, respectively, as r_3, r_5, and r_8. The changes in the sizes of these circles (that is, changes in the $r_{N's}$) are then studied as the cyclone changes in intensity. A change in r_N with time indicates a change in a circular area inside which values of satellite observed cloud cover N or more are most frequent. The fact that some cyclones develop an eye where cloud estimate is zero does not change the definition of r_N.

Figures 18, 29, 34, and 38 show the change in r_N as the cyclone develops. The changes in the spacing between the curves indicate the changes in the gradient of cloud intensity with respect to radial distances from the cyclone center. Another feature of the curves is that the r_N decreases during the tropical disturbance and tropical depression stages of the cyclone (stages are determined from the U.S. Weather Bureau

reports). When cyclones attain the states where they are regarded as tropical storms, the $r_{N's}$ increase and then decrease soon after the cyclones become a hurricane or a typhoon.

Observation of satellite photographs shows that the cloud structure of a cyclone as observed by the satellite changes as the cyclone develops. At the initial stages the clouds are usually of cumuliform structure with little or no cirrus canopy. At the time of rapid intensification, the internal cloud structures are hidden by the cirrus clouds produced by cumulus towers. At this stage, the cloud estimate is determined essentially by the cirrus shield. Since different locations of the cirrus shield exhibit varying amounts of whiteness depending upon whether cumulus clouds are immediately below at those locations, varying photometer readings are still obtained at different parts of the cirrus shield.

From Figures 29, 34 and 38, it is quite clear that the life circle of a tropical cyclone can be divided into three major stages, viz: the development stage, the intensification stage, and the hurricane or typhoon stage. The general decrease during the development stage indicates that the production of cloud is being concentrated into a smaller area as moist air converges on a large scale towards the center of the growing cyclone. Therefore, there is an aggregation of cumulus type clouds into the small area at this stage of development.

Frictional convergence of moist air is the mechanism, Charney, et al. (1964), believed to be responsible for the forced ascent of air parcels in the synoptic scale organization of upward motion in a tropical cyclone. The ordinary conditional instability has been found to be incapable of explaining the synoptic scale organization of motion, as the mechanism only leads to the formation of motion on the scale of individual cumulonimbus clouds. Unless the flow pattern over the ocean provides the dynamical conditions for wider up current, than those of ordinary cumulonimbus, no tropical cyclone can form. The necessity for a large region of low level convergence at the initial stages of tropical cyclone formation is emphasized by the observation that the relative humidity in the tropical atmosphere is about 80 percent, even in the boundary layer. Large scale low level convergence provides forced ascent of moist air which subsequently condenses and provides the latent heat necessary for the growth and the maintenance of the tropical cyclone.

By visual inspection of satellite photographs, it is impossible to distinguish between the tropical disturbance (indicated by the presence of cloud clusters) which will later develop into a tropical cyclone and those that will not. This study suggests that any consistent tendency of a group of cloud clusters to concentrate into a smaller area may be indicative of the likelihood that the cloud clusters may develop into a tropical cyclone. However, more research is needed to clarify all the conditions under which a tropical cyclone develops from the clusters.

A form of the vorticity equation can be used to relate qualitatively the changes in the values of r_N to the changes in the dynamics of the developing cyclone. Vorticity in the atmosphere and the divergence produce and shape the cloud patterns. The vorticity equation can be written as:

$$\frac{d}{dt}(\zeta + f) = -(\zeta + f)\nabla_h \cdot V_e \qquad 7.1(i)$$

where f = coriolis parameter

ζ = relative vorticity

$\zeta_a = \zeta + f$ the absolute vorticity

$\nabla_h \cdot V_e$ = horizontal velocity divergence

$\frac{d}{dt}$ = total differential with respect to time .

In this formulation, the terms representing the vertical vorticity arising from vertical motion gradients and the solenoidal terms representing the baroclinicity arising from horizontal density gradients have been neglected. For large scale processes in the tropics, these terms are at least one order of magnitude less than the terms shown in expression 7.1 (i). The expression can be rewritten in the form that defines the divergence with respect to a given area occupied by clouds. The definition relates the percentage change of the horizontal area A_r occupied by the cloud mass, to the divergence of clouds that is

$$\nabla_h \cdot V_e = \frac{1}{A_r}\frac{dA_r}{dt} . \qquad 7.1(ii)$$

$\nabla_h \cdot V_e$ may be regarded here as cloud divergence and the term on the right hand side is the percentage change of the horizontal area with time, occupied by clouds. The expression 7.1 (ii) is customarily employed in estimating the rate of change of cirrus shield over cumulonimbus clouds with time. In this instance the expression is used to show the change of a general cloud area with time. 7.1 (i) can then be rewritten as

$$\frac{1}{\zeta_a}\frac{d}{dt}\zeta_a = -\frac{1}{A_r}\frac{dA_r}{dt} . \qquad 7.1(iii)$$

The parameter r_N derived from the computation on the cloud cover can be identified with horizontal area A_r equal to πr_N^2 at the initial stages of the development of the cyclone.

The introduction of πr_N^2 in equation 7.1 (iii) yields

$$\frac{1}{\zeta_a}\frac{d}{dt}\zeta_a = -\frac{2}{r_N}\frac{dr_N}{dt} .$$

At the initial stages $\frac{dr_N}{dt}$ is negative. This means that the fractional change in absolute vorticity with time is positive at those stages. The decrease in r_N can, therefore, be identified with the gradual development of the vortical structure of the cyclone.

Synoptic experience (through cross section analysis and aircraft observation) indicates that the cyclone structure at the stages described above has a cold core area of shower activity. The coolness of the lower regions of an incipient tropical cyclone has been attributed to evaporation of rain with a descent of air with low θ_e from middle levels in the general area of cyclone development. As moist air continues to converge into vertical columns in the general area of the incipient cyclone, moisture condenses out as rain and the latent heat released is distributed in the vertical. The source of energy for the maintenance of the tropical cyclone is the latent heat due to the moisture which frictional convergence supplies to the vertical columns. The cyclone then gradually develops into a warm core system. To a good approximation, the radial force balance in the cyclones at this stage satisfies the gradient wind relationship. With the warm core cyclones, the radial pressure gradient decreases upwards and rising air is brought to a level where the centrifugal and coriolis forces corresponding to their initial momentum overbalances the weaker pressure gradients aloft and therefore must move outwards. This phenomenon is reflected in satellite photographs by the development of cirrus canopy over the cyclone system.

From Figures 29, 34 and 38 the increase in r_N at this stage expresses quantitatively the expansion of the cirrus shield. The cyclone becomes a warm core system at approximately the time the cirrus canopy covered the storm system. The expansion of the cirrus canopy continues until the winds in the cyclone system attain hurricane strength. The decrease in the cirrus canopy as cyclone becomes mature is manifested in the decrease of r_N in Figures 29, 34 and 38. The decrease in r_N is evidence that at mature states the tropical cyclone has become more compact and has also modified its environment. The clear zone which usually surrounds the cyclone at this stage is evidence that downward motion is occurring at the periphery of the cyclone. The downward motion is the outer column (although less organized) of the thermally direct circulation which is an important feature of the tropical cyclone.

From the foregoing, two conclusions can be made concerning the relationship between the intensity of the tropical cyclone and the satellite cloud cover of the cyclone.

First, the values of r_N vary in the same manner for all tropical cyclones studied, but the values of r_N are not necessarily the same for the same stage of development of all the cyclones. This fact emphasizes the difficulty encountered in the process of developing a useful relationship between the cloud patterns of tropical cyclones as shown in satellite pictures and their maximum wind speed. Some researchers (e.g., Fritz et al., 1966), established some relationship between cloud patterns and the intensity of cyclones which permits the estimation of the intensity of the tropical cyclone from the satellite-observed cloud patterns alone. The relationship often underestimated the intensity of the cyclone when used with independent data, partly because the photographs used in establishing the relationship for the various levels of cyclone intensity were from different cyclones, and partly because of the considerable subjectivity in the determination of the cloud pattern sizes and 'category' of the cyclones. These rendered the relationship between cloud patterns and intensity of cyclones developed by Fritz and others, only of limited use. Direct proportionality between the intensity of cyclone and the size of the cirrus shield, seem only likely during the period of rapid intensification. Before and after this period such direct proportionality does not exist.

Secondly, observations of cloud patterns during the course of this study suggest that three major 'species' of tropical cyclones can be classified. Those whose patterns are small and remain so during their lifetime. Their r_N values are small but still vary with their intensities. Those whose cloud patterns are large, that is, characterized by large cirrus shield during their intensification and mature stages, and those that may be classified as 'run of the mill' cyclones, with moderately sized cloud patterns.

7.2 Interpretation of amplitudes and phases of the harmonic components obtained from the harmonic analysis of the satellite observed cloud patterns

The application of the principles of harmonic analysis to the study of the cloud distributions in the patterns of clouds exhibited by tropical cyclones as seen from satellite photographs provides a statistical method for determining the deviation from the mean of the cloud cover estimates (determined as explained in earlier chapters) along a concentric circle drawn around the centers of the cyclones. The positions along the circles (relative to the North) at which the deviations are most pronounced are also indicated by the method.

The distribution of amplitudes and phase spectrums has been computed up to wave number four for every circle. These spectrums are discrete line spectrums and hence have meanings only for discrete integer values of wave numbers. Shown in Appendix I, Tables 2 to 7 are the amplitudes expressed as percentages of the mean, and the percentage variance of cloud cover accounted for, by each harmonic component for the various cloud patterns of the tropical cyclones analyzed. Further discussions of these amplitudes and the corresponding phase angles are given in subsequent paragraphs.

(a) The distribution of amplitudes

Tables 2, 4 and 6 in Appendix I show the distribution of amplitudes $\hat{H}_n$ expressed as percentages of the mean for the series of photographs of the three tropical cyclones discussed in this investigation. From these tables, it is clear that the first and the second harmonic components are the most prominent. Tables 1, 3, 5, and 7 show the percentage of variance of the cloud cover accounted for by each harmonic component for the photographs analyzed. The first and the second harmonic components account for more than seventy-five percent of the total variance of cloud cover, especially within the radial distance six degrees from the center of the cyclone. In many instances, the two components account for better than ninety percent of the total variance of the cloud amount at all radii distances. At distances beyond seven degrees, there are sometimes large contributions to the total variance of cloud cover estimates from the third harmonic. Such contributions at those distances from the center of the cyclone are assumed to be either due to the presence of clouds unrelated to the cyclone system, or due to the fact that cyclone related clouds are less organized at those distances.

Since the behavior of the actual cloud field in the cyclone cloud pattern is similar to the behavior of the field obtained by adding graphically the amplitudes of the first harmonic to the mean cloud field (Appendix II), the cyclone cloud structure can be characterized by the first harmonic during most of its life time as explained in the

previous section. When the incipient cyclone lies totally within the I. T. C. Z. cloudiness, there is little or no contribution from the first component. In this case, the second harmonic is the most dominant. The amplitudes of the second harmonic have the largest magnitudes when the incipient cyclones are along the I. T. C. Z. and diminishes as the cyclones move out of the cloud band. There is, however, a substantial contribution from this component throughout the life time of the cyclones.

(b) The distribution of phase angles

The azimuth distances in degrees from the North, on each circle drawn on the photographs, at which the maximum amplitude of cloud cover exist for the different components are interpreted as the phases of the cloud distribution for that component. For each of the cloud patterns, a curve is drawn to connect all the phase positions at all the radial distances from the center of the cyclone. The shift in the position of the curves, referred to as 'phase curves', from one pattern to another for a tropical cyclone, is studied with a view to understanding the relationship between the shift in the phase curves which are here identified with cloud bands in the hurricane system and the air motion in a hurricane system. From the series of photographs for a particular cyclone, the phase curves for the first and second harmonics are drawn separately. Figures 46 and 47 show the curves from hourly analysis of the ATS photographs for Hurricane Debbie. Figures 48-50 show such curves for the three tropical cyclones studied.

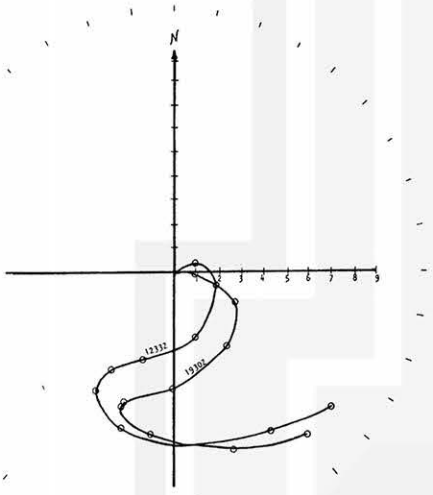

Fig. 46. Polar diagram showing lines joining the phase angles for the first harmonic component at various radial distances from cyclone center at 1233 Z and 1930 Z on August 16, 1969 for hurricane Debbie.

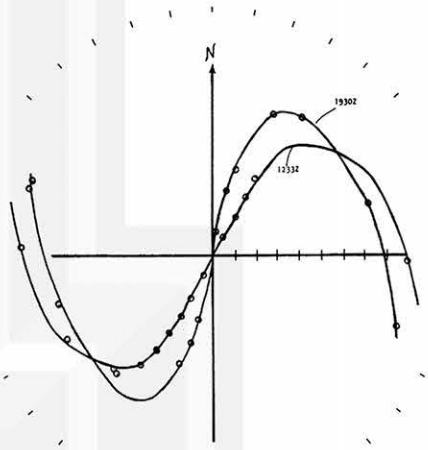

Fig. 47. Polar diagram showing lines joining the phase angles for the second harmonic component at various radial distances from cyclone center at 1232 Z and 1930 Z on August 16, 1969 for hurricane Debbie.

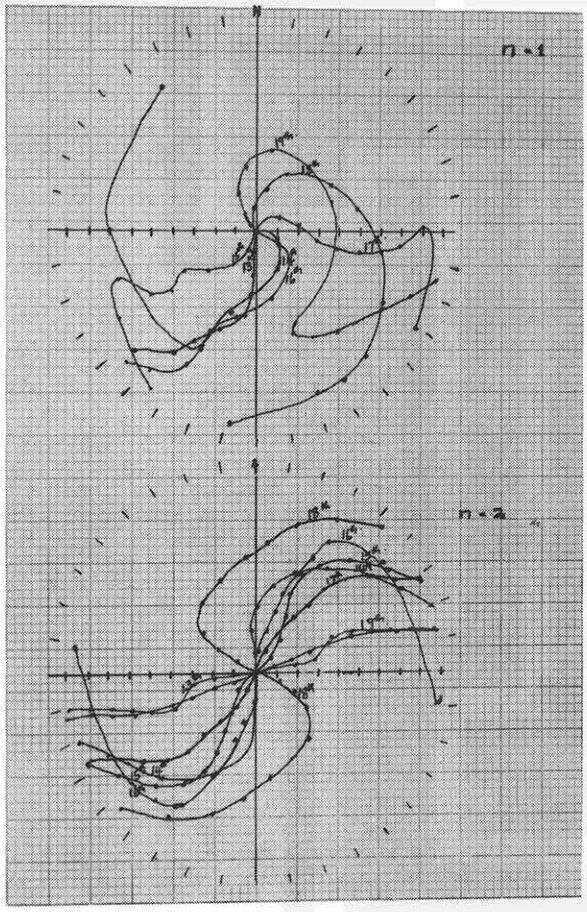

Fig. 48. Phase curves for the first and the second harmonic components for hurricane Debbie.

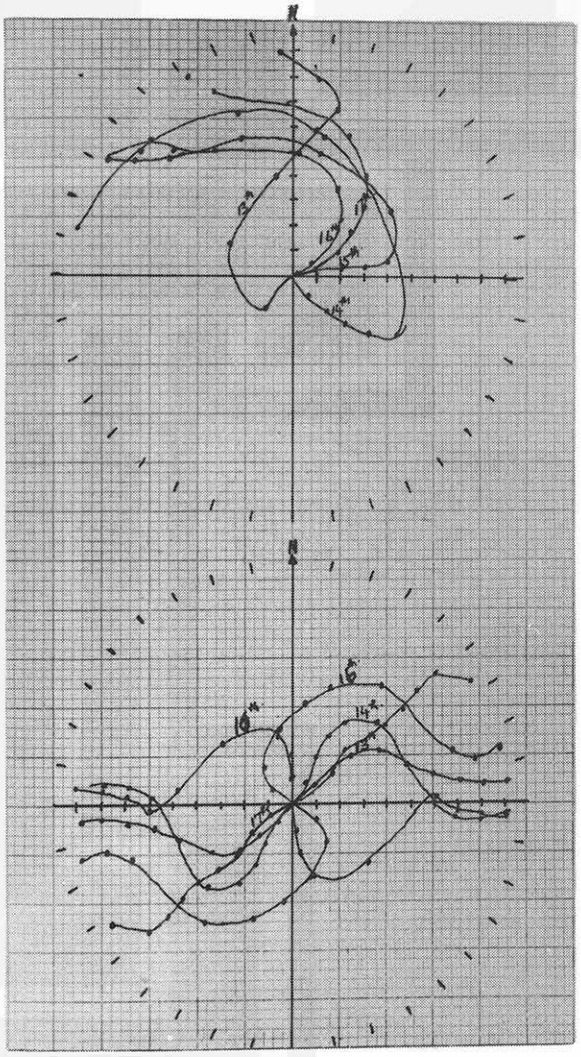

Fig. 49. Phase curves for the first and the second harmonic components for hurricane Holly.

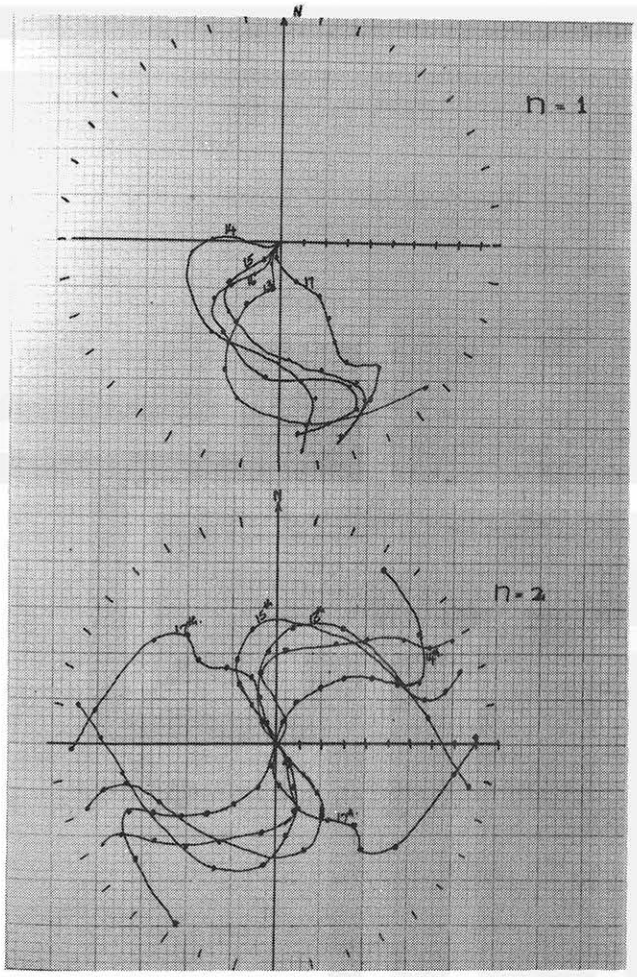

Fig. 50. Phase curves for the first and the second harmonic components for typhoon Cora.

Before further discussions on the relationship between the shift in the phase curves and the air motions in a hurricane system, it is necessary to discuss the various scales of motion in the tropics so that the relationship can be put in the proper perspective.

Three major scales of motion have been recognized in the tropical circulations, viz:

(i) The meso-convective scale motions (wave length 10 km - 100 km). On this scale are groups of convective systems made of cumulus and cumulonimbus towers (1 km - 10 km). Several mesoconvective-scale clouds then group together to make up the cloud cluster scale (100 km - 1000 km).

(ii) The synoptic or the long wave scale motions (2 km - 10,000 km). Easterly waves, tropical cyclones, waves in the upper troposphere, etc., belong to this scale of motion. There seems to be two principal types of these waves, namely those with wave lengths 200 km - 5000 km, which have maximum intensity in the lower troposphere, and the others with wave lengths from 5000 km - 10,000 km, which have maximum intensity in the upper troposphere. The mesoscale and the cloud cluster scale motions are embedded in the synoptic or long wave scale motion.

(iii) The planetary scale motions: (wave lengths greater than 1000 km and up to hemispheric scale). The equatorial trough, the trade wind regime, sub-tropical highs and jets, tropical monsoon, etc., belong to the planetary scales of motion.

The relationship between the motions of the cloud systems of tropical cyclones and the cyclone circulation is that between the first two scales of motion discussed above. The one scale of motion is embedded in the other.

Cloud materials of small dimensions (small cumulus clouds, small cirrus elements) often move with the air in which they are embedded and they are sometimes used in estimating the air motion. Observations show that deep clouds (of cumulus variety or middle layer clouds) do not move with the air in which they are embedded. The present investigation shows that the shift of the phase curves for both harmonic components in the azimuthal direction was very small in comparison with the azimuthal flow of air around the circumference of the cyclone.

Figures 46 and 47 show the shift in the phase curves in seven hours for both the first and the second harmonic component for hurricane Debbie, August 16, 1969. Within a radial distance of 7°, the shift is cyclonic for both harmonic components. Outside this radial distance, the shift is anticyclonic.

From Figures 46 and 47 the rotation rates of the phase curves are computed for the cyclonic turning part of the curves. These rates are compared with the rotation rates of air particles in a hurricane with maximum wind equal to 40 m/sec. and a wind profile of $V_e r^{0.5}$ = constant outside the radius of maximum wind (taken as 50 km).

Before discussing the curves in Figures 46 and 47 further, it is necessary to consider also the daily variations of the phase curves for the three cyclones studied. The phase curves for the first and second harmonic components are drawn separately for each cyclone (Figs. 48-50). For Hurricane Debbie and Typhoon Cora, the curves for the first harmonic have a general southwesterly orientation. At the initial stages of the cyclones the phase curves oscillate about a southwesterly direction especially within the radial distance six degrees from the center with the orientation of curves essentially towards the southwest. As the cyclones become full grown, the curves rotate cyclonically within about 6° - 7° of the center and also anticyclonically outside the area. This feature is best expressed by the curves for Hurricane Debbie for this harmonic. The curves for Hurricane Holly have an unusual orientation which is here attributed to the erratic development of the cyclone. Even in that case, there is some constancy in the orientation of the phase curves.

The curves for the second harmonic exhibited the same characteristics as those of the first harmonic. At the initial stages the phase curves oscillate about a southwesterly direction inside the 6 degrees radius. The fluctuations (cyclonic - anti-cyclonic) from day to day of the two sets of curves, within these radial distances at the initial stages of the cyclones, is noteworthy. Since there are no reasons to attribute these fluctuations to errors in the photographic processing or errors due to changes in the direction of motion of the cyclones, these oscillations indicate that at the early stages of development of tropical cyclones the cloud bands tend to oscillate about a particular direction.

After the cyclones have developed hurricane strength winds, phase curves rotate cyclonically within 7° of the cyclone center. This rotation appears to be an indication of the cyclonic rotation of the cloud bands. Comparing the hourly phase curves for Hurricane Debbie on August 16, 1969, with the daily curves for the same cyclone, it is observed that the daily movement of phase curves cannot be extrapolated from the rate of rotation of the phase curves computed from the hourly curves. In fact, the phase curves for the second harmonic for August 16 and August 17, 1969, show a recession of the phase curves. Local oscillation and cyclonic rotation are also observed in the phase curves for Typhoon Cora and Holly.

The possible conclusions that can be drawn from these observations is that the cloud bands and hence the field of low level convergence of the hurricane systems oscillate locally and they also undergo cyclonic rotation about the center of the cyclone. The rate of the rotation of the cloud bands is usually less than the rate of the cyclonic rotation of air particles about the center of the cyclone. From Figure 51 the rate of

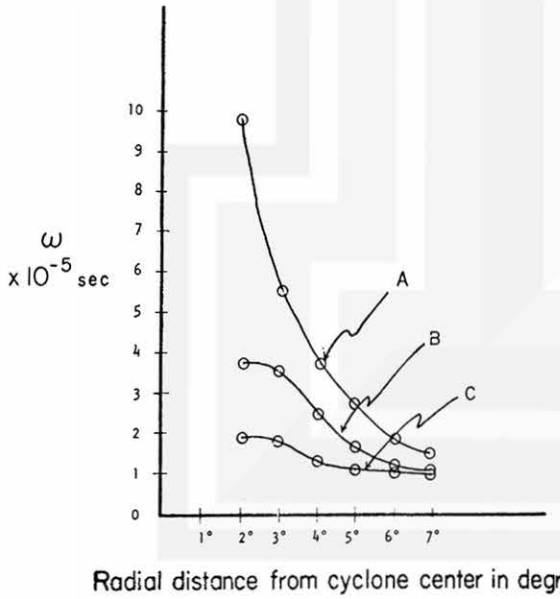

Fig. 51. Rotation rates of phase curves and air particles as function of radial distances. Curve A shows rotation rates of air parcels. Curve B shows rotation rates of phase curves for the first harmonic component. Curve C shows rotation rates of phase curves for the second harmonic component.

rotation of the cloud bands is about fifty to seventy-five percent of the rate of rotation of air particles. The movement of the phase curves suggests that the above estimates of the rate of rotation are high. Because the net motion of the phase curves from one day to the other sometimes show recession, it can be said that the rate of rotation of the cloud bands is not uniform in time and is generally lower than that indicated in Figure 51. A three-hourly or six-hourly computation of the phase curves, although at present not possible because photographs are not available for night time hours, is needed for proper identification of the mode of propagation of the cloud bands about the center of the cyclone. The motion of the cloud bands may in the future be interpreted from the point of view of an inertial instability in the air flow around the cyclone center. These instabilities may depend on horizontal shear, variation of the Coriolis parameter, the influence of friction, and on many other factors. At the moment there is no explanation for the motion of the cloud bands or the field of convergence which the cloud bands represent. How the motion of the cloud bands modifies the convective motion within the cloud bands and how it modifies the motion of air in the tropical storm will become clarified when the relationship between the three scales of motion stated earlier is firmly established.

7.3 Convective clouds and the numerical modelling of tropical cyclones

The relevance of the discussion on the numerical modelling of the tropical cyclones to the present investigation stem from the fact that the results of this study emphasizes some aspects of the tropical cyclone which are not normally taken into account in the numerical simulation of the cyclones. Some of the assumptions on which the numerical modelling of tropical cyclones are predicated are discussed below.

In most of the theoretical studies of the cyclone up to the present time, an assumption that the cyclone is an axially symmetric system is usually made. This assumption implies that clouds and the associated thermodynamic and dynamic quantities are distributed uniformly about the central axis of the cyclone. Evidence from the study of satellite photographs show that convective motion which is the main feature of the cyclone tends to concentrate along spiral bands which radiates from the center of the cyclone. The harmonic analysis of the cloud cover of the cyclone indicates that the first harmonic component is very prominent throughout the life time of the cyclone. This emphasizes the asymmetric nature of the cyclone. This asymmetry no doubt plays an important part in the evolution of tropical cyclones. Anthes (1970) in a theoretical study of tropical cyclones suggested that large scale asymmetry in the windfield of tropical cyclones may be important in satisfying the angular momentum budget of steady state cyclones. Asymmetry must, therefore, be included in the numerical modelling of tropical cyclones.

Another assumption is that deep convective clouds are the most important forms of moist convection with respect to the vertical transport of heat and moisture in the tropical cyclone system and therefore the effect of this convective cloud must be incorporated into the equation of motion used in the simulation of these cyclones. It is believed that the principal source of energy for the maintenance of tropical cyclones is the latent heat released by the cumulonimbus clouds. Given the field of large scale velocity, temperature and humidity of the cyclone environment a method of including the contribution of the convective motions to the changes and the rate of changes of

these fields must be found. The methods now employed to parameterize the convective scale motions in the tropical cyclone so as to include the net effect of these motions without the use of a model to describe the motions in detail can be divided into three categories.

In the first category are those methods that depend on the convergence of moisture in the boundary layer. The contribution of moist convection to the heating of the large scale environment is made proportional to the convergence of moisture in the planetary boundary layer. This method was first suggested by Ooyama (1964), Charney and Eliassen (1964), Ogura (1964), and was later improved upon by Rosenthal and Koss (1968) and Sunquist (1970).

In the second category, parameterization of cumulus convection was made dependent upon the moisture convergence integrated through the atmosphere. The work of Kuo (1965) and Rosenthal (1970) fall into this category. The details of these methods and some of their limitations can be found in the literature cited.

The two methods mentioned above are dependent on the convergence of moisture. An important aspect of the present study is the observed rotation of the field of convergence. This observation may play an important role in the dynamics of the hurricane system. Since the observed distribution of cumulus clouds in a tropical cyclone system must have a bearing on the formulation of methods used to include the effects of latent heat release in the system, future theoretic studies of cumulus parameterization in tropical cyclones must include the effect of rotation of the field of convergence.

The methods of cumulus parameterization in the third category are those that are dependent upon lapse rate adjustment. This method is more frequently used in planetary general circulation modelling than in the study of tropical cyclones. The important aspect of this method is that convective heating is allowed for by a direct adjustment of the lapse rate when instability occurs. This method is explained by Manabe et al. (1965) and by Oliger et al. (1970). The methods assume that convection is a function of lapse rates alone. In subsequent sections it is illustrated that there are clouds and active convection in areas where the lapse rate is moist adiabatic.

With the methods described above researchers have been able to simulate some characteristics of the tropical cyclone. The results obtained, however, often depend on the assumptions made. The present study points to some features of the cyclone that must be considered in the numerical simulations of tropical cyclones.

7.4 Satellite observed cloud cover of tropical cyclone and vertical structures of tropical cyclones

For a complete understanding of the tropical cyclone cloud cover as seen from satellite attitudes, it is necessary to look at some aspects of the vertical structure of the cyclones. Some radiosonde data collected from stations scattered in the Caribbean, Florida and around the Gulf of Mexico are used to construct a vertical profile of the troposphere near Hurricane Abby located in the Gulf of Mexico on June 3, 1968 (see Fig. 52). An ESSA satellite photograph showing the cloud patterns about the same

Fig. 52. Photograph of hurricane Abby, 3 June 1968.

time as the radiosonde observation was analyzed according to the procedure explained earlier. In doing this, the earlier requirement that any tropical cyclone whose cloud pattern is being studied must be far removed from land areas is relaxed to take advantage of the location of Hurricane Abby.

On June 3, 1968, about 1800 Z , Hurricane Abby, then a weak hurricane, was located approximately at Lat. 25°N long. 84°E so that the cloud cover was partly over the ocean and partly over the Florida peninsular and some Caribbean Islands. At that location, the center of the cyclone was about 5° - 7°from seven radiosonde stations, namely Jacksonville (206), Cape Kennedy (794), Grand Bahama (063), Grand Cayman (384), Swan Island (501), Merida (644), and Boothsville (232), (see Figures 53 and 54). Figures 55 to 57 represent the vertical profiles of the tangential and radial components of winds; relative humidity and the total static energy Q at an average distance of six degrees from the centers of the cyclone.

The cloud cover estimate N at thirty-six regularly spaced points along circles drawn on the ESSA photographs are determined and analyzed as explained earlier. The result of the analysis is shown in Figure 53 and Figure 54. The figures show the distribution of amplitudes, superimposed on maps showing the location of radiosonde stations for the first and second harmonic components, as functions of the azimuth distances from the north.

The approximate positions of the stations are indicated along the azimuth distances. From the graphs in Figures 53 and 54, the following observations are made:

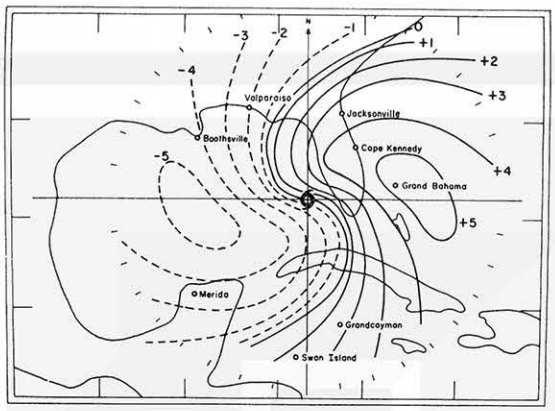

Fig. 53. Polar diagram showing distribution of amplitudes and phase for the first harmonic component for hurricane Abby, 3 June 1968.

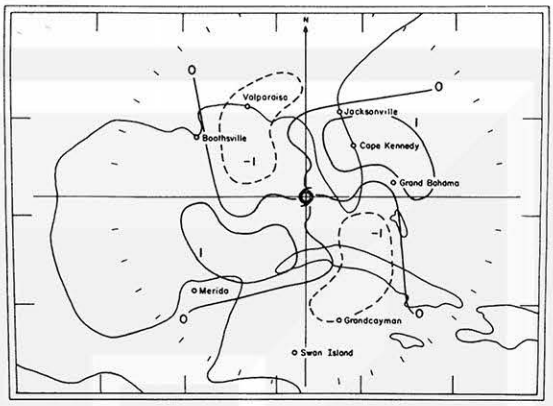

Fig. 54. Polar diagram showing distribution of amplitudes and phase for the second harmonic component for hurricane Abby, 3 June 1968.

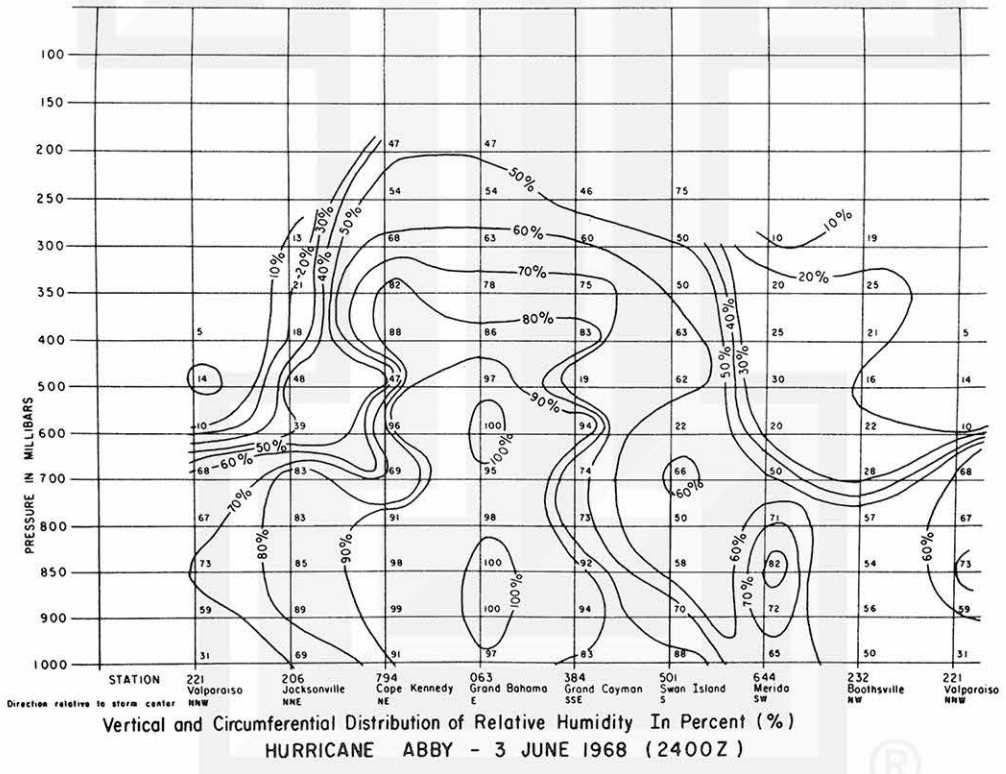

Fig. 55. Vertical and circumferential distribution of relative humidity in percent. Hurricane Abby, 3 June 1968.

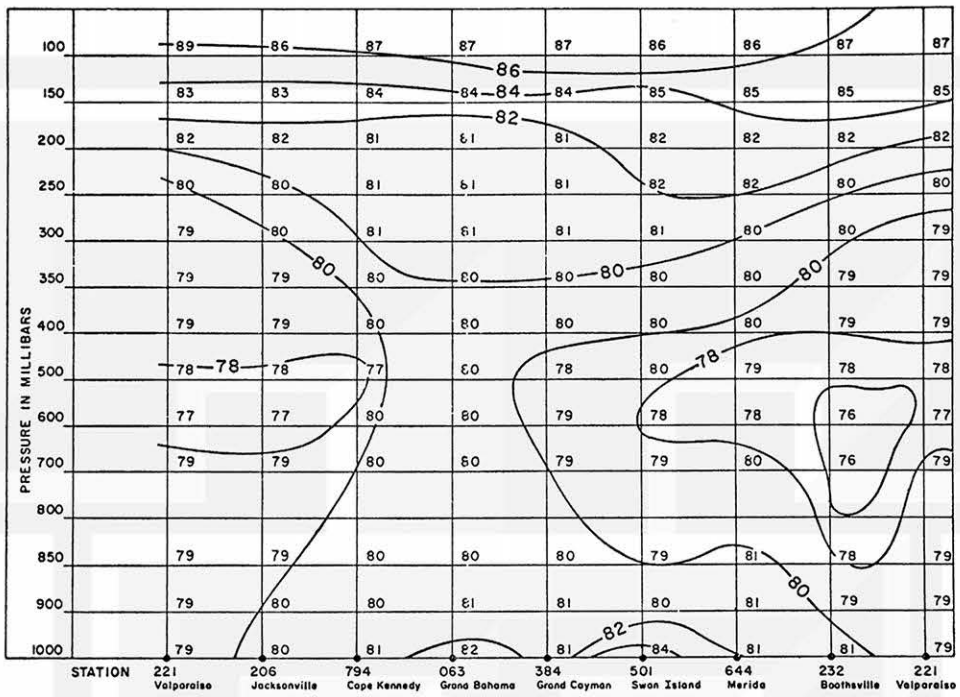

Fig. 56. Vertical and circumferential distribution of 'Q' in calories per gram. Hurricane Abby, 3 June 1968.

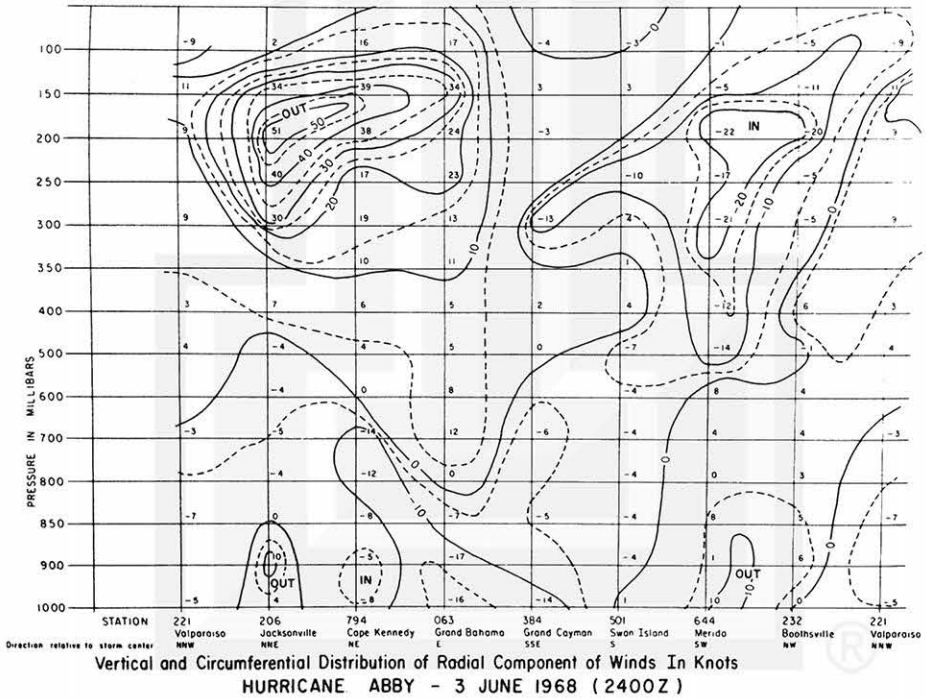

Fig. 57. Vertical and circumferential distribution of radial components of winds in knots. Hurricane Abby, 3 June 1968.

(a) The first harmonic component is the most prominent. It accounts for more than ninety percent of the total variance of cloud cover estimates along the concentric circles around the cyclone center. The distribution of the amplitudes, Figure 53, of the component shows maximum positive value over Grand Bahama. The analysis of the radiosonde data over Grand Bahama shows 100% relative humidity (Fig. 55) from the ground up to about 500 mb level. Elsewhere and at approximately the same distances from the center of the cyclone, the analysis of the radiosonde data shows relative humidity less than 100 percent.

The analysis of total static energy $Q = C_p T_e + L\alpha_g + g^z$ in calories per unit mass (Fig. 56) shows that no tropospheric minimum of Q is observed over Grand Bahama. The vertical profile of Q at the other stations shows a minimum at the 600 mb level. The uniform value of Q up to 400 mb level indicates that the upward transport of mass and energy is more vigorous over the general area of Grand Bahama. The profile of Q can also be identified with the profile of the equivalent potential temperature ($\theta_e \sim \frac{Q}{C_p}$). Over areas around Grand Bahama shown to have the highest cloud cover estimate, θ_e is conserved up to about 400 mb level. Above this level θ_e increases upwards. It is important to note here that over this cloudy area, convection still remained vigorous despite the fact that the lapse rate is practically most adiabatic. In fact above 400 mb $\frac{\partial \theta_e}{\partial z} > 0$ which is a condition of stability.

(b) Figure 57 indicates that cyclonic tangential winds and low level inward flow of air towards the center of the cyclone are more prominent over Grand Bahama than over other stations (also see Fig. 58). There is a prominent jetlike outflow of air

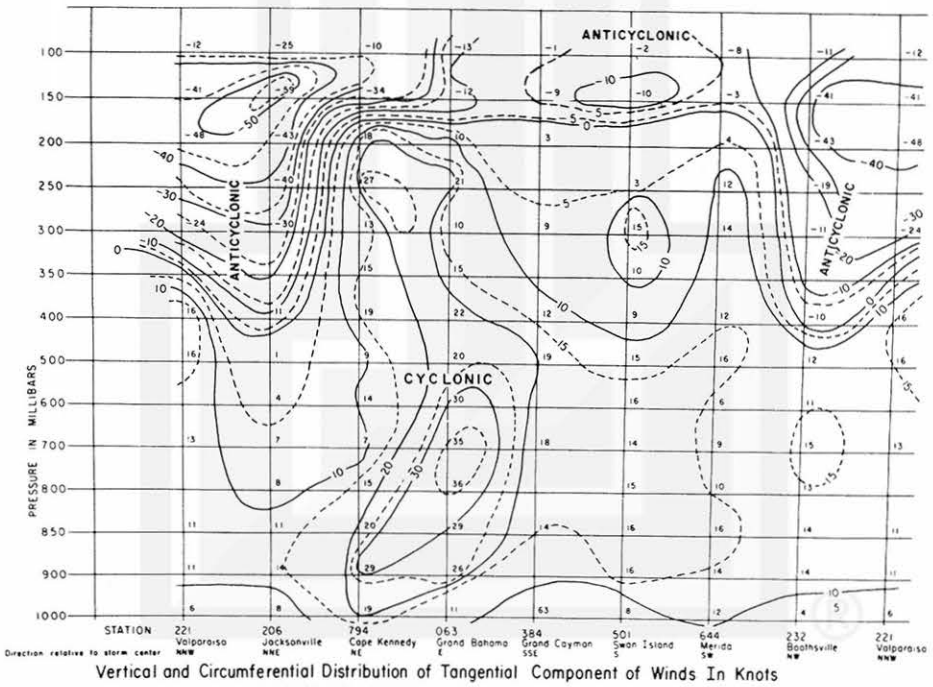

Fig. 58. Vertical and circumferential distribution of tangential components of wind in knots. Hurricane Abby, 3 June 1968.

over Jacksonville at the upper levels. Figures 53 to 56 show this station to be within cloud area but the low relative humidity at the upper levels over this station may be indicative also of subsiding air at that level. Clear areas over Valparaiso, Boothsville and Merida may also be evidence of subsiding air over those areas.

(c) The first maximums of the second, third, and fourth harmonic components are located over the general area of Grand Bahama. The amplitudes of these components are, however, small compared to those of the first harmonic component. The distribution of amplitudes for the second harmonic are shown in Figure 54.

In the above discussions, it is demonstrated that the cloud patterns of tropical cyclones reflect the thermodynamic processes going on beneath the cloud patterns.

CHAPTER VIII

SUMMARY AND CONCLUSIONS

The suitability of satellite photographs for tropical cyclone research depends on how well the currently accepted views on the tropical cyclone system are reflected in the satellite photographs of the system and how much of the characteristics of the tropical cyclones beyond the familiar ones can be further identified from such photographs.

Two fundamental characteristics of satellite observed cloud patterns of the tropical cyclone are apparent from this study. First, the variety of forms these patterns can assume and secondly, the orderly changes in the appearance and orientation of these patterns as the cyclones develop. In this study some aspects of these characteristics have been represented quantitatively and have been explained in terms of the physical processes suspected to be taking place in the system. On the other hand, some observed characteristics of the cloud patterns suggest some physical processes whose existence has hitherto not been demonstrated.

Through detailed analysis of series of satellite photographs depicting the various stages of three tropical cyclones, the following conclusions are drawn:

(a) The gradual changes in the cloud cover estimates as the cyclones develop are indicative of an orderly physical process taking place in the cyclone system. Only small fluctuations in cloud cover estimates, one to two-tenths, are found in the cloud cover estimates for tropical cyclones developing in favorable circumstances. Large fluctuations in the cloud cover estimates of the order of three-tenths or more may be evidence of an unusual development of the cyclone. Cyclones exhibit such characteristics when they are in hostile atmospheric environments and they may not develop hurricane or typhoon force winds before they dissipate.

(b) The spatial distribution of the cloud cover estimates vary with the development of the cyclones. There is similarity in the way the spatial distributions vary with time in all the cyclones studied but no unique cloud distribution parameter can be associated with a particular stage of development of the cyclones. This conclusion emphasizes the difficulty of formulating a correlation relationship between the size of the cloud cover as seen from satellite photograph and the intensity (maximum winds and lowest pressure) of the cyclone.

The curves showing the changes in the spatial distribution of cloud patterns (Figs. 29, 34 and 38) illustrated the three major periods into which the life history of the tropical cyclone can be divided. These three periods are: the early development period during which the aggregation of cumulus cloud into smaller area gives an indication of the incipient cyclone, the period of rapid intensification characterized by the development of cirrus shield over the cyclone system. The cirrus shield increases with time during this period. The third period is the period between the time the cyclone is recognized as having hurricane or typhoon strength winds and the time the cyclone attains its maximum intensity. During this period the rate of expansion of the cirrus shield first increases and then decreases as the cyclone modifies its environment; thereafter the cyclone slowly degenerates.

(iii) The harmonic analysis of the cloud cover estimates provides a statistical method for determining the deviations from the mean cloud cover estimates along concentric circles drawn around the center of the cyclones. It also facilitates the study of the orientation of the cloud patterns by providing a means of determining the positions from the north (i.e., phases of the harmonic components) along each circle at which the cloud cover is most pronounced.

The harmonic analysis of the cloud cover estimates for the cyclone patterns studied shows that the first two harmonic components are the most important. They both account for about seventy-five to ninety percent of the total variance of the cloud cover estimates especially within six to seven degrees of the center of the cyclone. The first harmonic is the more prominent of the two. For each cloud pattern, the ratio of the amplitudes of the first harmonic to the mean cloud cover estimate along each circle, denoted by a_r, is used as a parameter that describes the asymmetric distribution of the cloud cover with respect to the center of the cyclone. The parameter has maximum values along circles near the center of the cyclone during the early stages of the development of the cyclone. As the cyclone cloud cover becomes uniform on the circles close to the center of the cyclone, the maximum value of the parameter is found at outer radii. The ratio, therefore, provides a quantitative means of investigating the symmetrization process of the cyclone cloud cover. The symmetrization process first takes place near the center of the cyclone and then extends outwards as the cyclone matures; figures 41 to 45 illustrate this process.

To study the changes in the orientation of cloud patterns of the cyclones as the cyclone develops, phase curves are drawn for the first and the second harmonics. These phase curves are curves joining the phase position along each circle for all the nine circles drawn on each cloud pattern. The phase curves are identified with cloud bands and hence with the field of low level convergence. The curves tend

to oscillate in preferred directions with respect to the center of the cyclone at the initial stages of development of the cyclone and rotate cyclonically, in general within seven degrees of the cyclone center at later stages. Outside this distance, the curves in general rotate anticyclonically. The rotation and the oscillation of the curves near the center of the cyclone is identified with motions of the cloud bands. The modes and the origins of these motions are at present not clear. A possible explanation of the origin of such motions may be found in some form of inertia instability in the air flow around the center of the cyclone. The anticyclonic motion of the curve can be attributed to the outflowing cirrus clouds from the convective clouds that make up the cloud bands. Estimates of the rate of cyclonic rotation of the phase curves show that the phase curves for the first harmonic will undergo a complete rotation (360°) in about two days (for points on the curves near the center) to seven days for points on the curves between four and seven degrees from the center. For the second harmonic, a 360° rotation will take about four to seven days.

Compared to the rotation of air particles around the center of the cyclone, the rotation of the phase curves is very slow. Estimates of the rates of rotation are compared in Figure 51. Although the rates of rotation of the first and second harmonic are rather high, the fundamental fact that they are lower than those of air particles is indicated.

The procedures followed in this study offer a quantitative method of diagnosing the cloud patterns of tropical cyclones. Such diagnosis used in conjunction with conventional data may help in the better understanding of the tropical cyclone. In data sparse regions of the tropics where the satellite photograph becomes the primary source of information about the tropical cyclone, the computation of the satellite observed cloud cover estimates N, the changes in the area covered by cloud as indicated by the variation of r_N with time, the asymmetry parameter a_r and the phase curves are capable of providing quantitative information about the tropical cyclone not presently provided by mere inspection of the photographs. Since these parameters vary in orderly pattern, they also possess some prognostic values.

Refinement of the results obtained here will be possible when three hourly or even six hourly analysis of the cloud cover of tropical cyclones becomes possible throughout the life time of the cyclone. It will be possible for example to clarify the modes of propagation of the phase curves and to establish a better relationship between the satellite-observed cloud cover of the cyclones and the intensity of the cyclone (maximum wind and lowest pressure) with a continuous six hourly analysis of the cloud patterns. Much more so if there are adequate supplementary observations of the cyclones by conventional means at the time of the cloud analysis. This may be possible in the near future with the launching in 1973 of an operational SMS/GOES satellite equipped with infrared sensors so that night time cloud patterns of the cyclones can also be analyzed.

REFERENCES

Anthes, R. A., 1970: The role of large scale asymmetries and internal mixing in computing meriodinal circulations associated with steady state hurricanes. Mon. Wea. Rev., 98, 521-528.

Arnold, J. E., 1965: The time change of cloud features in Hurricane Anna 1961. The University of Chicago, SMRP Research Paper 64.

_____, 1966: Easterly wave activity over Africa and in the Atlantic with a note on the intertropical convergence zone during early July, 1961. The University of Chicago, SMRP Research Paper 65.

Barret, E. W., 1961: Some applications of harmonic analysis to the general circulation. Beitr. Phys. Atmosphere, 34, 167-197.

Booth, A. L and V R. Taylor, 1969: Mesoscale Archive and Computer Products of Digitized Video Data from ESSA Satellites. Bull. of the Amer. Met. Soc., 50, 431-438.

Charney, J. and A. Eliassen, 1964: On the growth of hurricane depression. J Atmos. Sci., 21, 68-75.

Clapp, P F , 1964: Global cloud cover for seasons using TIROS nephanalysis. Mon. Wea. Rev., 97, 256-276.

_____, 1968: Northern Hemispheric cloud cover for selected late fall season using TIROS nephanalysis. ESSA Technical Memorandum WBTM NMC 44.

Depperman, C. E , 1947: Notes on the origin of Phillipine typhoons. Bull. Am. Meteor. Soc., 28, 399-404.

Dunn, G. E., 1940: Cyclogenesis in the tropical Atlantic. Bull. Amer. Meteor. Soc., 21, 215-229.

Erickson, C. O., 1963: An incipient hurricane near the West African coast. Mon. Wea. Rev., 91, 61-68.

_____, 1971: Diagnostic study of a tropical disturbance. Mon. Wea. Rev., 99, 68-78.

Ferrell, W., 1911: A Popular Treatise on Winds, 2nd E., John Wiley & Sons, N.Y.

Fett, R. W., 1964: Aspect of hurricane structure: New model considerations suggested by TIROS and Project Mercury Observations. Mon. Wea. Rev., 92, 43-60.

Fett, R W , 1966: Upper level structure of the formative cyclone. Mon. Wea. Rev., 94, 9-18.

Frank, N. L., 1963: Synoptic case study of tropical cyclogenesis utilizing TIROS data. Mon. Wea. Rev., 91, 355-366.

_____, 1969: The 'inverted V' cloud pattern - an easterly wave? Mon. Wea. Rev., 97, 130-140.

Fritz, S., 1962: Satellite pictures and origin of Hurricane Anna. Mon. Wea. Rev., 90, 507-513.

Fritz, S., L. F. Hubert, A. Timchalk, 1966: Some inferences from satellite pictures of tropical disturbances. Mon. Wea. Rev., 94, 231-236.

Fujita, T. T., 1969: Formation and structure of equatorial anticyclones caused by large-scale cross-equatorial flows determined by ATS photographs. J. App. Meteor., 8, 649-667.

Hubert, L. F., A. F. Krueger and J. S. Winston, 1969: The double Intertropical Convergence Zone - Fact or Fiction? J. Atmos. Sci., 26, 771-773.

Kornfield, J., A. F. Hasler, K. J. Hansen and V. E. Suomi, 1967: Photographic cloud climatology from ESSA III and V computer produced mosaics. Bull. of the Amer. Meteor. Soc., 48, 878-883.

Kuo, H-L., 1965: On formation and intensification of tropical cyclones through latent heat release by cumulus convection. J. Atmos. Sci., 22, 40-63.

Malkus, J. S., C. Ronne, M. Chaffee, 1961: Cloud patterns in Hurricane Daisy, 1958. Tellus, 13, 8-30.

Manabe, S., J. Smagorinsky, and R. F. Strickler, 1965: Simulated climatology of a general circulation model with a hydrologic cycle. Mon. Wea. Rev., 93, 769-798.

Merrit, E. S., 1964: Easterly wave perturbation, a re-appraisal. J. App. Meteor., 3, 367-382.

_____ and R. Wexler, 1967: Cirrus canopies in tropical storms. Mon. Wea. Rev., 95, 111-120.

Ogura, Y., 1964: Frictionally controlled, thermally driven circulations in a circular vortex with application to tropical cyclones. J Atmos. Sci., 21, 610-621.

Oliger, J. E , R. E Wellck, A Kasahara, W M. Washington, 1970: Description of NCAR global circulation model. Lab. of Atmos. Sciences Publication, Boulder, Colorado.

Oliver, V. J., 1969: Tropical Classification System. Proceedings of the Interregional Seminar on the Interpretation of Meteorological Satellite Data. Melbourne, Australia.

Ooyama, K., 1964: A dynamical model for the study of tropical cyclone development. Geofisica Internacional Mexico, 4, 187-198.

Panofsky, H. A., 1968: Some Applications of Statistics to Meteorology. Pennsylvania State University, University Park, Pa.

Palmen, E., 1948: On the formation and structure of tropical hurricanes. Geophysica (Helsinki) 3, 26-38.

Piexoto, J., B. Saltzman, 1964: Harmonic analysis of the topography along parallels of earth. J. Geophysical Research, 69, 1501-1505.

Regular, H., 1936: Barometrische Shwankungen and Tornadoes an der Westkuste von Africa. Annal. Hydrograph (Berlin).

Riehl, H., 1945: Waves in the Easterlies and Polar Front in the Tropics. Miscellaneous Report 17, Department of Meteorology, University of Chicago.

_____, 1948: On the formation of typhoons. J. Meteorology, 5, 247-264.

_____, 1954: Tropical Meteorology, McGraw-Hill, New York.

_____ and J. S. Malkus, 1961: Some aspects of Hurricane Daisy, 1958. Tellus, 13, 181-213.

Rosenthal, S. L , 1970: A circularly symmetric primitive equation model of tropical cyclone development containing explicit water vapor cycle. Mon. Wea. Rev., 98, 643-663.

Rosenthal, S. L. and W. J. Koss, 1968: Linear analysis of a tropical cyclone model with increased vertical resolution. Mon. Wea. Rev , 96, 858-866.

Sadler, J. C., 1964: Tropical cyclones of the eastern North Pacific as revealed by TIROS observations. J. Appl. Meteor., 3, 347-366.

_____, 1968: Average Cloud Cover in the Tropics from Satellite Observations. East-West Center Press, Honolulu, Hawaii.

Sundquist, H., 1970: Numerical simulation of the development of tropical cyclones with a 10 level model. Part 1. Tellus, 22, 359-390.

Visher, S. S., 1925: Tropical Cyclones of the Pacific. Honolulu, T.H.: Bernice T. Bishop Museum.

Wexler, H., 1954: Observing the weather from a satellite vehicle. Jour. of British Interplanetary Soc., 13, 269-272.

_____, 1945: The Structure of the September 1944 hurricane when off Cape Henry, Virginia. Bull. Am. Met. Soc., 26, 156-159.

Yanai, M., 1968: Evolution of a Tropical disturbance in Caribbean Sea region. J. Met. Soc. of Japan, Ser. II, 46, 86-109.

Young, M. I., 1967: Variability in estimating total cloud cover from satellite pictures. J. Applied Meteor., 6, 573-579.

APPENDIX I

TABLES SHOWING RELATIVE AMPLITUDES OF HARMONIC COMPONENTS AND THE PERCENTAGE VARIANCE ACCOUNTED FOR BY EACH COMPONENT

TABLE 1. Percentage variance of cloud cover accounted for by the harmonic components for model cloud patterns.

Stage 1

$n \backslash \hat{\eta}$	0	0	100	94	90	82	75	68	60	52	49	43
4	0	0	34	28	30	32	31	29	27	24	23	20
3	0	0	0	0	0	0	0	0	0	0	0	0
2	0	29	66	66	60	50	44	39	33	28	26	23
1	0	0	0	0	0	0	0	0	0	0	0	0
radial distance	1	2	3	4	5	6	7	8	9	10	11	12

Stage 2

$n \backslash \hat{\eta}$	0	80	89	89	83	75	69	63	59	55	51	46
4	0	39	4	9	13	18	21	23	23	22	21	20
3	0	14	27	20	16	11	7	4	3	3	2	2
2	0	19	48	54	51	44	41	36	33	30	28	24
1	0	8	10	6	3	2	0	0	0	0	0	0
radial distance	1	2	3	4	5	6	7	8	9	10	11	12

Stage 3

$n \backslash \hat{\eta}$			96	95	86	43	61	53	49	46	41	37
4	0	0	0	0	1	0	3	7	9	11	12	12
3	0	0	41	45	44	35	25	16	13	11	6	5
2	0	0	18	18	25	29	29	28	25	24	23	20
1	0	0	37	27	16	9	4	7	7	0	0	0
radial distance	1	2	3	4	5	6	7	8	9	10	11	12

TABLE 1. Continued

Stage 4

$n \backslash \hat{\eta}$			96	84	89	81	70	58	50	45	41	36
4	0	0	6	11	14	8	3	0	0	3	4	6
3	0	0	17	15	35	43	39	31	25	19	15	11
2	0	0	30	20	5	12	17	20	21	20	20	19
1	0	0	43	48	35	18	11	7	5	3	2	0
radial distance	1	2	3	4	5	6	7	8	9	10	11	12

Stage 5

$n \backslash \hat{\eta}$			94	94	94	85	67	68	71	64	58	39
4	0	0	6	9	10	10	25	29	28	21	14	8
3	0	0	5	14	18	10	10	16	24	27	28	27
2	0	0	11	16	25	21	3	0	0	2	5	6
1	0	0	72	56	41	44	29	23	19	14	11	8
radial distance	1	2	3	4	5	6	7	8	9	10	11	12

Stage 6

$n \backslash \hat{\eta}$	0	0	96	98	92	80	77	55	53	55	60	45
4	0	0	0	4	10	13	13	12	12	12	10	8
3	0	0	8	15	19	18	16	13	12	13	11	8
2	0	0	5	17	24	23	18	15	14	15	13	15
1	0	0	63	62	39	26	20	15	15	15	16	24
radial distance	1	2	3	4	5	6	7	8	9	10	11	12

TABLE II. Relative amplitudes for the first four harmonic components for the cloud analysis of hurricane Debbie August 13, 14, 15, 16 and 19, 1969.

August 13

n	$\hat{H}n$								
4	0	0	0	10	19	24	30	33	30
3	0	4	7	4	14	29	38	40	42
2	0	8	12	15	29	49	67	77	72
1	0	10	37	40	37	35	31	15	8
0	1	2	3	4	5	6	7	8	9

Radial distance from cyclone center in degrees

August 14

n	$\hat{H}n$								
4	0	5	10	12	16	13	5	4	11
3	0	0	9	8	7	0	8	16	17
2	0	5	10	23	39	46	57	67	83
1	0	10	46	72	74	54	38	31	30
0	1	2	3	4	5	6	7	8	9

Radial distance from cyclone center in degrees

August 15

n	$\hat{H}n$								
4	0	0	0	12	0	17	23	20	11
3	0	7	15	16	20	37	56	59	47
2	0	9	13	28	50	60	52	48	47
1	0	20	45	65	75	71	64	75	87
0	1	2	3	4	5	6	7	8	9

Radial distance from cyclone center in degrees

TABLE II. Continued

August 16

n	$\hat{H}n$								
4	0	0	0	8	0	9	12	19	16
3	0	0	6	8	0	9	19	30	14
2	0	5	16	25	37	47	41	10	44
1	0	0	11	26	47	69	81	73	58
0	1	2	3	4	5	6	7	8	9

Radial distance from cyclone center in degrees

August 19

n	$\hat{H}n$								
4	0	0	10	15	10	43	60	58	55
3	0	0	11	16	33	50	45	21	15
2	0	0	31	57	73	68	62	74	85
1	0	0	5	5	17	35	48	59	63
0	1	2	3	4	5	6	7	8	9

Radial distance from cyclone center in degrees

TABLE III. Percentage variance accounted for by the first four harmonic components at various radial distances for hurricane Debbie August 14, 15, 16, and 19, 1969.

August 13

n \ $\hat{\eta}$		99	99	97	79	88	92	90	89
4	0	0	0	5	3	10	10	10	10
3	0	4	3	1	11	15	17	17	18
2	0	14	10	12	21	42	54	60	55
1	0	81	86	79	44	21	11	3	6
r°	1	2	3	4	5	6	7	8	9

August 14

n \ $\hat{\eta}$	0	90	98	98	98	90	87	90	85
4	0	5	4	2	3	3	1	0	1
3	0	0	3	1	1	0	1	4	3
2	2	5	4	9	20	37	59	71	72
1	0	80	87	86	74	50	26	15	9
r°	1	2	3	4	5	6	7	8	9

August 15

n \ $\hat{\eta}$		99	98	100	96	93	87	77	68
4	0	0	0	3	0	3	5	3	1
3	0	7	10	5	5	12	26	23	12
2	0	10	7	14	28	32	22	15	12
1	0	82	81	78	63	46	34	36	43
r°	1	2	3	4	5	6	7	8	9

TABLE III. Continued

August 16

$n \backslash \hat{\eta}$		100	97	98	100	98	95	90	76
4	0	0	0	5	0	1	1	5	4
3	0	10	10	5	3	1	4	12	3
2	0	54	59	42	38	31	18	1	27
1	0	36	28	46	59	65	72	72	42
r°	1	2	3	4	5	6	7	8	9

August 19

$n \backslash \hat{\eta}$			97	98	94	89	86	83	85
4	0	0	6	6	1	16	26	21	18
3	0	0	7	6	14	22	15	3	1
2	0	0	56	81	74	41	28	36	43
1	0	0	28	5	5	10	17	23	23
r°	1	2	3	4	5	6	7	8	9

TABLE IV. Relative amplitudes for the first four harmonic components for the cloud analysis of hurricane Holly September 13 - 17, 1969.

					September 13				
					$\hat{H}n$				
4	0	0	6	0	10	14	22	25	24
3	0	0	5	0	7	6	10	18	26
2	0	10	24	35	45	52	51	50	50
1	0	8	7	24	44	55	52	38	22
r°	1	2	3	4	5	6	7	8	9

					September 14				
					$\hat{H}n$				
4	0	0	0	0	11	15	18	22	31
3	0	0	0	9	15	0	0	0	16
2	0	9	19	28	17	32	60	67	55
1	0	15	24	18	10	13	24	27	37
r°	1	2	3	4	5	6	7	8	9

					September 15				
4	0	0	12	10	15	26	22	17	27
3	0	9	28	43	45	45	52	47	63
2	0	0	15	24	28	21	32	60	68
1	20	48	68	55	26	29	49	62	65
r°	1	2	3	4	5	6	7	8	9

TABLE IV. Continued

September 16

					$\hat{H}n$				
4	0	0	0	5	6	17	37	57	55
3	0	6	14	24	27	23	17	0	21
2	3	10	15	10	33	45	43	33	28
1	12	20	30	37	27	32	46	57	60
r°	1	2	3	4	5	6	7	8	9

September 17

					$\hat{H}n$				
4	0	0	0	0	18	18	13	0	25
3	0	7	0	37	57	78	84	71	53
2	5	15	34	61	86	97	84	63	55
1	30	50	72	87	98	93	78	67	47
r°	1	2	3	4	5	6	7	8	9

TABLE V. Percentage variance accounted for by the first four harmonics at various radial distances for hurricane Holly, September 13 - 17, 1969.

September 13

n \ $\hat{\eta}$		86	97	89	89	83	80	75	80
4	0	0	6	0	2	3	6	10	11
3	0	0	4	0	1	0	1	5	12
2	0	50	81	60	44	38	36	38	48
1	0	36	6	29	42	42	37	22	9
r°	1	2	3	4	5	6	7	8	9

September 14

n \ $\hat{\eta}$		99	93	95	87	71	80	80	73
4	0	0	0	0	13	11	6	7	4
3	0	0	0	6	27	0	0	0	4
2	0	18	36	62	36	51	64	62	45
1	0	81	57	27	11	9	10	11	20
r°	1	2	3	4	5	6	7	8	9

September 15

n \ $\hat{\eta}$	96	95	99	99	95	76	74	84	88
4	0	0	2	2	6	13	5	2	5
3	0	4	15	32	52	39	31	28	26
2	0	0	4	11	20	8	11	26	30
1	96	91	78	54	17	16	27	28	27
r°	1	2	3	4	5	6	7	8	9

TABLE V. Continued

September 16

n \ $\hat{\eta}$	100	99	97	98	93	89	87	87	89
4	0	0	0	1	2	7	21	33	36
3	0	5	11	27	25	11	4	0	3
2	7	15	13	5	40	48	28	14	10
1	93	79	73	65	26	23	34	40	43
r°	1	2	3	4	5	6	7	8	9

September 17

n \ $\hat{\eta}$	98	100	93	100	96	92	82	75	71
4	0	0	0	0	1	1	1	0	5
3	0	1	0	11	16	23	28	28	23
2	3	7	17	30	34	35	28	22	25
1	95	92	76	59	45	33	25	25	18
r°	1	2	3	4	5	6	7	8	9

TABLE VI. Relative amplitudes for the first four harmonic components for the cloud analysis of typhoon Cora, August 13 - 17, 1969.

August 13

				$\hat{H}n$					
4	0	2	4	6	5	26	0	17	20
3	0	2	8	12	14	40	15	11	10
2	0	13	14	6	8	25	29	39	50
1	0	0	15	30	45	13	35	25	31
r°	1	2	3	4	5	6	7	8	9

August 14

				$\hat{H}n$					
4	0	0	0	0	0	0	41	58	70
3	0	0	9	14	10	5	7	18	24
2	0	0	30	58	74	61	33	16	19
1	0	0	53	45	32	33	40	41	40
r°	1	2	3	4	5	6	7	8	9

August 15

				$\hat{H}n$					
4	0	0	8	5	7	8	0	10	18
3	0	0	0	22	19	8	8	13	13
2	0	3	12	15	10	34	26	42	47
1	0	29	47	38	34	45	57	64	69
r°	1	2	3	4	5	6	7	8	9

TABLE VI. Continued

August 16

				$\hat{H}n$					
4	0	0	0	0	10	22	33	38	39
3	0	3	4	3	7	6	11	10	11
2	0	2	6	9	20	34	42	49	47
1	0	24	42	47	44	38	25	12	16
r°	1	2	3	4	5	6	7	8	9

August 17

				$\hat{H}n$					
4	0	0	0	0	14	22	24	13	9
3	0	2	3	4	15	24	24	18	9
2	0	7	11	15	29	35	24	20	7
1	0	5	20	38	48	41	33	33	51
r°	1	2	3	4	5	6	7	8	9

TABLE VII. Percentage variance accounted for by the first four harmonics at various radial distances for typhoon Cora, August 13 - 17, 1969.

August 13

n \ $\hat{\eta}$		95	93	94	93	93	83	69	63
4	0	1	3	2	1	5	0	8	6
3	0	2	10	9	8	12	9	3	2
2	0	85	36	2	3	5	30	41	39
1	0	7	44	81	81	71	44	17	16
r°	1	2	3	4	5	6	7	8	9

August 14

n \ $\hat{\eta}$		98	100	99	93	76	69	70	69
4	0	0	0	0	0	6	27	42	45
3	0	0	2	3	1	0	0	4	6
2	0	6	23	60	78	54	17	3	3
1	0	92	75	36	14	16	25	21	15
r°	1	2	3	4	5	6	7	8	9

August 15

n \ $\hat{\eta}$		97	97	75	56	83	62	55	78
4	0	0	3	1	2	1	0	1	3
3	0	0	0	20	12	40	1	2	2
2	0	1	6	10	3	0	11	21	22
1	0	97	88	44	39	43	51	51	51
r°	1	2	3	4	5	6	7	8	9

TABLE VII. Continued

August 16

$n \backslash \hat{\eta}$		99	99	97	98	92	90	85	76
4	0	0	0	0	6	14	28	30	26
3	0	2	1	0	2	1	3	2	3
2	0	1	2	4	16	34	44	50	42
1	0	96	96	93	74	43	75	3	5
r°	1	2	3	4	5	6	7	8	9

August 17

$n \backslash \hat{\eta}$	0	99	96	92	93	92	83	59	58
4	0	0	0	0	5	11	17	5	2
3	0	4	2	0	6	13	18	10	2
2	0	39	23	12	22	28	17	12	1
1	0	56	71	80	60	40	31	32	53
r°	1	2	3	4	5	6	7	8	9

APPENDIX II

CONTOURS SHOWING ACTUAL CLOUD FIELD AND THE FIELD OF THE MEAN CLOUD COVER ESTIMATES PLUS AMPLITUDES OF FIRST HARMONIC FOR HURRICANE DEBBIE, 1969

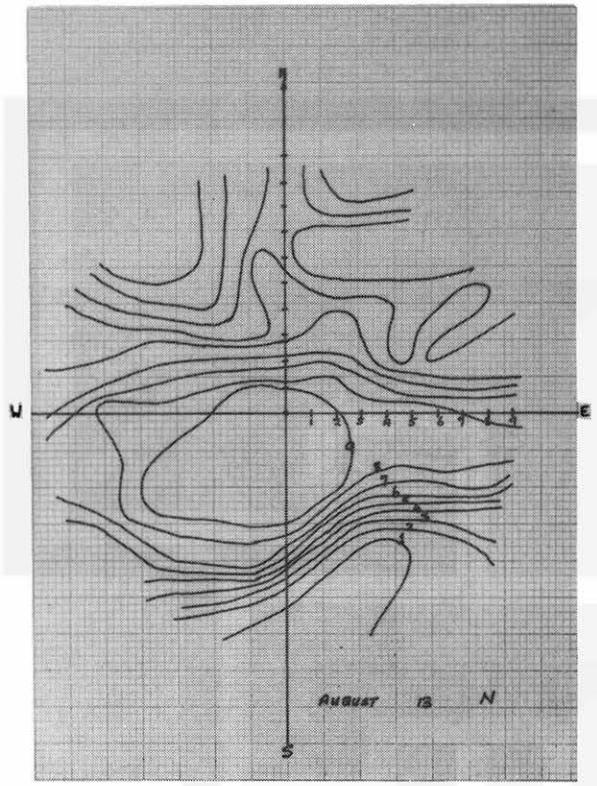
N
W
E
S
AUGUST 13 N

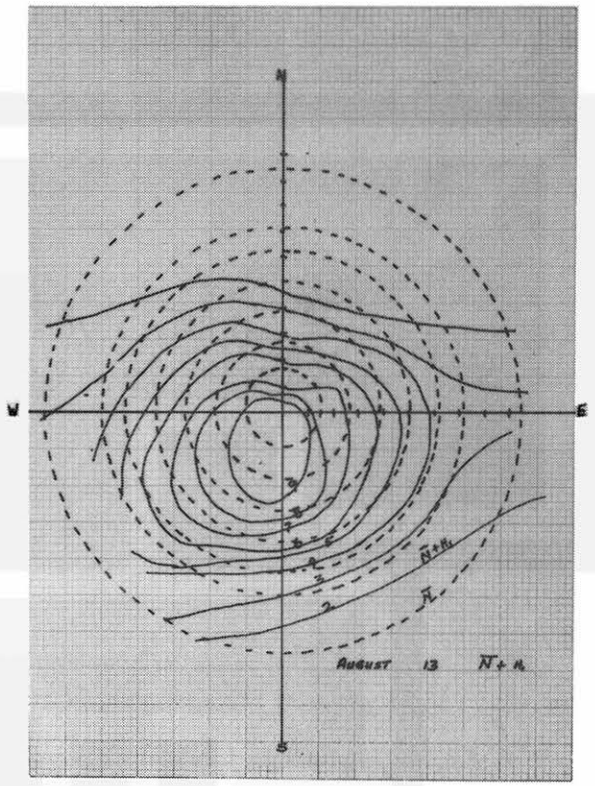
N
W
E
S
AUGUST 13 $\overline{N}+H_1$

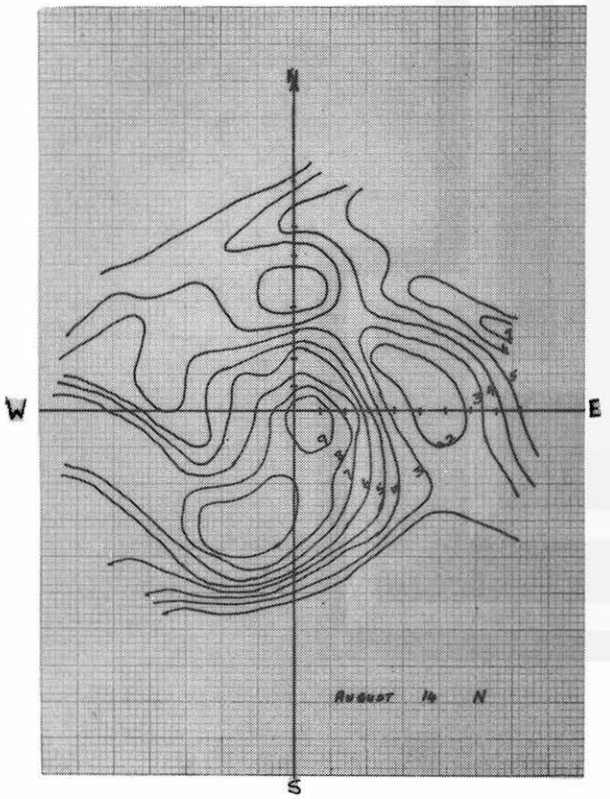
N
W
E
S
AUGUST 14 N

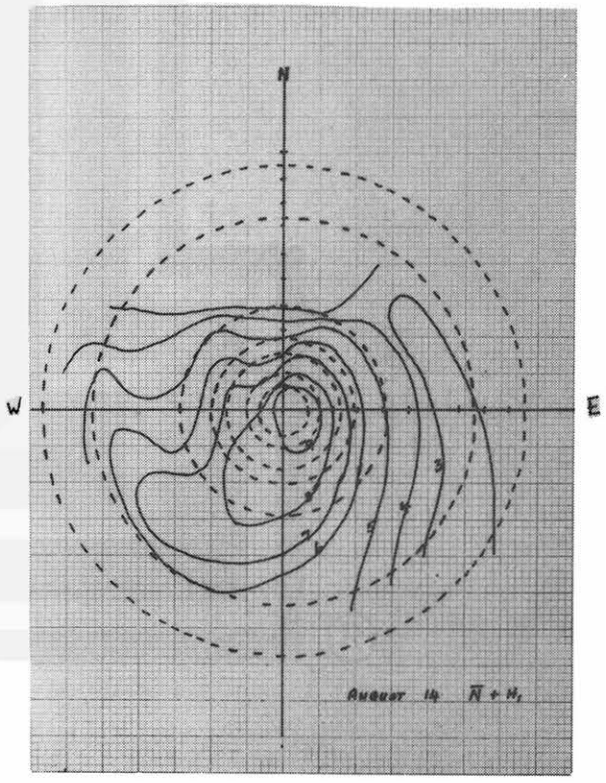
N
W
E
AUGUST 14 $\overline{N}+H_1$

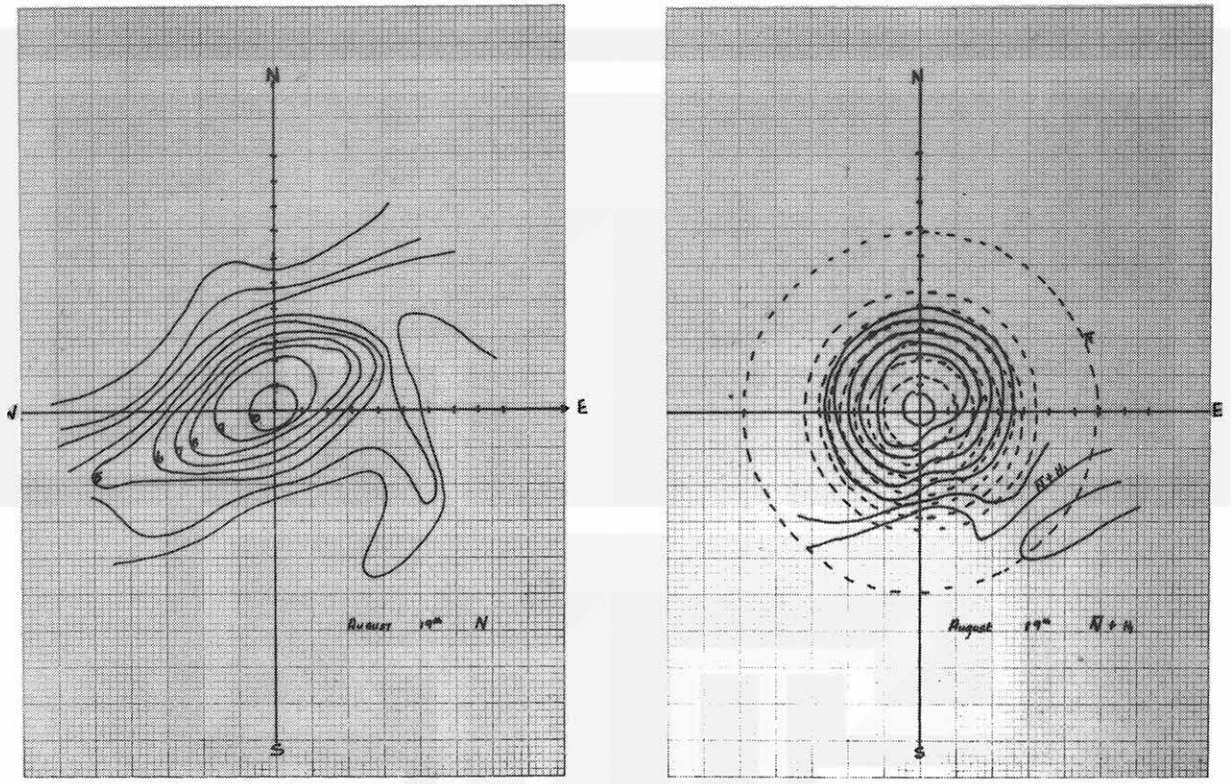
N
W
E
S
August 19th N
N
W
E
S
August 19th N + H

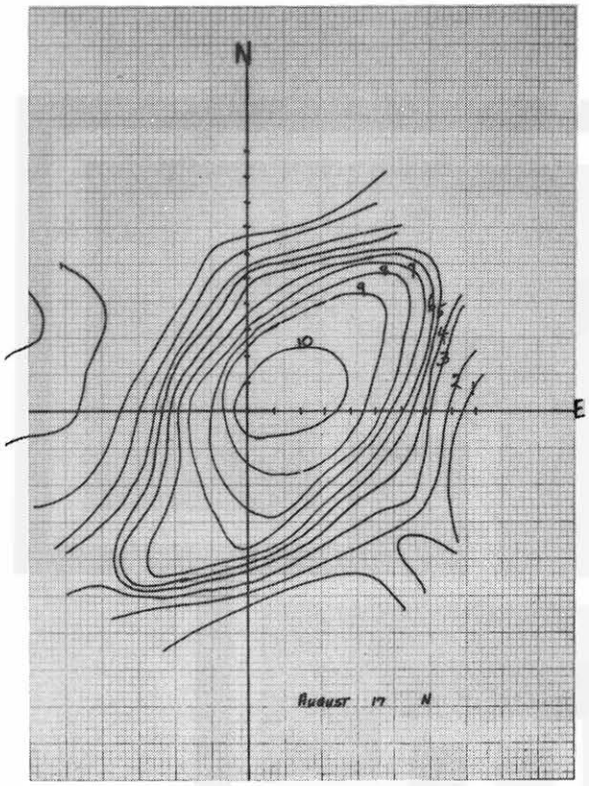
N
E
August 17 N

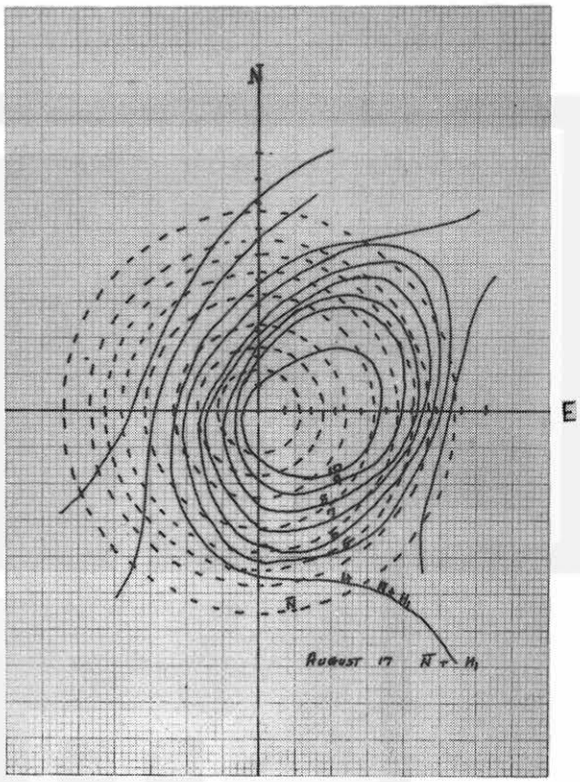
N
E
August 17 $\overline{N} + H_1$

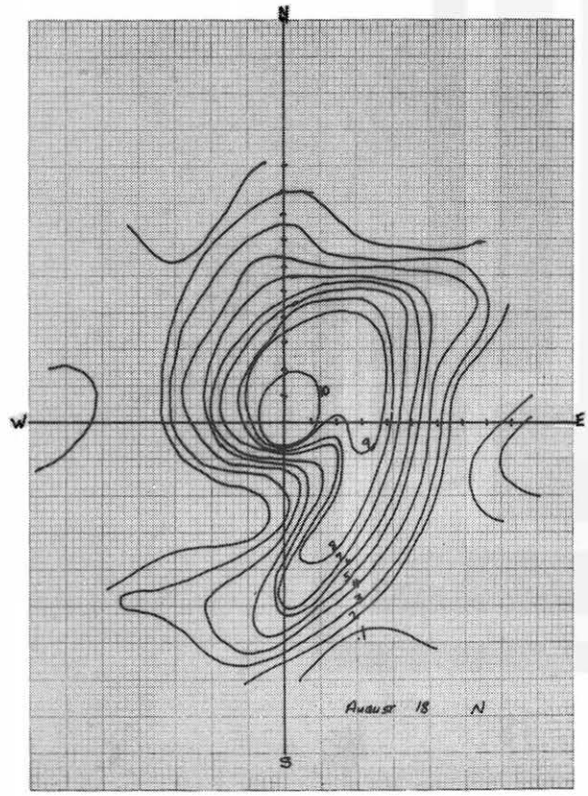
N
W
E
S
August 18 N

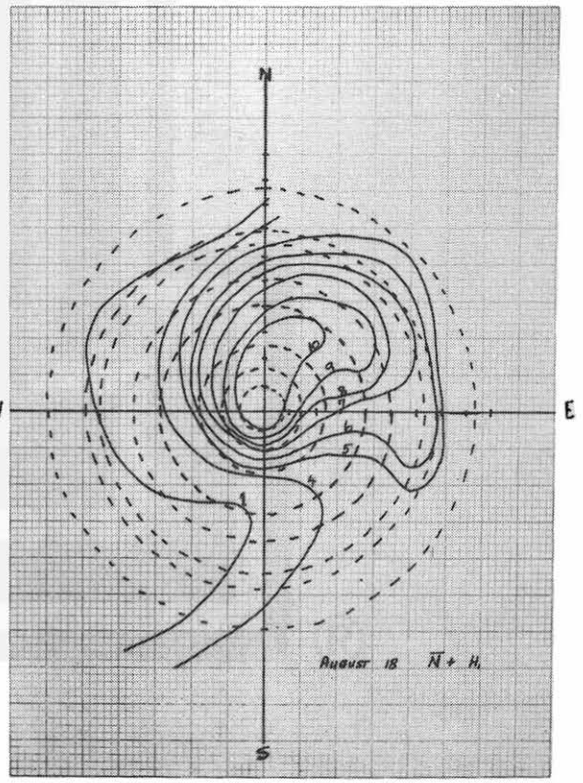
N
W
E
S
August 18 $\overline{N} + H_1$

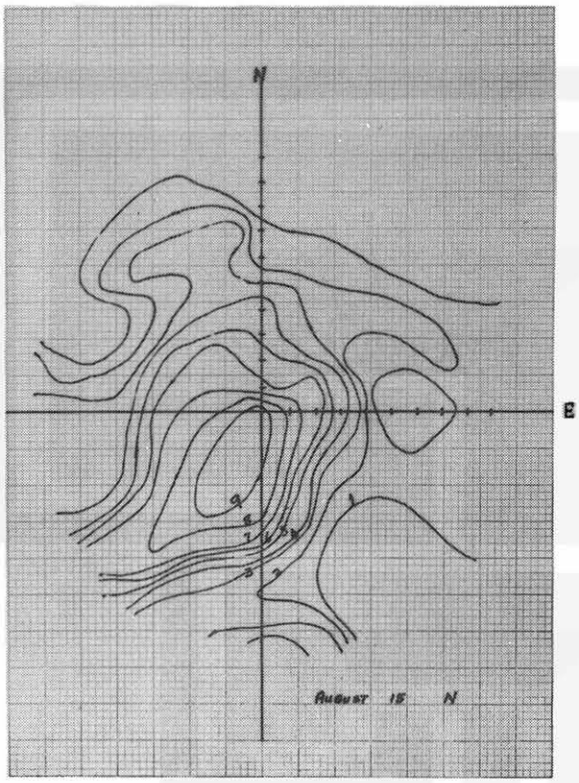
N
E
AUGUST 15 N

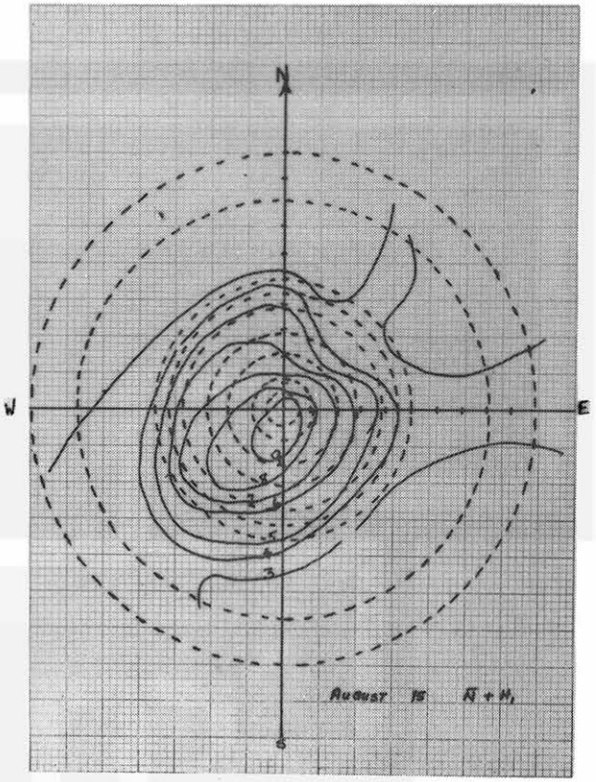
N
W
E
S
AUGUST 15 N + H

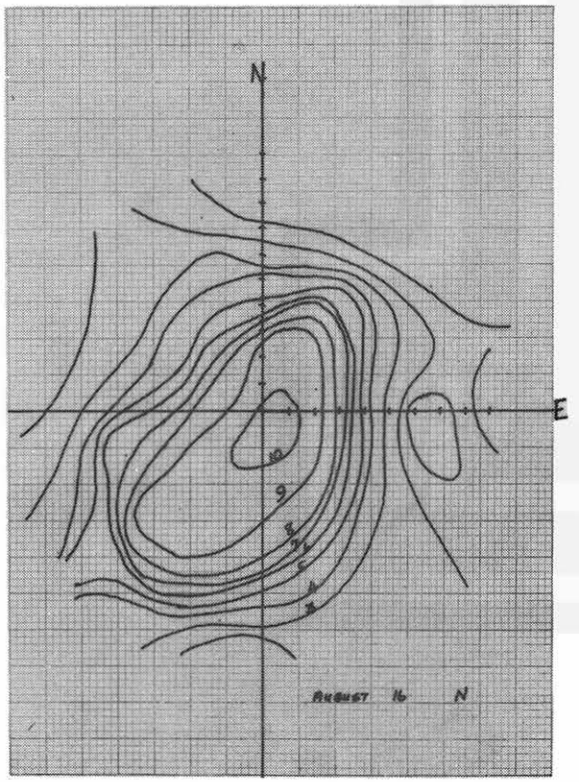
N
E
AUGUST 16 N

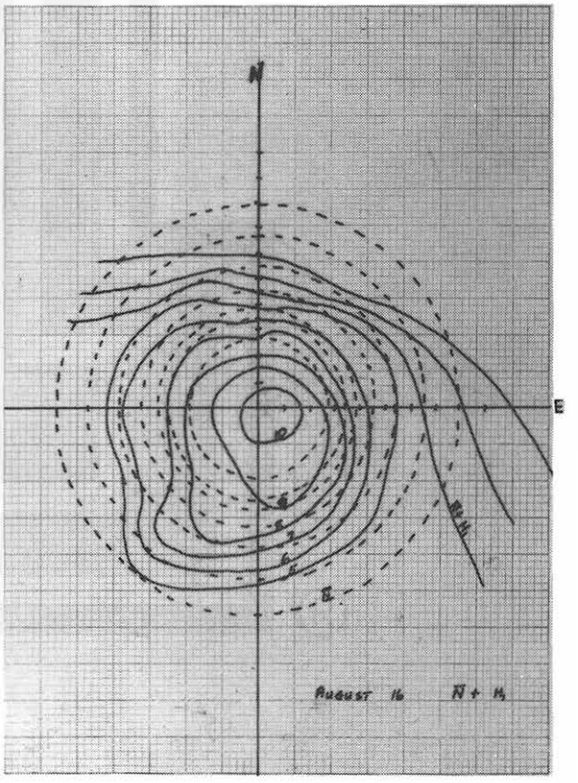
N
E
AUGUST 16 N + H

MESOMETEOROLOGY PROJECT - - - RESEARCH PAPERS

(Continued from front cover)

42.* A Study of Factors Contributing to Dissipation of Energy in a Developing Cumulonimbus - Rodger A. Brown and Tetsuya Fujita

43. A Program for Computer Gridding of Satellite Photographs for Mesoscale Research - William D. Bonner

44. Comparison of Grassland Surface Temperatures Measured by TIROS VII and Airborne Radiometers under Clear Sky and Cirriform Cloud Conditions - Ronald M. Reap

45. Death Valley Temperature Analysis Utilizing Nimbus I Infrared Data and Ground-Based Measurements - Ronald M. Reap and Tetsuya Fujita

46. On the "Thunderstorm-High Controversy" - Rodger A. Brown

47. Application of Precise Fujita Method on Nimbus I Photo Gridding - Lt. Cmd. Ruben Nasta

48. A Proposed Method of Estimating Cloud-top Temperature, Cloud Cover, and Emissivity and Whiteness of Clouds from Short- and Long-wave Radiation Data Obtained by TIROS Scanning Radiometers - T. Fujita and H. Grandoso

49. Aerial Survey of the Palm Sunday Tornadoes of April 11, 1965 - Tetsuya Fujita

50. Early Stage of Tornado Development as Revealed by Satellite Photographs - Tetsuya Fujita

51. Features and Motions of Radar Echoes on Palm Sunday, 1965 - D. L. Bradbury and T. Fujita

52. Stability and Differential Advection Associated with Tornado Development - Tetsuya Fujita and Dorothy L. Bradbury

53. Estimated Wind Speeds of the Palm Sunday Tornadoes - Tetsuya Fujita

54. On the Determination of Exchange Coefficients: Part II - Rotating and Nonrotating Convective Currents - Rodger A. Brown

55. Satellite Meteorological Study of Evaporation and Cloud Formation over the Western Pacific under the Influence of the Winter Monsoon - K. Tsuchiya and T. Fujita

56. A Proposed Mechanism of Snowstorm Mesojet over Japan under the Influence of the Winter Monsoon - T. Fujita and K. Tsuchiya

57. Some Effects of Lake Michigan upon Squall Lines and Summertime Convection - Walter A. Lyons

58. Angular Dependence of Reflection from Stratiform Clouds as Measured by TIROS IV Scanning Radiometers - A. Rabbe

59. Use of Wet-beam Doppler Winds in the Determination of the Vertical Velocity of Raindrops inside Hurricane Rainbands - T. Fujita, P. Black and A. Loesch

60. A Model of Typhoons Accompanied by Inner and Outer Rainbands - Tetsuya Fujita, Tatsuo Izawa, Kazuo Watanabe and Ichiro Imai

61. Three-Dimensional Growth Characteristics of an Orographic Thunderstorm System - Rodger A. Brown

62. Split of a Thunderstorm into Anticyclonic and Cyclonic Storms and their Motion as Determined from Numerical Model Experiments - Tetsuya Fujita and Hector Grandoso

63. Preliminary Investigation of Peripheral Subsidence Associated with Hurricane Outflow - Ronald M. Reap

64. The Time Change of Cloud Features in Hurricane Anna, 1961, from the Easterly Wave Stage to Hurricane Dissipation - James E. Arnold

65. Easterly Wave Activity over Africa and in the Atlantic with a Note on the Intertropical Convergence Zone during Early July 1961 - James E. Arnold

66. Mesoscale Motions in Oceanic Stratus as Revealed by Satellite Data - Walter A. Lyons and Tetsuya Fujita

67. Mesoscale Aspects of Orographic Influences on Flow and Precipitation Patterns - Tetsuya Fujita

68. A Mesometeorological Study of a Subtropical Mesocyclone -Hidetoshi Arakawa, Kazuo Watanabe, Kiyoshi Tsuchiya and Tetsuya Fujita

69. Estimation of Tornado Wind Speed from Characteristic Ground Marks - Tetsuya Fujita, Dorothy L. Bradbury and Peter G. Black

70. Computation of Height and Velocity of Clouds from Dual, Whole-Sky, Time-Lapse Picture Sequences - Dorothy L. Bradbury and Tetsuya Fujita

71. A Study of Mesoscale Cloud Motions Computed from ATS-I and Terrestrial Photographs - Tetsuya Fujita, Dorothy L. Bradbury, Clifford Murino and Louis Hull

72. Aerial Measurement of Radiation Temperatures over Mt. Fuji and Tokyo Areas and Their Application to the Determination of Ground- and Water-Surface Temperatures - Tetsuya Fujita, Gisela Baralt and Kiyoshi Tsuchiya

73. Angular Dependence of Reflected Solar Radiation from Sahara Measured by TIROS VII in a Torquing Maneuver - Rene Mendez.

74. The Control of Summertime Cumuli and Thunderstorms by Lake Michigan During Non-Lake Breeze Conditions - Walter A. Lyons and John W. Wilson

75. Heavy Snow in the Chicago Area as Revealed by Satellite Pictures - James Bunting and Donna Lamb

76. A Model of Typhoons with Outflow and Subsidence Layers - Tatsuo Izawa

* out of print

(continued on outside back cover)

SATELLITE AND MESOMETEOROLOGY RESEARCH PROJECT --- PAPERS
(Continued from inside back cover)

77. Yaw Corrections for Accurate Gridding of Nimbus HRIR Data - Roland A. Madden

78. Formation and Structure of Equatorial Anticyclones Caused by Large-Scale Cross Equatorial Flows Determined by ATS I Photographs - Tetsuya T. Fujita and Kazuo Watanabe and Tatsuo Izawa.

79. Determination of Mass Outflow from a Thunderstorm Complex Using ATS III Pictures - T. T. Fujita and D. L. Bradbury.

80. Development of a Dry Line as Shown by ATS Cloud Photography and Verified by Radar and Conventional Aerological Data - Dorothy L. Bradbury.

81. Dynamical Analysis of Outflow from Tornado-Producing Thunderstorms as Revealed by ATS III Pictures - K. Ninomiya.

82. ** Computation of Cloud Heights from Shadow Positions through Single Image Photogrammetry of Apollo Pictures - T. T. Fujita.

83. Aircraft, Spacecraft, Satellite and Radar Observations of Hurricane Gladys, 1968 - R. Cecil Gentry, Tetsuya T. Fujita and Robert C. Sheets.

84. Basic Problems on Cloud Identification Related to the Design of SMS-GOES Spin Scan Radiometers - Tetsuya T. Fujita.

85. Mesoscale Modification of Synoptic Situations over the Area of Thunderstorms' Development as Revealed by ATS III and Aerological Data - K. Ninomiya.

86. Palm Sunday Tornadoes of April 11, 1965 - T. T. Fujita, Dorothy L. Bradbury and C. F. Van Thullenar (Reprint from Mon. Wea. Rev., 98, 29-69, 1970).

87. Patterns of Equivalent Blackbody Temperature and Reflectance of Model Clouds Computed by Changing Radiometer's Field of View - Jaime J. Tecson.

88. Lubbock Tornadoes of 11 May 1970 - Tetsuya Theodore Fujita.

89. Estimate of Areal Probability of Tornadoes from Inflationary Reporting of Their Frequencies - Tetsuya T. Fujita.

90. Application of ATS III Photographs for Determination of Dust and Cloud Velocities Over Northern Tropical Atlantic - Tetsuya T. Fujita.

91. A Proposed Characterization of Tornadoes and Hurricanes by Area and Intensity - Tetsuya T. Fujita.

92. Estimate of Maximum Wind Speeds of Tornadoes in Three Northwestern States - T. Theodore Fujita.

93. In- and Outflow Field of Hurricane Debbie as Revealed by Echo and Cloud Velocities from Airborne Radar and ATS-III Pictures - T. T. Fujita and P. G. Black (Reprinted from preprint of Radar Meteorology Conference, November 17-20, 1970, Tucson, Arizona).

94. Characterization of 1965 Tornadoes by their Area and Intensity - Jaime J. Tecson.

95. * Computation of Height and Velocity of Clouds over Barbados from a Whole-Sky Camera Network - Richard D. Lyons.

96. The Filling over Land of Hurricane Camille, August 17-18, 1969 - Dorothy L. Bradbury.

97. Tornado Occurrences Related to Overshooting Cloud-Top Heights as Determined from ATS Pictures - T. Theodore Fujita.

98.** F P P Tornado Scale and its Applications - T. Theodore Fujita and A. D. Pearson.

99. Preliminary Results of Tornado Watch Experiment 1971 - T. T. Fujita, J. J. Tecson and L. A. Schaal.

100. F-Scale Classification of 1971 Tornadoes - T. Theodore Fujita.

101. Typhoon-Associated Tornadoes in Japan and New Evidence of Suction Vortices in a Tornado near Tokyo - T. Theodore Fujita.

102. Proposed Mechanism of Suction Spots Accompanied by Tornadoes - T. Theodore Fujita.

103. A Climatological Study of Cloud Formation over the Atlantic During Winter Monsoon - H. Shitara

104.** Statistical Analysis of 1971 Tornadoes - Edward W. Pearl

105. Estimate of Maximum Windspeeds of Tornadoes in Southernmost Rockies - T. Theodore Fujita.

106. Use of ATS Pictures in Hurricane Modification - T. Theodore Fujita.

107. Mesoscale Analysis of Tropical Latin America - T. Theodore Fujita.

108. Tornadoes Around The World - T. Theodore Fujita. (Reprinted from Weatherwise, Vol 26, No. 2, April 1973)